Nanocarriers for simultaneous delivery of structurally different polynucleotides encoding antigens and adjuvants

Dissertation

zur Erlangung des Grades

des Doktors der Naturwissenschaften

der Naturwissenschaftlich-Technischen Fakultät

der Universität des Saarlandes

von

Sarah Samir Mahmoud Nasr

Saarbrücken

2022

Tag des Kolloquiums: 14.07.2022

Dekan: Prof. Dr. Jörn Walter

Berichterstatter: Prof. Dr. Claus-Michael Lehr

Prof. Dr. Anna K. H. Hirsch

Vorsitz: Prof. Dr. Thorsten Lehr

Akademischer Mitarbeiter: Dr. Jessica Hoppstädter

The present work was conducted from January 2018 to November 2021 under the supervision of Prof. Dr. Claus-Michael Lehr and Dr. Brigitta Loretz at the Helmholtz Institute for Pharmaceutical Research Saarland

This thesis was conducted as part of a Full Ph.D. Scholarship, funded by the Egyptian Ministry of Higher Education Mission's Sector.

‘***Cogitatio in vero exquirendo maxime versatur. Appetitus impellit ad agendum.***

The Intellect engages us in the pursuit of Truth. The Passions impel us to Action.’

— Marcus Tullius Cicero

Contents

List of Abbreviations

APCs	Antigen-presenting cells
ASOs	Anti-sense oligonucleotides
CCL4	Chemokine ligand 4
CCR7	chemokine receptor 7
CD	Circular Dichroism
CMV	Cytomegalovirus
CoAc	Gelatin-pDNA complex coacervate
CPP	Cell Penetrating Peptide
DLS	Dynamic light Scattering
EMA	European medical Agency
FACS	Fluorescence activated cell sorting
FCS	Fetal calf serum
HBSS	Hanks' Balanced Salt Solution
HIV	Human immunodeficiency virus
HMWT	High Molecular weight Heparin
LNP	Lipid Nanoparticles
MFI	Mean fluorescence intensity
MHC I	Major Histocompatibility Complex I
MHC II	Major Histocompatibility Complex II
miRNA	micro RNA
mRNA	Messenger ribonucleic acid
NA	Nucleic acid
ANTA	Nanoparticle Tracking Analysis
PBS	Phosphate buffer saline
P-CoAc	Protamine-coated Gelatin-pDNA complex coacervate
pDNA	Plasmid deoxyribonucleic acid
PEI	Polyethyleneimine
PRRs	Pattern recognition receptors

P-TS-CoAc	Protamine-coated Thermally-stabilized Gelatin-pDNA complex coacervate
RSV	Respiratory syncytial virus
saRNA	Self-amplifying RNA
SD	Standard deviation
SI	Separation index
siRNA	Short-interfering RNA
TLR	Toll-like Receptor
TS-CoAc	Thermally-stabilized Gelatin-pDNA complex coacervate

List of Figures

List of tables

Kurze Zusammenfassung

Die rasche Zulassung von mRNA-basierten Impfstoffen für den menschlichen Gebrauch nach der Covid-19-Pandemie hat ihren Wert für die öffentliche Gesundheit bewiesen. Dennoch gibt es Raum für Verbesserungen, um die Anzahl der erforderlichen Auffrischungsdosen zu verringern. Ziel dieser Studie war es, einen Nanoträger zu entwickeln, der Nukleotid (NT)-kodierte Antigene und Adjuvantien gemeinsam abgibt und deren zeitversetzte Expression ermöglicht, so dass die Adjuvantexpression dem Priming der Zielzellen (APC) mit der Antigenexpression folgt.

Daher wurde ein Kern-Schale-System konstruiert, das auf einem Plasmid-DNA (pDNA)-Gelatine-Koazervat-Kern basiert, der thermisch zu einem Nanogel stabilisiert, mit Protamin (P-TS-CoAc) beschichtet und an der Oberfläche mit mRNA beladen wurde. Das System zeigte eine einzigartige Co-Transfektion für beide NT, die für fluoreszierende Reporterproteine kodieren, im Vergleich zu mehreren etablierten Kontrollen in einer dendritischen Mäusezelllinie (DC2.4). Ebenso zeigte das System eine zeitversetzte Expression der beiden NT, mit einer schnellen,vorübergehenden Expression der mRNA und einer verzögerten, längeren Expression der pDNA.

Es wurden NT-kodierte Adjuvans-Kandidaten ausgewählt, um die Transfektionsfähigkeit von P-TS-CoAc in DC2.4 zu prüfen. Diese waren CCL4 und CCR7, die an der Mobilisierung von Immunzellen zu Entzündungsherden bzw. drainierenden Lymphknoten beteiligt sind. CCL4-kodierende NT induzierten die Freisetzung von CCL4 aus DC2.4 nach Elektroporation, jedoch nicht nach Behandlung von DC2.4 mit entsprechend beladenen P-TS-CoAc. Weitere Studien könnten durchgeführt werden, um die Leistung des Systems zu verbessern.

Short Summary

The rapid approval of mRNA-based vaccines for human use following the Covid-19 pandemic established their public health value. Yet, room for improvement to reduce number of required booster doses still exists. This study aimed to investigate the development of a nanocarrier to co-deliver NA-encoded antigens and adjuvants and achieve their time-resolved expression, such that adjuvant expression follows target cell (APC) priming with antigen expression.

Hence, a core-shell system was constructed based on a plasmid DNA (pDNA)-gelatin coacervate core, thermally stabilized into a nanogel, coated with protamine (P-TS-CoAc), and surface loaded with mRNA. The system showed unique co-transfectional ability for two such NAs encoding fluorescent reporter proteins when compared to several established controls in dendritic murine cell line (DC2.4). The system also showed time-resolved expression of the two NAs, with a rapid and transient expression of mRNA on the shell and a delayed, prolonged-expression of pDNA in the core.

NA-encoded adjuvant candidates were selected to assess P-TS-CoAc's capacity to transfect them into DC2.4, namely, CCL4 and CCR7, involved in mobilizing immune cells towards inflammation sites or draining lymph nodes, respectively. CCL4 encoding NAs induced CCL4 release from DC2.4 following electroporation, yet, not upon DC2.4 treatment with P-TS-CoAc loaded with CCL4 encoding-NAs. Further studies could still be conducted to improve system performance.

Chapter I: General background

Throughout the 20th century and so far in the 21st century, vaccines have been one of the major factors revolutionizing public health[1]. They have helped to either eliminate or eradicate the majority of childhood diseases. This includes the eradication of smallpox, and the almost entire elimination of poliomyelitis, as well as a reduction in the incidence of measles, mumps, diphtheria, pertussis, tetanus, and rubella by more than 95%[2–4]. Many of the aforementioned infections account for major purging events throughout human history[5]. More recently vaccines against Hepatitis A and B, Haemophilus influenza b, and pneumococcus as well as tumor eliciting infectious agents are further decreasing infectious diseases related mortalities[2]. Such impact of vaccines is transforming our world from one in which one in four children used to reach the age of twenty[6], and life spans averaged at 49.5 years at the dawn of the 20th century into the very different world we inhabit today[7–9]. As vaccines continue to play their major role, safeguarding the world's population against both old and emerging infectious diseases, the battle against infectious diseases is far from over and the challenges faced by vaccines continue to metamorphose with the shifting public health challenges, and the never-ceasing capacity of pathogens to adapt and mutate thus continually fueling the need for improved vaccine technologies.

Many challenges remain to be addressed by modern vaccines, where many pathological agents still lack an effective vaccine on the market including Mycobacterium tuberculosis, malaria, Zika virus, HIV, Respiratory syncytial virus, Cytomegalo virus[1,10]. Dose number reduction of currently available multi-dose vaccines can prove instrumental in outbreak situations and low in-come country endemics[11–15]. The changing age demographics, with life expectancies, approximately doubling within a century pose a challenge associated with the declining quality of immune response with age also known as immunosenescence, which can negatively impact vaccine responsiveness in elder populations [16–19]. Hence, prompting the need not only for safer vaccines but also technologies capable of antigen sparing, that can still produce an adequate immune response in elder individuals using equal antigen doses to those used for younger populations. Vaccines more prone to precipitating a balanced adaptive immune response with adequate T-cell component and long-lasting memory are also in demand[1,10] Emerging anti-infectives-resistant superbugs and our hyperconnected world where endemics can much easier turn into pandemics overnight dictate the need for flexible, efficient, and safe vaccine technologies that can be rapidly developed and widely deployed at affordable prices, to both developed and developing countries.

Currently, two approaches seem like the most viable means for meeting the aforementioned requirements of modern vaccines namely, nucleic acid-based vaccines, mRNA-based vaccines in specific[20] as well as adjuvantation[21].

Adjuvants can guide a quantitative enhancement of the resulting immune response by producing higher antibody titers and seroconversion rates even in immunologically

challenged populations such as infants, the elderly, and immunosuppressed individuals[15,22–25]. This quantitative enhancement can also promote vaccine dose sparing[10,11,13,14,26–28] with all the public health, economic and logistic benefits to ensue. Such quantitative impact was most clearly demonstrated by the antigen sparing impact of incorporating emulsion-based adjuvants MF59 and AS03 in H_5N_1 vaccines[15,28]. Yet, adjuvantation can additionally promote the quality of vaccine evoked immune response in terms of speed of response to the vaccine[29,30], enhancement in Th-1 biased responses[31], or at least balanced Th-1 to Th-2 responses, the generation of long-lasting immune memory[32–34], as well as promoting adequately high CD8+ responses alongside the CD4+ response[35–37]. This particular feature and capability of the appropriate adjuvant to promote adequate CD8+ responses[38–40], especially in the absence of direct intracellular infection and endogenous antigen expression and hence eventual presentation on MHC I, may also be what had placed nucleic acid-based vaccines and viral vector-based vaccines at the forefront of the Covid-19 vaccine market. A key feature distinguishing mRNA-based vaccines from live-attenuated or viral-vector DNA-based vaccines is the non-existent risk of infection or genome integration, as well as the possibility for repeated administration with minimal acquired immunity against the carrier[41].

With the aid of reverse vaccinology techniques that are now becoming key in vaccine design[42,43], nucleic acid-based vaccines provide the opportunity for precise epitope selection, prominent examples of the value of such a feature can be derived from Covid-19 vaccine development. Several epitopes of SARS-CoV-2 were investigated for their immunological outcomes including the Spike protein (S)[44–46], Envelope proteins (E)[47], Nucleocapsid proteins (N)[48], Membrane proteins (M)[49], non-structural proteins (nsp) as well as several Open Reading Frames (ORF) on the viral RNA. Where some epitopes generated a strong CD4+ response primarily S, M, and N proteins, and to a lesser extent nsp3, nsp4, and ORF840. Whereas CD8+ T-cell responses were mostly elicited by M and S proteins, nsp6, ORF3a, and the N protein could also elicit a significant reaction[50]. Some epitopes on the other hand generated undesirable immunological outcomes, for example, nsp15 disrupted IFN production, thus hurdling the inflammatory cascade by associating with RNF41[51], whereas ORF8 was reported to downregulate MHC I expression and hence impaired the cellular arm of adaptive immunity[52].

The superior overall performance of the receptor-binding domain (RBD) of S-Protein as a safe and effective vaccine epitope evident in its pre-dominant neutralizing antibody titers in convalescent subjects [53–55] encouraged NA vaccine manufacturers to adopt it as their NA encoded antigen of choice[56,57]. The flexibility of the platform further allowed BionTech/Pfizer to fine-tune for safety by comparing their two mRNA candidates BNT162b1 (encoding for RBD site of the S protein) to BNT162B2 (encoding full-length S-protein in pre-fusion conformation) In a phase 1/2/3 study, where the RBD-encoding candidate displayed higher local and systemic adverse events compared to full-length S-Protein encoding candidate, where eventually BNT162B2 was adopted in further vaccine development[58]. Additionally, the endogenous expression of antigen(s) by host cells allows for post-translational modifications of these antigens such as appropriate protein folding, glycosylation, cleavage, or other modifications as would initially happen in case of an

actual infection. The flexibility of the technology also provides crucial benefit in the case of conformation-dependent antigens such as the Spike protein (S-protein) of MERS-CoV, where sequence modification of the S-protein encoding mRNA of MERS-CoV allowed the production of pre-fusion stabilized S protein through a double proline replacement (MERS-CoV 2P S), where studies showed that membrane-displayed MERS-CoV 2P S was more effective than either secreted MERS-CoV 2P S or wild-type MERS-CoV S in eliciting neutralizing antibodies[59]. This feature later also proved to be instrumental in developing the mRNA-based vaccines against SARS-CoV-2, where Moderna, BioNTech/Pfizer as well as CureVac all adopted mRNA sequences coding for double proline substituted, pre-fusion S membrane proteins for their vaccines[56].

All the aforementioned examples highlight the necessity and clear advantage of vaccine technologies that allow the precise selection of class I epitopes and preferably mixing and matching such epitopes to reach the most optimized immune response against a specific therapeutic target while avoiding immune-impairing epitopes. Such a feature can be very challenging to achieve using 'whole-virus vaccines' such as inactivated and live-attenuated vaccines[57]. A comparative systematic meta-analysis of SARS-CoV-2 vaccines' efficacy and immunogenicity showed that mRNA-1237 generated neutralizing antibody (nAb) titers approximately two orders of magnitude higher than CoronaVac (β-propiolactone inactivated SARS-CoV-2 adjuvanted with Aluminium Hydroxide)[45]. In general, mRNA based vaccines displayed overall efficacy at preventing symptomatic disease of over 90% against the Alpha strain compared to 63% efficacy reported for Oxford–AstraZeneca's ChadOx-1 (viral vector) when it was initially listed by WHO, whereas the inactivated vaccines CoronaVac and Sinopharm displayed 51% and 79% respectively[60].

It is hence becoming more evident that combining vaccine technologies that permit precise epitope(s) selection and design, alongside effective adjuvantation can allow for much safer, cheaper, longer-lasting, and more efficient vaccines.

1.1. Structure and pharmacology of mRNA-based vaccines

In this section, the pharmacology and structural modifications regarded as the current state of the art of mRNA-based vaccines design will be discussed in more detail. According to the central dogma of biology mRNA, is a single-stranded nucleic acid corresponding to a DNA-encoded genetic sequence in the cell nucleus. mRNA is transcribed in the nucleus on the DNA sequence template of the gene of interest and acts as a mediator carrying this genetic message to the cytoplasm where it is translated into proteins by the ribosome[61]. Typically, an mRNA molecule is comprised of 5 structurally and functionally distinct regions namely, 5′ cap, 5′-untranslated region (5' UTR), an open reading frame (ORF) encoding for the antigen, 3′ UTR, and a poly(A) tail[20] **(Figure 1).**

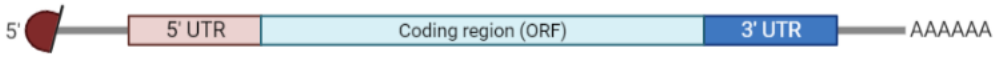

Figure 1.*The basic structure of messenger RNA (mRNA).*

Investigating the use of mRNA as a protein source for various therapeutic applications has been actively ongoing for three decades[62], with a particular focus on mRNA-based vaccines against both pathogens and tumors[20]. The principle upon which mRNA vaccines are based is the delivery of antigen encoding mRNA to the cytoplasm of host cells, preferably, antigen-presenting cells (APCs), the encoded antigens could be associated with an infectious pathogen, as well as tumor-associated or specific antigens. The antigen is then endogenously translated by the host's APCs allowing its intracellular processing and presentation on MHC I, synonymous with the course of events in case of an actual intracellular infection/mutation. Such MHC I mediated presentation, in turn, allows the activation of CD8+ mediated cytotoxic T-cell responses[63]. Also, subsequent extracellular release of these endogenously expressed antigens during cellular turnover, renders them accessible to MHC-II processing and presentation by bystander cells, thus eliciting CD4+ and B-cell mediated humoral immunity[64]**(Figure 2).**

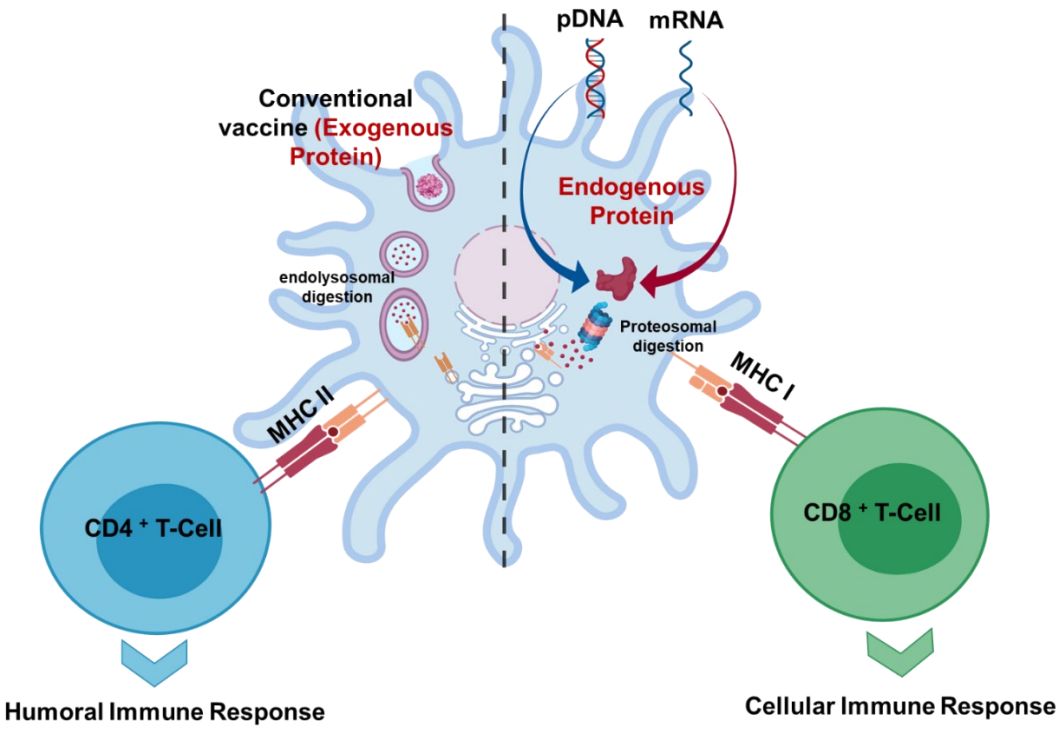

Figure 2. *proposed mechanism of action of mRNA-based vaccines.*

Currently, three main classes of RNAs are under investigation as vaccines, namely unmodified non-replicating mRNA, modified non-replicating mRNA, and Self-amplifying mRNA (saRNA). In-Vitro transcription (IVT) has been routinely used to produce the aforementioned mRNA classes. IVT mainly relies on the use of bacteriophage DNA-based

RNA polymerases such as T3, T7, or Sp6 to produce the desired mRNA sequence from a linearized DNA template, where the gene of interest is preceded with that specific polymerase compatible primer[65]. The technique is cell-free thus eliminating several regulatory concerns, alongside being faster and cleaner compared to protein production and purification involved in the preparation of subunit and virus-like particle (VLP) based vaccines[66].

Several drawbacks curbed the initial application of mRNA-based vaccines. First, the enzymatic instability of mRNA via the environmentally abundant extracellular RNases as well as its anionic charge and large molecular weight render its intracellular uptake challenging[67]. Its internalization mainly takes place through phagocytic mechanisms where the uptaken mRNA most likely ends up degraded in the endolysosomal compartment before reaching its site of translation in the cytoplasm[20]. mRNA free of modified nucleosides can trigger innate immunity, which despite rendering mRNA vaccines self-adjuvanting, can trigger IFN type I mediated responses which initiates several genetic pathways to curb mRNA translation and hence reduced antigen expression[68]. Double-stranded RNA impurities (dsRNA), a common bi-product of IVT can also trigger innate immunity via TLR3 receptors, further curbing mRNA translatability[56,69]. IVT product purification of dsRNA showed a significant improvement in its translatabilty[69]

Unmodified mRNA possesses self-adjuvanting properties, as it is largely associated with prokaryotes hence serving as pathogen-associated molecular patterns (PAMPS). mRNA molecules free of modified nucleosides can trigger innate immunity through their recognition by a range of pattern recognition receptors (PRR) in the cell membrane, cytoplasm, and the endosomal TLR3, 7,8 as well as MDA-5 and RIG-I RNA cellular recognition systems[70]. Such innate immunity recognition mechanisms do not only apply to pathogen-related RNAs but also apoptosis-related host-specific RNAs, as well as in-vitro transcribed RNA using unmodified bases. The most prominent cytokine triggered by RNA is IFN I, which can paradoxically impact vaccine efficacy, where on the one hand IFN I promotes APC activation, maturation, and antigen presentation yet, it also acts to curb the translatability of such mRNAs to avoid viral propagation or dissemination of apoptotic proteins[70].

In nature, mammalian cells tend to include modified bases at significantly higher frequencies than prokaryotic cells in their (ribosomal RNA (rRNA), Transfer RNA (tRNA), and mRNA. For instance, mammalian rRNA contains ten folds of pseudouridine (Ψ) and twenty-five folds 2′-O-methylated nucleosides compared to bacterial rRNA[71]. tRNA is often more densely modified than either mammalian rRNA or mRNA, overall 25% of its nucleosides are modified. When it comes to mRNA, while bacterial mRNA is largely devoid of nucleoside modifications, mammalian mRNA features a range of base modifications such as 5-methylcytidine (m5C), N6-methyladenosine (m6A), inosine, and many 2′-O-methylated nucleosides in addition to N7-methylguanosine (m7G)[72]. These modified nucleosides curb the immunogenic potential of mammalian mRNA by distinguishing it from prokaryotic mRNA[63,73]. Yet while base-modification of mRNA allows for immune evasion and enhanced translatability, A conundrum remains as to how

to achieve an acceptable balance between antigen expression efficiency as a proponent of the adaptive immune response, and mRNA self- adjuvanting properties as a proponent of the equally crucial innate immune response to a vaccine[74].

Several other structural modifications of mRNA contributed to boosting its structural stability and in-vivo expression, A eukaryotic cap structure is required at the 5' end of the molecule to prevent its recognition by PRR[75–77], such cap structures include Cap-1, Anti-reverse cap analogs (ARCA) and Clean cap technologies[78]. All these cap structures can be added either during or after transcription using vaccinia capping systems. The cap structure mainly serves as the anchor binding mRNA to eukaryotic translation initiation factor 4E (EIF4E), hence allowing its translation via ribosome.

The 5' and 3' UTR on either side of the ORF, routinely derived from either viral or eukaryotic sources, can when appropriately designed and incorporated dramatically prolong the half-life and hence the protein expression of mRNA[79,80]

On the ORF, in addition to base modifications, codon modifications can also be applied, where by replacing codons of lower cognate tRNA frequency in the cytosol with others of higher tRNA recognition frequency, possible improvements in the rate and extent of translation can be incurred[81]. G: C enrichment[82] and uridine depletion[83] are also codon modifications that can effectively enhance protein expression.

The ploy A tail structure length can also significantly impact the stability and translatability of the mRNA[76], and should hence be incorporated in an appropriate length ideally about 50-200 bases [65,75] in clinical settings[70,80], either directly from the DNA template or post-transcriptionally using poly (A) polymerase.

Self-amplifying mRNA (saRNA) is the next generation of RNA-based therapies and a further attempt to extend the half-life and maximize protein expression while minimizing RNA doses. The concept is based on combining two distinct ORFs on the same mRNA molecule, one encoding for the protein or in the case of vaccination, the antigen of interest, yet the second ORF on codes for the alphaviral RNA-dependent RNA polymerase among other non-structural proteins that upon translation can assemble in-situ into multi-enzyme replicase complex that can further self-amplify using the originally administered saRNA as a template. Early studies had reported effective immunization against RSV, and influenza with doses as low as 10 μg in mice[84]. Subsequent studies showed that using saRNA complexed in LNPs could further reduce that dose to 100ng to produce potent T and B cell-mediated responses in mice against RSV[85]. Nowadays the higher and more persistent antigen expression from saRNA-based vaccine candidates compared to conventional non-replicating mRNA is being explored for a range of infectious diseases including influenza, SARS-CoV-2, Rabies, Zika, and HIV[86].

More recently trans-saRNA in which the replicase and antigen encoding ORFs are co-delivered in two separated mRNA molecules is proposed as a very promising technique

that can drastically enhance saRNA delivery efficiencies, as well as enhance its structural stability. Beissert *et al.* reported that trans-saRNA showed 10-100 fold higher expression of trans-saRNA compared to single piece saRNA, also this technology could provide an effective Haemagglutinin encoding mRNA vaccine against influenza at doses as low as 50 ng[87]. Yet two major concerns regarding the clinical application of SAM, remain to be the size of the samRNA compared to conventional mRNA, as well as the presence of potentially immune triggering viral genome in its structure, which may limit its use in multi-dosing requiring regimens[86].

All the aforementioned structural modifications contributed to revolutionizing the therapeutic potential of mRNA transforming it from a molecule of limited structural stability, limited half-life, and low expression levels to the powerful therapeutic tool it is currently becoming.

1.2. Structure and pharmacology of pDNA-based vaccines

A lot of the performance aspects and mechanisms of adaptive immunity induction of mRNA vaccines also apply to DNA-based vaccines, with few differences[88]. pDNA is generally quite simple to manipulate and cheaply propagate with high yields in prokaryotic cells[89]. A pDNA molecule typically consists of a promotor region, most commonly of viral origin, an antibiotic resistance selection gene, and the antigen encoding gene followed by a poly-A tail encoding region[90]. The first key difference between DNA and mRNA is the superior structural and enzymatic stability of DNA, supercoiled pDNA can remain stable for up to 7 years at -20 ˚C, or several months at 2-4 ˚C, whereas mRNA requires constant storage in -70 ˚C, and even after formulation into LNPs.
The second difference between DNA and mRNA vaccines is the requirement for nuclear barrier crossing by DNA for its successful translation[91], such feature renders DNA-based vaccines generally less effective in quiescent cells, thus requiring the inclusion of nuclear-translocating signal(s) in the carrier system[92]. pDNA-based vaccines have also been repeatedly reported to induce a less intense immune response in primates and humans compared to smaller animals, owing to both a lower level of antigen expression as well as inferior self-adjuvanting properties compared to mRNA[93,94].

1.3. Non-viral delivery systems for NA-based vaccines, composition, modes of actions, and immune reactive properties

The anionic macromolecular nature of both mRNA and DNA still hinders their efficient uptake into host cells, and delivery systems that can shield the nucleic acid cargo

from environmental degradation, promote cell membrane crossing, as well as endosomal escape, are essential for the functionality of NA-based vaccines[67,95].

Currently, LNPs are the gold standard for mRNA delivery in clinical settings. All mRNA-based SARS-CoV-2 vaccines currently on the market rely on LNP technology. LNPs can encapsulate mRNA with high efficiency, and promote its cellular uptake, and endosomal escape. The formulation technique is straightforward and scalable, and the system is overall well-tolerated by the vast majority of recipients[96]. LNPs currently in clinical use are routinely comprised of four lipid components, namely ionizable lipid, helper lipid, cholesterol, and PEGylated lipid, which together can encapsulate mRNA in the system's core[97].

Cationic lipids were the prior generation to ionizable lipids used in LNPs, such as DOTMA and DOTAP, which were the first reported cationic lipids to successfully deliver mRNA in 1989[98]. Yet these perpetually cationic lipids promoted cell apoptosis and inflammatory responses at their sites of application[99,100]. Ionizable lipids, on the other hand, are a second generation that was able to overcome these effects, by their pH-dependent ionization state, where they are only positively charged in acidic pH while remaining neutral at physiological pH[101]. DODAP and DODMA[102,103] were the first reported ionizable lipids for mRNA delivery. The mRNA is encapsulated within such lipids in their cationic state under slightly acidic conditions, the formulation can later be readjusted to the physiological pH before administration without any perceived system dissociation. The ionizable lipids would hence regain their cationic charge in the endolysosomal compartment following cellular uptake, these cationic lipids can then interact with the anionic phospholipid endosomal membrane resulting in its disruption and hence promoting the endosomal escape of the mRNA cargo to the cytoplasm[104,105]. Later generations of ionizable lipids have been generated through rational design[103] and combinatorial approaches [106,107], such as Dlin-MC3-DMA [108], which besides showing efficiency for mRNA delivery (43-46) was the ionizable lipid component of the first FDA-approved LNP system for siRNA delivery in Onpattro's Patisiran. Other efficient ionizable lipids for RNA delivery include C12-200[109], 503O13[110], 306Oi10[111], OF-02[112], TT3[113], 5A2- SC8[114,115], SM-102 (used in the Moderna vaccine mRNA-1273 against SARS- CoV-2)[116]53and ALC-0315 (used in the Pfizer–BioNTech vaccine BNT162b2)[117], all of which have been almost exclusively discovered through combinatorial approaches. The combinatorial synthesis of vast lipid libraries allowed an in-depth understanding of their structure-activity relationships, pinpointing the most influential factors on the performance of such lipids being the lipid's pKa[110], its surface charge at pH 5[118] as well as its hemolytic activity at pH 5.5 [106,107], the size of the ionizable head group, steric hindrance between tail groups as well as the length and size of connector groups between the head and the tail(s)[119]. As previously mentioned limited options exist for achieving cell targetted expression of mRNA via sequence manipulation or other structural modification means. Yet several approaches have been implemented to delegate this targeting functionality of the carrier system, part of which focuses on its ionizable lipid component. For example, Lokugamage *et al.* reported the success of structurally constrained ionizable lipids with polycyclic adamantane tails to

target T-cell in-vivo[120], whereas Zhao *et al.* on the other hand showed such feature feasible using lipidoids with cyclic imidazole head structures [121], though the underlying mechanism remain unclear.

While ionizable lipid remains the most crucial lipid component of LNPs, helper lipids, cholesterol, and PEGylated lipids are still integral components of the system serving various roles. Helper lipids for example can significantly influence membrane fusion dynamics with both cell and endosomal membranes given their significant influence on membrane fluidity and phase transitions[122]. Helper lipid selection is primarily influenced by the ionizable lipid material, the mRNA cargo as well as the targeted cell population. For instance, LNPs for siRNA delivery showed the highest efficiency upon incorporating a saturated helper lipid such as DSPC [120], while for mRNA, delivery by unsaturated helper lipids such as DOPE is generally superior [123,124]. Yet, interestingly, all SARS-CoV-2 mRNA vaccines employed DSPC as their helper lipid component, given its previous approval within the Patisiran LNP[56]. Further studies are still required to compare the performance of DOPE and DSPC for the delivery of these vaccines.

Cholesterol can enhance LNPs fluidity and particle stability by incorporating among the hydrophobic tails of the rest of the lipid components filling the gaps and promoting stronger hydrophobic interactions[125]. The enhanced overall LNP fluidity promotes more efficient cell and endosomal membranes fusion and hence better cellular uptake and endosomal escape[126]. More recently cholesterol analogs have been explored for their ability to promote LNPs cell retention after uptake. In a study conducted by Moderna, β-Sitosterol showed enhanced intracellular mobility, fragility, and endosomal escape upon incorporation in LNPs compared to cholesterol, which resulted in 600 fold increase in luciferase expression from the mRNA cargo [127].

The PEGylated lipid component serves to prolong the LNPs circulation half-life and shield it from early non-specific PRR mediated recognition and elimination by the innate immune system[128,129]. The length of the PEG chain will vary according to the desired half-life of the formulation. The lipid anchor would range from 10 to 18 carbons[130,131], whereas the PEG chain may vary between 350 and 3000 Da in length[132]. For all the LNPs employed by either Moderna, CureVac, or Pfizer/Biontech for their SARS-CoV-2 vaccines DMG-PEG2000 was used[56].

Eventually, the lipid components and the mRNA are formulated as LNPs using the nanoprecipitation technique within a microfluidic assembly, which exerts minimal shear on the mRNA cargo, is easily tunable, and usually results in highly reproducible LNP batches in terms of physicochemical properties and in-vivo performance. generally, the staggered herringbone micromixer is commonly used for small-scale production, whereas the more durable T-mixers are used for large-scale production[133,134].

Cationic and ionizable polymers have also been developed for mRNA delivery, yet they remain of limited clinical application compared to lipids[135]. Such polymers can

electrostatically assemble with mRNA forming stable polyplexes capable of shielding mRNA cargo against enzymatic degradation as well as promoting endosomal escape, the most commonly proposed mechanism for the endosomal escape of polyplexes is the proton sponge effect[136].

One of the oldest and most studied polymers for mRNA delivery is polyethyleneimine (PEI). Despite its excellent efficacy, its in-vivo application remains largely limited by its toxicity [137,138] (81-82). In addition to toxicity, the use of high Mwt PEI has also been associated with lower transfection efficiency due to diminished NA cargo release[139,140]. Yet it has generally been observed that the use of low Mwt PEI or its PEGylation [141] or cyclodextrin conjugation [142–144] has been associated with reduced toxicity and improved transfection performance.

More biocompatible and biodegradable polymeric PEI alternatives have also been developed. One of the most prominent candidates is Poly(β- amino ester)s, especially its hyperbranched forms which have shown highly localized lung expression of co-formulated mRNA upon pulmonary administration in mice[145–147]. They have also shown success in cutaneous[148,149] and retinal delivery[150] of mRNA cargos. In addition to their DNA delivery capacitices[151] the synthesis of Poly(β- amino ester)s is simple and straightforward using Michael's addition, allowing the facile preparation of extensive libraries that could further deepen the understanding of their structure-activity dynamics[151].

Poly(amidoamine)s can similarly be synthesized using Michael addition as well, they tend to form dendrimer-like branched structures that still allow accessibility for core and peripheral modifications[114] using disulfide linkages or core pegylation [138,152] to mitigate potential toxicity. The branched dendrimer-like structure and the high amine group density at the periphery allow for efficient mRNA complexation and shielding [138].

In parallel to the paradigm shift from cationic to ionizable lipids in LNPs, similar trends have been undertaken for polyplexes, where pH-responsive polymers have also been proposed. For example, poly(aspartamide) cores conjugated to amino ethylene side chains have exhibited protonation under endosomal pH, and a subsequent enhancement in mRNA cargo's endosomal escape and subsequent translation[153]. Transfection efficiency is also tunable by manipulating chain length and degree of pegylation with demonstrated successful mRNA delivery to brain [153,154] spinal cord [155], knee joint [156], liver [157], and olfactory nerves [158].

BioDynamers have also been recently reported as dynamic biopolymers with acylcarbazone backbones, functionalized by basic amino acid side chains of either lysine, arginine, histidine, or a combination of the three[159]. BioDynamers assume a nanorod conformation that is both pH and concentration responsive, where it can degrade at lower pH and concentrations in the endosomal compartment, triggering efficient endosomal escape and high transfection efficiencies in human cell lines[159]. Similar systems have also

been reported[160,161] that rely on such intra-endosomal dissociation for efficient cytoplasmic mRNA delivery.

Cell-penetrating peptides have also been extensively investigated for their ability to deliver NAs. Their exact mechanisms could vary according to structure[162]. Yet they are generally rich in basic amino acids, and their overall cationic nature is hypothesized to interact with the negatively charged membrane phospholipid heads or glycosaminoglycans hence disrupting the bilayer structure of either cell or endosomal membranes[163,164]. RALA peptide comprised mainly of a repetitive arginine, alanine leucine, and alanine sequence have been reported to target DC transfection, promoting an efficient T-cel response against mRNA encoded antigen in-vivo[165]. Pepfects were also a series of cell-penetrating peptides optimized for mRNA delivery and largely relying on histidine-rich side chains could induce mRNA efficient transfection in-vitro[166]. CPP-coated viral-like particles are also emerging as efficient NA carriers [167]. Other systems also include Zr-based Metallo-organic frameworks cationized using ethanolamine [168].

Most of the systems that have been already described for mRNA delivery have also been employed with relative success for pDNA delivery. Nuclear translocation remains the main barrier and rate-limiting step to pDNA mediated transfection, where passive diffusion through nuclear pore complex (NPC) remains restricted to DNA fragments less than 300 bP. To date, most studies have shown the high reliance of pDNA transfection on nuclear membrane dissociation during cell division, where 85-90% transfection of pDNA lipoplexes[169] or polyplexes[170] treated cell lines occur in-vitro only after mitosis. Thus, modifying pDNA delivery systems with nuclear localizing signals (NLS) remains the most effective approach to ensure efficient DNA transfection. Some of the rather successful nuclear-translocation approaches in-vitro included nanocarrier conjugation with either all-trans-retinoic-acid (ATRA)[171] or glucocorticoids, the stimulation of both their cognate receptors has been shown to induce NPC dilation and promote nuclear translocation of pDNA cargo in-vitro, yet only dexamethasone conjugated nanocarriers could show in-vivo tumor regression in murine model[172].

All the aforementioned systems could enable NA-based vaccines by helping them overcome the cellular and intracellular barriers to eventually achieve intracellular antigenic protein expression which can promote more efficient CD8+ mediated adaptive immune responses. Yet, garnering innate immune responses and also occasional augmentation and optimization of adaptive immune response can further enable NA-based vaccines, and hence adjuvantation is explored in the next section.

1.4. Recent developments in adjuvantation concepts

Despite the establishment of the concept of adjuvantation by Gaston Ramon and Alexander Glenny Over a century ago, the number of clinically used adjuvants remains limited[23]. Many of the currently available whole viral vaccines, being either live-attenuated or inactivated vaccines have been proven to possess spontaneous endogenous adjuvantation properties through their inclusion of PAMPs [173–177]. For example, the Yellow fever live-attenuated vaccine (YF-17D) has been found to express PAMPs in-vivo able to trigger TLR2, TLR3, TLR7, TLR9, the retinoic acid-inducible gene I (RIG-I), and the melanoma differentiation-associated protein MDA5[178] (24). The Bacillus Calmette–Guérin (BCG) tuberculosis vaccine has also been demonstrated to initialize TLR2, TLR4, and TLR9 innate immunity pathways, as well as, dendritic cell-specific ICAM-grabbing non-integrin (DC-SIGN)[174,175]. Yet as previously described, some of the structural components of whole pathogens could on the other hurdle the innate and/or adaptive immune response against the pathogen and promote immune evasion. Hence the use of defined adjuvants in terms of both structural and innate and sometimes even adaptive immunity engaging pathways should be the next endeavor.

For the majority of the 20th-century insoluble aluminium salts have been the only clinically applied adjuvants, enhancing the efficiency and durability of the immune response of vaccines against Hepatitis B, tetanus, and diphtheria among others[23]. It was not until the 90s when the emulsion-based adjuvant MF59 was incorporated as part of Fluad seasonal influenza vaccine[179], since then several novel particulate adjuvants were introduced, mainly AS01[180,181], AS03[182], AS04[183], each of these adjuvants can stimulate a range of immune pathways depicted in **(Table 1),** yet for many of them, the exact mechanisms involved in innate immunity are still not fully understood, including mechanisms for T-helper cell recruitment, pathogen-specific antibody induction, their role in stress signal induction such as tissue damage, as well as metabolic changes that may play a further role in the immune response. Alum and Alum containing adjuvants such as AS04 also partially exert their adjuvanting effect via adsorbing the antigen and sustaining its release, resulting in a prolonged and stronger antibody response. This effect has been mainly resorted to the prolonged exposure of the lymph node germinal centers to the antigen[184]

Table 1. *Key adjuvants currently in application**

Adjuvant	Composition	Mode of action	Tested disease(s)
Alum	Insoluble aluminium salts	NLRP3 inflammasome, Th2 responses (+Th1 in humans), Ab	DTaP, pneumococcus, influenza, hepatitis A, B, HPV, COVID19.
MPL	Chemically modified LPS	TLR4 agonist	Pollen induced allergies
AS01	Liposome (MPL, DOPC, cholesterol, QS21)	TLR4 agonist, Th1	Malaria, TB, shingles

AS02	O/W emulsion (MPL, QS21)	TLR4 agonist, Th1	HIV, TB, malaria
AS03	Oil-in-water emulsion (α-tocopherol, Tween80, squalene)	Immune cell recruitment	Influenza
AS04	MPL + Alum	TLR4 agonist, Th2	HPV, hepatitis B
AS015	Liposome (AS01, CpG)	TLR4 agonist, TLR9 agonist, immune cell recruitment	Lung cancer, melanoma
AF03	O/W emulsion (Span80, mannitol, polyoxyethylene cetyl stearyl ether, squalene)	Immune cell recruitment	Influenza
AS37	TLR7 agonist adsorbed to Alum	TLR7 agonist	Meningococcal serogroup C
MF59	O/W emulsion(Span85,Tween80, squalene)	Th1 + Th2, Ab	Influenza
CpG	Synthetic DNA	TLR9 agonist	Hepatitis B

*Table is reproduced from Ref. 185

Yet much emerging research in the field of adjuvantation opens up the door for a range of concepts that can and should be considered in modern vaccine design and where the concept of NA-encoded adjuvants can allow their flexible and feasible adoption and variation according to the singular requirement of the pathogen of concern or the target group of recipients. For instance, a body of research solely focuses on adjuvants aimed at the induction of DCs via TLR mainly, given the central role of DCs in the adaptive immune response[37,185] and the central role of TLR in DC induction, proliferation, and maturation[176,186,187]. Yet, other cell types and pathways can also be triggered using different adjuvants, for instance, the mechanism of MF59 and alum which relies on impacting muscle cells more than other cell types upon intramuscular injection, triggering ATP release, and where monocytes and granulocytes have been observed as the fastest and most abundant immune responders at its site of release, fuel the consideration of such pathways alongside DC and TLR mediated adjuvantation pathways. Direct stimulation of B-cells either on the level of TLR [186] or through triggering its cytosolic MyD88 pathway[188] has also been found impartial to an efficient and pathogen-specific and long-lasting antibody response. Also, the interest in adjuvants capable of discretely inducing higher levels of CD8+ cells and tissue-resident memory cells is growing, yet before the emergence of mRNA vaccines, this adjuvantation pathway was mainly initiated by inactivated or live-attenuated vaccines[189]. STING [190], RIG-I, and RLR [191,192] pathways targeted adjuvants have been shown to discretely potentiate CD8+ response in mice. Also, molecules targeting

metabolic regulators of APC such as mTOR complex [193] and GCN2 [194] in DCs have been proven to alter the T_H cell response towards antigens and hence the ensuing adaptive immune response. Mediators associated with tissue damage and different modes of cell death have also been reported to release damage-associated molecular patterns (DAMPs) such as ATP and uric acid that can promote IFN-I, IL-1ß, and IL-18 by DCs[195]. Such DAMPs associated pathways have also been reported as part of the adjuvanting activity of the ionizable lipid component LNPs[196]

As the paradigm shifts towards more stringently tailored epitope expression to harness the most effective, safe, balanced, and disease-tailored immune response using NA-expressed antigens, similar concepts and approaches can be extended towards adjuvantation. This can be made possible in next-generation vaccines, by encoding immunomodulating molecules that would take into consideration some of the aforementioned pathways and concepts. From a formulation and a technological point of view, it could advantageous to simply attempt the delivery of desired immune mediators of the innate immunity and even some aspects of the adaptive immune response (mainly cytokines/chemokines/as well as their receptors) alongside the antigenic mRNA. The concept will also minimize the possibility of a loss of synchronicity between the sites of antigen and adjuvant action, which has previously been shown to compromise the efficacy of antigen-adjuvant combinations[197–199].

1.5. Nucleic acid-based adjuvant cargos

Generally, both mRNA and double-stranded DNA possess inherent adjuvanting properties. Double-stranded DNA can have a mild self-adjuvanting effect via the STING pathway resulting in IL-6 release and proliferation of Th1 and cytotoxic T cells[10,23]. The adjuvant effect of DNA is all the same well established to be inferior to that mediated by unmodified mRNA[10,200,201]. mRNA incorporating unmodified bases can trigger endosomal TLR7/8 as well cytoplasmic RIG-I and MDA5 pathways that can stimulate a range of IRF3, IRF7, NF-kB mediated immune responses, resulting in the release of Type I interferon (IFNα, IFN_{β}), IL6 and TNFs as well as Th1 cells and cytotoxic T-cells proliferation. Several NA-based adjuvants are currently in use based on these generic immunostimulatory pathways, though they may be non-coding. Examples of such NA adjuvants include CPG and its derivatives, mainly acting as TLR9 agonists, as well as, polyIC, a double-stranded RNA synthetic analog, capable of triggering endosomal TLR3 and cytosolic RIG-I and MDA5[10].

Yet apart from their inherent adjuvanting properties, more recent studies have explored the potential of immunostimulatory encoding NAs in the context of vaccination either as standalone therapeutic entities or as adjuvants. In those different studies, specific immune pathways were targeted by the discrete expression of specific effectors in these pathways.

One of the most prominent studies was conducted by Moderna where they explored the impact of co-delivering mRNA encoding for constitutively active STING with antigen encoding mRNA on a single LNP carrier. The combination resulted in a significant enhancement in the Type I IFN mediated antigen-specific T-cells activation, leading to higher efficacy of human papillomavirus oncoprotein encoding mRNA vaccines in mice[202].

Hess *et al*. had also reported a significant enhancement of the specific cytotoxic T-cell response upon co-administration of granulocyte-macrophage colony-stimulating factor (GM-CSF) encoding mRNA as adjuvant along with OVA expressing mRNA as an antigen when compared to a combination of GFP and OVA encoding mRNA as negative control[203] to Ovalbumin expressing tumor mice models.
In a recent study reported by BioNTech, Hotz *et al.* administered a mixture of naked modified mRNA encoding for IL-12, IFN-α, GM-CSF, and IL-15, without co-administration of tumor-specific antigen encoding mRNA in a range of syngeneic tumor models in mice. The cytokine cocktail managed to induce a significant increase in the number of tumor-infiltrating CD4+, CD8+, and granzyme B+ cells, with no significant changes to tumor T_{reg} content compared to control mRNA. The synergistic effect of the three genetic adjuvant candidates was also demonstrated in their significantly higher capacity to repress tumor growth in subcutaneous tumor models in comparison to each single cytokine encoding mRNA administered alone. The cytokine encoding mRNA cocktail showed delayed tumor regression and enhanced animal survival compared to control-treated mice at both its tumor site of injection but also in uninjected distal and disseminated tumors, and hurdled tumor growth upon rechallenge[204].

TriMix is a cocktail of mRNA encoding for CD40 ligand, CD70, and constitutively active TLR4 (caTLR4). This combination has demonstrated effective and successful adjuvantation to tumor-associated antigen (TAA) encoding mRNA vaccines in several preclinical and clinical trials that spanned several tumor classes[205–211]. Dewitte *et al.* used DC sonoporated with mRNA-loaded microbubbles, they used either GFP encoding mRNA as a negative control, OVA mRNA alone, OVA mRNA on DC prestimulated with LPS, or a combination of OVA mRNA and TriMix. They demonstrated superior tumor antigen-specific cytotoxic T cell response, tumor size reduction, and overall survival in several different melanoma murine models using the OVA mRNA-TriMix combination. The combination showed an average animal survival time of ≥31 days compared to 24 days for OVA mRNA only. Additionally, complete tumor regression was achieved in 30% of combination-treated mice, along with long-term immunological memory[208]. Whereas, Lint *et al.* demonstrated the superior performance of ex-vivo electroporated DCs with a combination of TAAs encoding mRNA and TriMix to TAA-mRNA treated DCs following intratumoral injection in 4 different tumor mouse models namely; E.G7-OVA, P815, TC-1, and A-20. TAA-mRNA. TriMix combination showed significantly higher specific lysis of TAA expressing cells, as well as delayed tumor regression and prolonged animal survival in all 4 tumor models[205]. The superior impact of these tumor-infiltrating DCs (TiDCs) in generating a systemic tumor neoepitopes specific immune response, also further indicates the capacity of such adjuvantation strategies to reverse the commonly reported

TiDCs immune suppression status[212,213]. In a clinical study that investigated the impact of co-electroporating TriMix with human leukocyte antigen class II-targeting signal encoding mRNA, patients with advanced melanoma showed antigen-specific tumor-infiltrating lymphocytes in 57.1% of patients after 4 vaccine doses, over 6 weeks, as opposed to 0% at the beginning of the vaccination regimen[209].

In the context of infectious diseases, a preclinical study conducted by iHIVARNA investigated the efficacy of HIV-2 vaccination using TriMix in combination with mRNA encoding for 16 selected HIV-1 epitopes (HTI). Where HTI-TriMix, HTI only, or TriMix only electroporated autologous immature DCs from patients were investigated for their antigen-specific immunostimulatory capacity in-vitro. The HTI-TriMix combination was significantly superior to either treatment alone in upregulating the DC maturation markers CD80, CD83, CD86, and CCR7, enhancing TNF-α, IFN-γ, IL2, CCL3 production as well as enhancing DCs capacity to instigate CD4+ and CD8+ proliferation. The findings were in agreement with those in murine model shown by superior antigen-bearing specific cell lysis using TriMix-HTI[207].

Chemokines encoding pDNAs have also been attempted as cancer vaccine adjuvants. For example, CCL4 (macrophage inflammatory protein-1ß, MIP-1ß) targets a broad range of innate and adaptive immune effectors expressing its cognate CCR5 including immature DC, Th1 cells, natural killer cells, and monocytes. Nguyen-Hoai *et al.* compared animal survival, tumor size reduction, and tumor-specific IgG2a titers in a Balb/c Her2/neu+ murine tumor model following vaccination with pDNA encoding Her2/neu, CCL4, or a combination of the two pDNAs, the combination showed superior performance to either pDNAs alone[214]. Comparable results were also demonstrated using pDNA encoding for CCL21, responsible for mobilization of mature DCs to secondary lymphoid organs via their CCR7 receptor[215].
Similar results were obtained using CCL19 encoding pDNA, co-delivered with (ß-galactosidase) encoding pDNA in MCA205 (ß-gal) tumor mouse model. Where CCL19 is a chemokine mainly expressed in secondary lymphoid organs, and also recognized by CCR7. Co-delivery of CCL19 and ß-galactosidase encoding pDNAs similarly to CCL4 co-delivery enhanced overall TH1 polarization compared to either pDNAs alone or the mock vector. The combination also resulted in superior T-cell infiltration into the tumor compared to either pDNAs or a mock vector with subsequently significantly smaller tumor size and higher animal survival rates both short and long term over 60 days and 25 weeks respectively[216].

In conclusion, the aforementioned data highlights the status and value that may lay in genetic adjuvantation approaches, especially alongside the now rising genetic vaccination approaches.

Aim of the thesis

Because mRNA-based vaccines continue to garner more attention as the next generation of vaccines, safe and efficient carrier systems for this class of molecules become increasingly important. Recently, the approval of the first mRNA-based vaccines for human use in the wake of the Covid-19 pandemic marked the fastest vaccine development, deployment, and approval procedure in vaccine history, further solidifying the value of this vaccine class generally as well as in emergency situations.

Yet, some issues such as the requirement for dose sparing, as all the available mRNA-based vaccines have been shown to require booster doses still allow room for improvement. This work aims to investigate the possibility of designing a nanocarrier capable of co-delivering protein-encoding polynucleotide species that can eventually produce a temporally-resolved expression of the encoded proteins by a cell population. This nanocarrier design is aimed at the eventual co-delivery of NA-encoded antigens and adjuvants, expressed by antigen-presenting cells in a time-resolved manner, to maximize vaccine efficacy and safety via proper adjuvant application both in the spatial and temporal sense.

To achieve such a goal, a carrier capable of co-delivering two protein-encoding polynucleotide species with varying expression kinetics was required. Preferably a carrier capable of successfully co-delivering pDNA with an inherent delayed and prolonged-expression pattern and mRNA with a rapid and transient expression pattern.

The design of the nanocarrier also needed to ensure some basic requirements such as:

(1) Nanocarrier's biocompatibility, where preferably bio-compatible, biodegradable matrix formers can be used, and also the use of potentially toxic chemical cross-linkers could be avoided.

(2) Nanocarrier's colloidal stability in challenging media.

(3) The inclusion of components that tend to the varying transfection requirements of both mRNA (strong shielding effects, assisting endosomal escape) and pDNA (assisting nuclear translocation)

(4) A further additional requirement in the nanocarrier's design was the potential to load the NA cargos such that pDNA is core loaded with delayed-release from the system, whereas mRNA is surface loaded, which may further ensure the time resolution of pDNA and mRNA expression.

Chapter II: Thermally Stabilized Coacervate-Based Nanocarrier for Co-delivery of Messenger RNA and Plasmid DNA

Parts of this Chapter have been previously published in

Nasr, S.S.; Lee, S.; Thiyagarajan, D.; Boese, A.; Loretz, B.; Lehr, C.-M. Co-Delivery of mRNA and PDNA Using Thermally Stabilized Coacervate-Based Core-Shell Nanosystems. *Pharm* **2021**, *13*, 1924, doi:10.3390/pharmaceutics13111924.

2.1. Abstract

The present study features a novel technique of gelatin-based nanocarrier fabrication for nucleic acid delivery. The technique dismisses previously used cationization of gelatin or multi-step nanoprecipitation techniques, that eventually rely on chemical crosslinking for particle stabilization. Instead, the reported method relies mainly on the spontaneous ability of gelatin type A and pDNA to electrostatically assemble into nano-dimensional complex coacervates of narrow size distribution. These Gelatin-pDNA complex coacervates are liable to thermal stabilization into nanogels, a previously unused feature for pDNA's gelatin-based nanocarrier fabrication. Modulation of the pDNA: Gelatin mass ratio controls the overall surface charge of the coacervate, which will also be maintained by the resulting nanogel. And hence we opted for preparing negatively charged nanogels that can later be surface-coated by the densely cationic peptide protamine sulfate which further allows additional surface loading with mRNA. The resulting system is characterized for size, size distribution, and particle stability over time before and after protamine coating using dynamic light scattering (DLS), where the thermally stabilized cores gave more stable core-shell systems than the non-stabilized cores. The core-shell morphology was confirmed using TEM. The NA protective capacity of the system was verified using nucleases' challenge followed by agarose gel migration assay, where stabilized system showed an approximately 4-fold increase in densitometric pDNA band intensity to the non-stabilized, while both systems showed a significant enhancement in mRNA cargo stability compared to free mRNA. The unique feature of this system is its capacity to successfully co-transfect murine dendritic cell line DC2.4 with pDNA and mRNA formats of fluorescent reporters simultaneously, showing a transfection efficiency of 61.4%±21.6 for mRNA and 37.6%±19.45 for pDNA, 48 h post-treatment. Meanwhile, a range of established commercial, experimental, and clinical controls failed at successfully co-transfecting DC2.4 in-vitro with both mRNA and pDNA. Given the established differences in expression kinetics of mRNA and pDNA, this system could become instrumental in the time-resolved expression of adjuvants from mRNA and antigens from pDNA within an NA based-vaccine delivery context.

2.2. Introduction

In the past three decades, nucleic acid-based therapies have been constantly gaining momentum toward clinical application. Starting with DNA and followed by various forms of RNA including short-interfering RNA (siRNA), micro-RNA (miRNA), messenger RNA (mRNA), self-amplifying RNA (saRNA) as well as antisense oligonucleotides (ASOs)[217,218] have all shown promise as therapeutics candidates against a range of health problems previously unaddressed by conventional therapeutics. Nucleic acid-based vaccines have been the most advanced research field of nucleic acid-based therapies, with a special focus on mRNA-based vaccines in later years. For years, numerous clinical trials investigated mRNA-based vaccines for influenza H7N9, influenza H10N8, rabies, human metapneumovirus, cytomegalovirus, respiratory syncytial virus, parainfluenza virus 3, and Zika, among others[219]. As for DNA based-vaccines, several had received approval for veterinary use[220].

Nevertheless, until COVID-19 became a global health issue no mRNA, nor DNA-based vaccines had ever made it to clinical approval. Within 10 months of the initial reporting of SARS-CoV-2 as an emerging virus and by September 2020, thirty-five SARS-CoV-2 vaccine candidates were undergoing various phases of clinical trials, while subunit vaccines dominated the race at that time, making up for 30% of the candidates, NA-based vaccines were closely following with an overall contribution of 29% (17% mRNA and 12% DNA)[41]. This highlighted the potential of NAs as a tool for the rapid development and deployment of vaccines in emergency situations. The first SARS-CoV-2 vaccine candidate to move into phase-one clinical trials was mRNA-1273 developed by Moderna[221], a mere 65 days after the publication of the full viral genome by Chinese authorities in January 2020[41]. The FDA approval of mRNA-based vaccines was closely followed by the EMA approval of ChAdOx1-S, featuring a Chimpanzee adenoviral vector delivering DNA encoding for SARS-CoV-2 viral spike protein[222]. As previously detailed in chapter 1, the appeal of such nucleic acid-based vaccines also lies in their ability to produce strong and balanced humoral and cellular immune responses compared to subunit vaccines while avoiding the risks and difficulties associated with the production of live-attenuated, inactivated, and subunit vaccines[20,45,56]. Successful transfection of antigen-presenting cells with a NA vaccine allows them to synthesize the encoded antigenic protein endogenously and subsequently present it on MHC I, which entails a more efficient $CD8^+$ mediated cellular immune response than more conventional vaccines[38,56,66,223].

From a drug delivery point of view, the key advantage of nucleic acids as a drug cargo is the overall uniformity of their physicochemical characteristics, yet simultaneously, the vast diversity of their pharmacological effects. Nevertheless, their delivery remains challenging due to various physical constraints, stability issues, and toxicity of the delivery vehicles[224]. The instability of nucleic acids in the harsh biological environment, as well as their hydrophilic macromolecular nature, demands a protective biocompatible carrier for their delivery. Thus, the successful development of safe and effective prototype delivery

vehicles for such therapeutic moieties is becoming a necessity that can dramatically impact the treatment options for an unlimited number of disorders, as previously detailed in section 1.3. The currently available delivery systems for clinically approved Covid-19 NA-based vaccines being either LNPs for mRNA or adenoviral vectors for DNA have both been reported to evoke allergic reactions in some individuals[225–227]. Viral vector-based carriers have also been reported to induce vector-specific antibodies following the initial dose, which could affect the efficiency of booster doses using the same vector[228–230]. Hence, the availability of viable alternatives for these established carriers can help address the aforementioned concerns when they arise.

Biopolymer-based carrier systems can present a promising alternative alongside the currently available lipid or viral-mediated nucleic acid delivery. Gelatin type A is the acidic denaturation product of collagen, a biopolymer of established and broad pharmaceutical applications. It is an amphiphilic protein, in which the charged portion is predominantly cationic, thus aiding in spontaneous electrostatic assembly upon mixing with anionic nucleic acids, while the hydrophobic portions of its structure aid in particle formation in aqueous media[231]. Being a denatured protein, gelatin possesses low antigenicity, thus rendering it suitable for repeated administration[231–233]. Yet given its low charge density, gelatin's coacervates with NAs can be rather colloidally unstable. Previously, techniques utilizing gelatin for NA delivery relied on either the chemical modification of gelatin into a cationized semi-synthetic polymer, chemically cross-linking the gelatin-NA combination using dialdehydes, or a combination of both techniques [234,235]. Such approaches result in covalently bound NA-protein cross-links which have been reported to pose translational and transcriptional errors in their host cell [236,237]. Electrostatically assembled Gelatin-DNA coacervates, on the other hand, are more synonymous with the physiological NA- protein interaction taking place in various cellular processes[238]. Gelatin-DNA coacervates were previously reported to transform from a coacervate to an irreversible anisotropic nanogel phase when heated above gelatin's helix-coil transition temperature, then cooled below that temperature[239]. Yet to the best of our knowledge that feature has not previously been used for establishing a NA nanocarrier.

In the current study, we aimed to prepare a gelatin-based system for NA delivery without opting for the cationization of gelatin, a two-step nanoprecipitation technique, or a final covalent cross-linking step. Instead, the assembly of a gelatin A-pDNA coacervate was attempted relying solely on the spontaneous electrostatic assembly of these two polyelectrolytes to form a liquid in liquid coacervate system. The resulting coacervate can then be physically cross-linked into a nanogel through thermal cycling above and below the helix coil transition temperature of gelatin. Thus we could for the first time harness a previously un-used feature of this gelatin-pDNA coacervate system to prepare a pDNA nanocarrier. In this context, pDNA can serve a double role in the formulation; both as therapeutic cargo as well as core component and stabilizer. The thermal stabilization of the coacervate core could allow its coating with strongly cationic peptides without discernible core disruption. Protamine sulfate was selected as a cationic coat given its nuclear-translocating properties essential for efficient pDNA transfection[240–242]. Achieving a surface charge reversal from negative to positive upon protamine coating may permit further surface loading of the nanocarrier with mRNA. As an arginine-rich peptide,

protamine is also capable of aiding endosomal escape and successful cytoplasmic delivery of its mRNA cargo[243–245].

In this chapter, the aim was to (i) assess the viability of thermal stabilization of pDNA-gelatin coacervate as a viable physical stabilization technique to formulate a stable nanocarrier for pDNA, (ii) whether this nanocarrier can withstand a strongly cationic coat without disruption, and (iii) following surface loading of mRNA, the system's capability of co-transfecting an immune cell line with the dual NA cargo simultaneously, in comparison to established transfection tools. To assess this dual-loaded core-shell system's potential for delivery and expression of both NAs, the transfection efficiency of the system was measured in murine dendritic cell line DC 2.4.

2.3. Methodology

2.3.1. Materials

Gelatin GELITA® MedellaPro® <=100, porcine gelatin, 228g Bloom, pharmaceutical-grade was purchased from GELITA® Deutschland GmbH, Eberbach, Germany. Protamine sulfate was purchased from Sigma-Aldrich, Darmstadt, Germany. Plasmid DNA encoding AmCyan fluorescent protein (pAmCyan1-C1) was purchased from Clontech Laboratories Inc., Mountain View, CA, USA. Subcloning Efficiency™ DH5α E. coli competent cells were purchased from Invitrogen, Thermo Fisher Scientific, Darmstadt, Germany, Qiagen EndoFree Plasmid Mega Kit was purchased from Qiagen, Hildesheim, Germany. CleanCap® mCherry mRNA was purchased from Tri-Link BioTechnologies LLC, CA, USA. Purified water was obtained from a Milli-Q water purification system (Merck, Millipore) and is referred to as MQ water.

JetMessenger (JetM) and JetPrime (JetP) were purchased from Polyplus-transfection®, Illkirch, France. Branched polyethyleneimine (PEI), M_w~25000 as well as Choletsterol were purchased from Sigma-Aldrich Darmstadt, Germany. Lipofectin was purchased from Invitrogen, Thermo Fisher Scientific, Darmstadt, Germany. DLin-MC3-DMA was purchased from MedChemExpress (New Jersey, USA), DSPE-PEG 2000 and DPPC were a kind gift from Lipoid GmbH (Ludwigshafen, Germany).

Agarose research grade was purchased from Serva®, Heidelberg, Germany. Disodium dihydrate ethylenediamine tetra-acetic acid (EDTA-Na_2) was purchased from Roth GmbH + Co. KG, Karlsruhe, Germany.DNA Ladder 250-10000 bp was purchased from PEQLAB Biotech GmbH, Erlangen, Germany. Ethidium bromide 10 mg mL^{-1} was purchased from Sigma-Aldrich, Darmstadt, Germany. Live/dead fixable stain (568/583) was purchased from PromoCell GmbH, Heidelberg, Germany. Quant-iT ™ PicoGreen ™ dsDNA Assay Kit and RiboGreen™ RNA Assay-Kit, DNase I, DNase I buffer, 50 mM EDTA, RNase A, DNA loading dye (6x), and Ribolock were purchased from Thermo Fisher Scientific, Darmstadt, Germany. Bovine collagen type I solution, Purecol was purchased from CellSystems, Troisdorf, Germany.

Murine dendritic cell line DC2.4 was purchased from Millipore Corporation, California, USA. Cells RMPI-1640, Fetal Calf Serum (FCS), non-essential amino acids (NEAA,100X), and HEPES buffer solution(1M) were all purchased from Gibco, Thermo Fisher Scientific, Darmstadt, Germany.
β-mercaptoethanol 100X was purchased from Merck, Darmstadt, Germany

2.3.2. Plasmid propagation, extraction, and quality assessment

Fluorescent reporter protein-encoding plasmid DNA (pAmCyan1) was used as a model pDNA molecule in the experiments throughout this chapter. pAmCyan1 was transformed into Subcloning Efficiency™ DH5α E. coli competent cells (Invitrogen, Thermo Fisher Scientific, Darmstadt, Germany). Briefly, 100 ng pAmCyan1 was gently mixed with 50 µL pre-thawed cell suspension. The mixture was then incubated on ice for 30 min, following which the cells were heat-shocked at 42˚C for 30 sec and immediately returned to the ice bath for 2 more minutes. Pre-warmed, antibiotic-free LB-Broth (950 µL) was then added to the transformed cells, which were then allowed to recover for 1hr at 37 ˚C while shaking at 225 RPM. Either 20 or 200 µL of this transformed cell suspension was then streaked on pre-warmed Kanamycin resistant selective LB Agar, and incubated overnight at 37 ˚C, 5% CO_2.

Pre-cultures were set using single colonies that were transferred to selective 1mL LB-Broth containing Kanamycin (50 µg/mL) and incubated for 1 h at 37, 225 RPM. The pre-cultures showing the highest optical density were later transferred to 500 mL of the same medium and further incubated for 12 h at 37 ˚C, 5% CO_2, shaking at 225 RPM. Following this cells were collected from 500 mL culture suspension via centrifugation at 300 g for 20 min at 4 ˚C and pAmCyan1 was extracted from the pellet using EndoFree Plasmid Mega Kit (Qiagen, Hildesheim, Germany) according to the manufacturer's protocol.

The resulting plasmid was spectrophotometrically assessed for yield and purity using NanoDrop™ 2000 (Thermo Fisher Scientific, Darmstadt, Germany). Two restriction enzyme digests followed by agarose gel electrophoresis were applied to map the plasmid product and confirm its identity. Where 0.5 µg of pAmCyan1 was incubated with 25 U of either StuI or ApaI for 1hr at 37 ˚C, afterwards restriction enzyme(s) were inactivated by heating the reaction mixture at 80 ˚C for 10 min. Samples were then run on a 1.3% Agarose gel, at 90 mV for 90 mins and visualized under UV light (Fusion FX7 imaging system, Peqlab, Erlangen, Germany).

2.3.3. Screening of gelatin-pDNA mass ratio to determine the optimal range for the coacervate formation

Gelatin Type A solutions of various concentrations **(Table 2)** were prepared in MQ water, by warming the dispersion at 55 ˚C. The resulting solutions were then mixed with 100 µg/mL aqueous solution of pDNA (pAmCyan1), in a ratio of 1:1 (v/v) via vortexing. These mixtures with different gelatin: pDNA mass ratios were then transfected to a 96-well plate and spectrophotometrically screened for changes in Transmittance (T%) at 450 nm.

The different mixtures were also assessed for changes in their zeta-potential (mV) using Dynamic light scattering (DLS) (Nano-ZS, Malvern Instruments, Worcestershire, U.K.), in the presence of free pDNA as a control. Nano-ZS. utilized at 4 mW He−Ne laser at a wavelength of 633 nm. Detection conditions were set to a backscattering angle of 173° at 25 °C, these settings were maintained throughout the study. Data were reported as intensity distribution (%) against particle size (nm).

Table 2. *Gelatin:pDNA mass ratios screened to determine optimal range for complex coacervate formation*

Gelatin concentration [mg mL^{-1}]	pDNA **concentration [µg mL^{-1}]**	**Gelatin : pDNA ratio[w/w]**
20	100	200:1
10	100	100:1
2	100	20:1
0.2	100	2:1
0.1	100	1:1

2.3.4. Gelatin-pDNA coacervate based particle core (CoAc) assembly

Following the selection of the gelatin: pDNA mass ratios range of interest for a stable complex coacervate formation, gelatin–pDNA coacervates (CoAc) were electrostatically assembled as previously described in MQ water using gelatin type A solutions with different concentrations (10 mg mL^{-1}, 7 mg mL^{-1}, 5 mg mL^{-1}, 3 mg mL^{-1}, 1 mg mL$^{-1,}$ and 0.1 mg mL^{-1}) that were mixed with pAmCyan (100 µg mL^{-1}) in a ratio of 1:1 *v/v* at 37 °C **(Table 3).** The corresponding gelatin:pDNA mass ratios are depicted in **(Table 3)** and the nomenclature of the different coacervates was denoted as CoAc$_{\#}$, where (#) is equivalent to the gelatin: pDNA mass ratio. Simultaneously, the optimum mixing temperature was also investigated by mixing 10 mg mL^{-1} gelatin solution with 100 µg·mL^{-1} pAmCyan1 solution at 1:1 *v/v*, at 3 varying temperatures of 23°C,37°C, and 55 °C. The resulting CoAcs were then screened for particle size, particle size distribution, and zeta-potential using DLS (Nano-ZS, Malvern Instruments, Worcestershire, U.K.).

Table 3. *Nomenclature and composition of gelatin-pDNA complex coacervates assembled at varying mass ratios.*

Sample name	**Gelatin concentration [mg mL^{-1}]**	**pDNA concentration [µg·mL^{-1}]**	**Gelatin to pDNA Ratio [*w/w*]**	**Protamine sulfate concentration [mg mL^{-1}]**	**Protamine sulfate to gelatin Ratio [*w/w*]**
CoAc$_{100}$	10	100	100:1	–	–
CoAc$_{70}$	7	100	70:1	–	–

$CoAc_{50}$	5	100	50:1	–	–
$CoAc_{30}$ *	3	100	30:1	–	–
$CoAc_{20}$	2	100	20:1	–	–
$CoAc_{1}$	0.1	100	1:1	–	–
TS-CoAc **	3	100	30:1	–	–
P-CoAc***	3	100	30:1	0.3	1:5
P-TS-CoAc**,***	3	100	30:1	0.3	1:5

* $CoAc_{30}$ was selected for further experiments, referred to as CoAc without a subsequent numerical value throughout the text; ** TS-CoAc is $CoAc_{30}$ exposed to four heating-cooling cycles; *** "P-'' stands for protamine sulfate coating.

2.3.5. Thermal stabilization of gelatin-pDNA coacervate system into anisotropic nanogel

The coacervate core with gelatin: pDNA mass ratio of 30:1 ($CoAc_{30}$) was eventually selected as the thermal stabilization candidate of choice due to its acceptable size, PDI, and most importantly overall negative zeta-potential. $CoAc_{30}$ would hence be simply referred to as CoAc throughout the text. To thermally stabilize CoAc, it was subjected to four alternating heating-cooling cycles at 55°C± 0.5 for 30 mins, then 0± 0.5 for 5 mins. Throughout the text, CoAc that has been subjected to four complete heating-cooling cycles are referred to as thermally-stabilized coacervates (TS-CoAc).

2.3.6 Assessment of the validity of gelatin-pDNA CoAc assembly and thermal stabilization for varying plasmid sizes in nanometric dimensions using DLS

Three plasmids other than pAmCyan1 (4701 bp), namely pUC19, pCCL4, pCCR7 which possess different sizes of 2686 bp,6380 bp, and 7240 bp, respectively were used as controls for TS-CoAc preparation instead of pAmCyan1. The experiment aimed to investigate the validity of the previously described CoAc assembly and stabilization procedure for plasmids of varying sizes. $CoAc_{30}$ of the three aforementioned plasmids were prepared as previously described and subjected to four thermal cycles to produce the corresponding TS-CoAc. Both CoAc and TS-CoAc were then characterized using DLS for particle size and PDI.

2.3.7. Assessment of comparative colloidal stability of CoAc and TS-CoAc in cell culture medium using Nanoparticle Tracking Analysis (NTA)

To assess the impact of physiologically relevant media on the colloidal stability of thermally stabilized vs non-stabilized CoAc and TS-CoAc prepared using pAmCyan1 were incubated with cell culture medium (RPMI-1640) in a ratio of (1:10 v/v) at 37 °C for 4 h. At zero time and the 4h time-point samples were withdrawn and diluted 100 folds in MQ to quench any ion-induced colloidal destabilization of the system. These samples were then analyzed for particle count using NTA (NanoSight LM10, Malvern Instruments, Worcestershire, U.K.), the analysis span 3 videos, 30 seconds each, at a camera level of 14 and a detection threshold set to 5. Data were analyzed using Nanosight 3.3 software.

2.3.8. Assessment of thermal stabilization on gelatin-pDNA coacervate using circular dichroism (CD)

A Gelatin solution (3 mg mL^{-1}) prepared by dissolving gelatin in MQ water at 55 °C was used to prepare CoAc with pAmCyna1, a portion of which was further used to prepare TS-CoAc. Either the original gelatin stock, CoAc, or TS-CoAc were placed in a 0.1-cm path-length quartz cell and brought to a temperature of 37 °C then analyzed using Jasco 810 spectropolarimeter (Jasco, Tokyo, Japan). MQ water was used as blank. Measurements were obtained from the average of 15 measurement rounds per sample after normalization to MQ water.

2.3.9. Shell Deposition and mRNA Loading

To prepare protamine sulfate coated CoAc and TS-CoAc, $CoAc_{30}$ or TS-$CoAc_{30}$ prepared using pAmCyan1 were introduced to one of two inlets of a microfluidic assembly meander chip, against protamine sulfate solution (0.3 mg mL^{-1}) from the other inlet, at 2 $mL.min^{-1}$ total flow rate and in a ratio of 1:1 v/v. the obtained protamine coated coacervate or protamine coated thermally stabilized coacervate (P-TS-CoAc) were stored at 4°C and characterized using DLS for particle size and PDI over three weeks. Samples concentrations were (1550 µg mL^{-1}) for non-coated particles and (925 µg. mL^{-1}) for protamine coated particles. Particle size is given as an intensity-based z-average.

2.3.10. Morphological assessment of nanocarrier using Transmission Electron Microscopy (TEM)

Four variations of the prepared nanocarriers, namely CoAc, TS-CoAc, P-CoAc, and P-TS-CoAc were morphologically assessed without staining using transmission electron microscopy (TEM). Briefly, 10 µL containing either 775 µg mL−1 of CoAc/TS-CoAc, or 925 µg mL−1 of P-CoAC /P-TS-CoAc were dried overnight on a copper grid (S160-4, Plano GmbH, Wetzlar, Germany) in a desiccator, following which samples were visualized under an accelerating voltage of 200 kV using TEM (JEM 2011, JEOL, St Andrews, UK). The overall particle assembly procedure is depicted in (**Figure 3**).

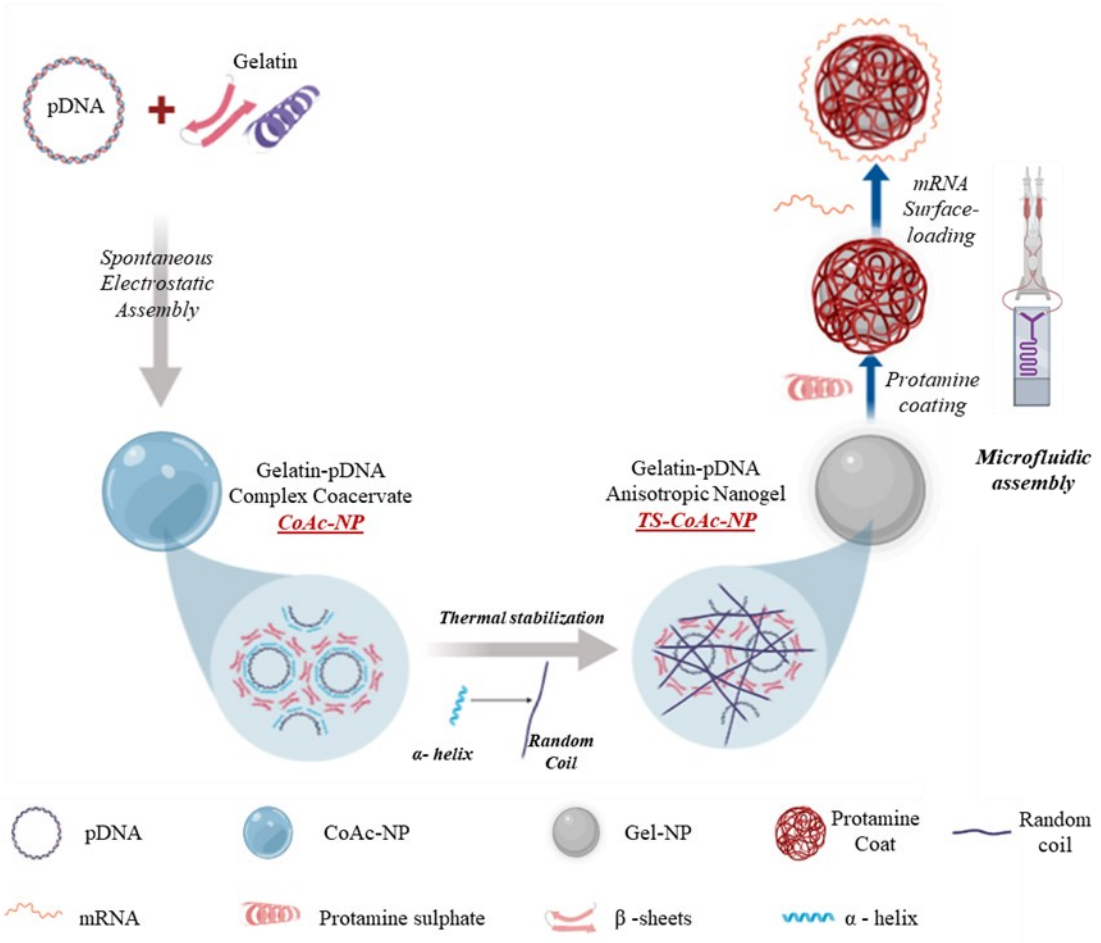

Figure 3. *The summarized preparation procedure of gelatin-pDNA coacervate (CoAc), thermally stabilized gelatin-pDNA coacervate (TS-CoAc), and protamine-coated thermally-stabilized gelatin-pDNA coacervate (P-TS-CoAc), with a depiction of the proposed mechanism of stabilization of CoAc into TS-CoAc thermally.P-CoAc is prepared via direct mixing of CoAc and protamine sulfate into a microfluidic coating system without thermal stabilization of CoAc.*

2.3.11. Assessment of entrapment efficiency (EE%), loading efficiency (LE%), and numeric molecular capacity per nanocarrier using PicoGreen and RiboGreen Assays

The thermally stabilized protamine coated core-shell particles (P-TS-CoAc) could be surface loaded surface-loaded with 1 µg mCherry per 170 µg of particles, mixed by simple pipetting to a final pDNA: mRNA mass ratio of 5:1 per particle. mRNA-loaded particles were allowed to stand for 15 minutes before further processing or application. The colloidal stability of this quaternary system, mRNA loaded P-TS-CoAc was followed using DLS throughout one week of storage at 4°C. Whereas the inherent instability of the P-CoAc did not allow for stable surface loading with mRNA.

Entrapment efficiency, loading efficiency, and the number of NA molecules per particle were determined for pDNA on P-TS-CoAc and P-CoAc, whereas for mRNA it was determined only for P-TS-CoAc due to the aforementioned instability of P-CoAc. This was performed by analyzing the mRNA or pDNA content of particle suspension supernatant obtained following 2h of ultracentrifugation at 58,000× *g*, 4 °C. Analysis was performed using PicoGreen and RiboGreen assays for pAmCyan1 and mCherry, respectively. Data were normalized to equivalent amounts of free pAmCyan or mCherry subjected to the same dilutions and ultracentrifugation conditions as the samples. Calibration curves were also established using pAmCyan1 for PicoGreen assay with a linearity range of (0.3-1000 $ng.mL^{-1}$), and mCherry for RiboGreen with a higher range of 1000-20 $ng.mL^{-1}$, and a lower range of 50-1 $ng.mL^{-1}$.

Using the method described by Zagato *et al.*[246], the number of mCherry and pAmCyan molecules per particle could be determined by the knowledge of the EE% determined using PicoGreen and RiboGreen assays and particle concentration ($particles.mL^{-1}$) in suspension determined using nanoparticle tracking analysis (NTA).

2.3.12. Assessment of NA cargo shielding by P-TS-CoAc and P-CoAc using agarose gel electrophoresis

Dnase I and Rnase A were used as nuclease(s) challenge against P-TS-CoAc and P-CoAc loaded mCherry and pAmCyan1, following which both NAs were released from the particle and subjected to gel migration assay to assess their integrity against equivalent masses of (1) intact mCherry and pAmCyan1 and (2) naked mCherry and pAmCyan1 subjected to a similar digestion procedure as controls. Briefly, mRNA-loaded P-TS-CoAc or P-CoAc (NA load of 1.5 µg mRNA and 7.5 µg pDNA) were incubated with 0.008 $U.mL^{-1}$ Dnase I and 0.027 µg mL−1 Rnase A (both Sigma-Aldrich, Darmstadt, Germany) in Dnase I working buffer at 37 °C for 30 and 60 min. following this, 20 µL were sampled from all reaction mixtures and its nucleases' content was quenched using 3 µL 50 mM EDTA for DNase I and 1 µL Ribolock for Rnase A (both Sigma-Aldrich, Darmstadt,

Germany), the nucleic acids were then released from P-TS-CoAc and P-CoAc via digestion with Trypsin (30 µL, 1.17 mg mL^{-1}) for 30 min at 37 °C, followed by addition of high molecular weight Heparin (HMWH)(10 µL, 300 mg mL^{-1}). Ethidium bromide (0.3 $\mu g \cdot mL^{-1}$) (Sigma-Aldrich, Darmstadt, Germany) containing agarose gel (1.3% *w/v*) (Serva, Heidelberg, Germany) was used to run and visualize the samples in TBE buffer (1×) at 90 mV for 90 min. followed by gel visualization under UV light (Fusion FX7 imaging system, Peqlab, Erlangen, Germany).

For further assessment of the difference in pDNA shielding effects between thermally stabilized and non-stabilized cores in a more challenging and physiologically relevant medium CoAc and TS-CoAc sample volumes equivalent to 3 µg pDNA were incubated with 10% FCS in HBSS for 3 h at 37 °C. Eventually, the serum nucleases' activity was then quenched using EDTA (150 µL, 50 mM). pDNA cargo was released via subsequent treatment with Trypsin (30 µL, 1.17 mg mL^{-1}) for 150 min at 37 °C, followed by HMWH (30 µL, 30 mg mL−1). Samples were run on a 0.7% *w/v* agarose gel for 60 min at 60 mV. Data were normalized to the equivalent amount of intact supercoiled pDNA as a control.
For both experiments, densitometric assessment of sample and control bands was performed using ImageJ-1.53k (National Institutes of Health, Bethesda, Maryland, USA) where sample bands were normalized to the corresponding intact controls.

2.3.13. In-vitro biological assessment of cytotoxicity of P-TS-CoAc in murine dendritic cell line DC2.4

Using dead fixable stain 568/583 (PromoCell GmbH, Heidelberg, Germany), the cytotoxicities of three concentrations of P-TS-CoAc were assessed in murine dendritic cell line DC2.4, Against untreated cells and heat-killed cells as controls. The used particles were not surface loaded with mRNA to exclude the interference of the spectral data pertinent to mCherry expression with that of the dead fixable stain. The three investigated P-TS-CoAc concentrations were (340 µg mL^{-1}, 170 µg mL^{-1}, or 85 µg mL^{-1}), and were equivalent to a pAMcyan1 cargo of 10, 5, and 2.5 µg respectively. In brief, DC2.4 (passages 10 to 12) were seeded in 24 well plates at a density of 50,000 cells per well, in a medium consisting of RPMI-1640 supplemented with FCS (10% *v/v*), HEPES (1%), NEAA (1%), β-mercaptoethanol (0.0054%). After 48 h incubation at 5% CO_2 and 37°C DC2.4 were approximately 80% confluent and were treated with either controls or samples. Cells were subjected to P-TS-CoAc treatment for 6 h at 5% CO_2 and 37°C under shaking at 250 RPM, following which the samples were removed. Cells were then washed twice with HBSS, then detached using 100 µL of Trypsin-EDTA, followed by the addition of 900 µL 2% FCS in HBSS. The cell suspension was then centrifuged at 4 °C and 300× *g* for 5 min, the pellet was rewashed in 1 mL HBSS then re-suspended, stained with dead fixable stain 568/583 (PromoCell GmbH, Heidelberg, Germany) according to the manufacturer's protocol and fixed in paraformaldehyde (4% *w/v*). The heat-killed control was prepared from untreated cells following pellet collection and washing by heating at 70 °C for 20 mins.

Dead fixable stain 568/583 exclusively stains dead cells with cell membrane-impermeable amine-reactive peptides, detectable on the PE-emission filter. The percentage of dead cells could be measured on a flow cytometer (BD LSRFortessa^{TM} Cell Analyzer Biosciences, Heidelberg, Germany) on the PE channel. Data were processed using Flowjo version 10.6.1. Cell viability was calculated according to **(Equation-1).**

$$\text{Cell viability (\%)} = \left(\frac{\text{total cell number} - \text{PE positive cell number}}{\text{total cell number}}\right) \times 100 \quad (1)$$

2.3.14. In-vitro biological assessment of transfection performance of P-TS-CoAc and P-CoAc against established clinical, experimental, and commercial controls in murine dendritic cell line DC2.4

Transfection efficiencies of mCherry and pAmCyan1 co-loaded P-TS-CoAc and P-CoAc were assessed in DC2.4 (passages 6 to 8). Cells were seeded in 24 well plates and allowed to reach approximately 80% confluency within 48h as previously described. Samples were either P-CoAc or P-TS-CoAc, at a concentration of 170 µg per well, equivalent to a dose of 1 µg mCherry and 5 µg pAmCyan. Untreated cells and cells treated with either naked mRNA or pDNA were used as negative controls.

Meanwhile, a range of positive controls was investigated against P-TS-CoAc and P-CoAc for their co-transfectional capacity. These positive controls included commercial transfections reagent such as (1) JetMessenger and JetPrime for mRNA and pDNA, respectively, in the single transfection mode, in which each transfection reagent was used with its NA of specialization according to the manufacturer's protocols (2) JetM and JetP as double transfection tools in which both reagents were mixed with mRNA and pDNA doses equivalent to those present in P-TS-CoAc/P-CoAc simultaneously and used as a double transfection control. (3) Lipofectin was used as a double transfection control with equivalent NA doses to P-TS-CoAc and P-CoAc. As an experimental positive control (4) High M_W branched polyethyleneimine (PEI) is a widely used polymer given its high transfection efficacy, despite its cytotoxicity. Thus, PEI-NPs were prepared using PEI: pDNA: mRNA mass ratio equivalent to the protamine sulfate: pDNA: mRNA mass ratio of 30:5:1 originally present in TS-CoAc. As a clinically relevant control, LNPs adapted from the current standard of mRNA/siRNA delivery were prepared. Briefly, an aqueous solution of mRNA and pDNA in a mass ratio of 1:5 (pH = 4) was mixed with an ethanolic solution of DLin-MC3-DMA, DPPC, Cholesterol, and DSPE-PEG2000, in molar ratios of 50:10:38.5:1.5 and a final N/P ratio of 6 [247]. As an internal control, a protamine sulfate solution (0.3 mg mL−1) was used to formulate a protamine sulfate coacervate with pDNA, to which mRNA was added immediately before cell treatment, in the same pDNA: mRNA mass ratio used for either P-TS-CoAc or P-CoAc. All the aforementioned treatments and

controls were incubated with the cells for 6 h at 5% CO_2 and 37°C under shaking at 250 RPM. Then samples were removed and replaced with fresh medium and cells were further incubated for 48 h. Cell harvesting was performed as previously described for the cytotoxicity assay with the exclusion of the dead staining step. Transfection efficiency was flow-cytometrically assessed (BD LSRFortessa^{TM} Cell Analyzer Biosciences, Heidelberg, Germany), using the PE-Texas red channel for mCherry and AmCyan channel for pAmCyan1. Flowjo version 10.6.1 was used for data processing.

2.3.15. Microscopical assessment of co-transfection using P-TS-CoAc and P-CoAc Confocal Laser Scanning Microscopy (CLSM)

For visualization and comparison of the transfection patterns of DC2.4 using P-TS-CoAc and P-CoAc, cells were seeded in 8 well glass bottom µ-slide (Ibidi, Gräfelfing, Germany), that has been coated with 1 mg/mL bovine collagen type I solution, Purecol (CellSystems, Troisdorf, Germany), at 25,000 cells/well. Cells were further allowed 48h to reach 80% confluency. Cells were treated with either (1) mCherry loaded P-TS-CoAc, (2) mCherry loaded P-CoAc, (3) JetM-mCherry combination (4) JetP-pAmCyan1 combination. The cell treatment procedure was performed as previously described. 48h following treatment and immediately before visualization, the cells were washed twice using HBSS and fixed for 5 min with 4% (*v/v*) paraformaldehyde (PFA; Electron Microscopy Sciences) in HBSS at room temperature. Cells were then mounted and stored at 4 °C for 30 mins before CLSM analysis (Leica TCS SP8, Leica Microsystems, Mannheim, Germany). Image acquisition was conducted on a Leica TCS SP8 confocal imaging microscope with a 25× water immersion objective (Fluotar VISIR 25×/0.95) at 1024 × 1024 resolution. For AmCyan, fluorescence was detected between 495–550 nm (excited at 405 nm; 24% laser intensity), for mCherry, fluorescence was detected between 683–784 nm (excited at 561 nm; 10% laser intensity), both using a HyD detector. Images were then processed with the Leica Application Suite (LAS) X software.

2.3.16. Statistical Analysis

Graph Pad Prism 8 for Windows (Version 8.01, GraphPad Software Inc.) was used for data analysis. Data are presented as the mean of individual values (generally 3–9 samples), and the standard deviation indicated by the error bars. (N) refers to the number of experiments, (n) refers to the number of samples per experiment. One-way ANOVA was performed for all test samples, and Tukey's post hoc test was used to assess inter-group differences. Data were considered statistically significant at a level of significance of $p < 0.05$ (* $p < 0.05$, ** $p < 0.01$, *** $p < 0.001$ and **** $p < 0.0001$).

2.4. Results and Discussion

2.4.1. identity and quality of in-house propagated plasmid

Spectrophotometric assessment of in-house propagated pAmCyan1 showed a yield of 2.6 mg as opposed to the expected 2.5 mg outcome of the Qiagen EndoFree Plasmid Mega Kit. The yielded pAmCyan1 also showed acceptable 260/280 and 260/230 ratios of 1.85 and 2.15 respectively, **(Table 4),** indicative of the absence of contaminants' content above the acceptable limits. Generally 260/230 ratios < 2.2 indicate the presence of unacceptably high phenol, glycogen, or carbohydrate contaminants which are common components used in extraction procedures. On the other hand, a 260/280 ratio < 1.8 may indicate protein or phenol contamination[248].

Table 4. *Spectrophotometric assessment of pAmCyan1 product quality*

Yield (mg)	260/ 280	260/230
2.62	1.85	2.15

Restriction enzyme mapping assay using StuI confirmed the identity of the pAmCyan1 product where two bands of approximately 1600 and 3000 bp could be visualized on the gel which is in line with the expected StuI digestion products **(Figure 4)**.

2.4.2. determination of gelatin-pDNA mass ratio coacervation range

Turbidimetric assessment of gelatin-pAmCyan1 mixtures spanning a range of mass ratios from 0:1 up to 200:1 gelatin to pAmCyan1 was carried out. The aim was to explore the useful mixing ratios range for gelatin-pDNA coacervate formation. Turbidimetric data showed a sharp increase in the light scattering of gelatin:pDNA ratios at 20:1 that plateaued up to 200:1 **(Figure 5-a)**. The Zeta-potential of coacervates approached neutrality between 20:1 and 100:1, also another indication of coacervate formation **(Figure 5-b).** Gel migration assay showed that gelatin:pAmCyan1 coacervates assembled in MQ water could fully bind and prevent migration of the plasmid starting from as low as 20:1 Gelatin: pAmCyan1, and even partially retard pAmCyan1 migration at a ratio of 1:1 **(Figure 5-c).** Based on this

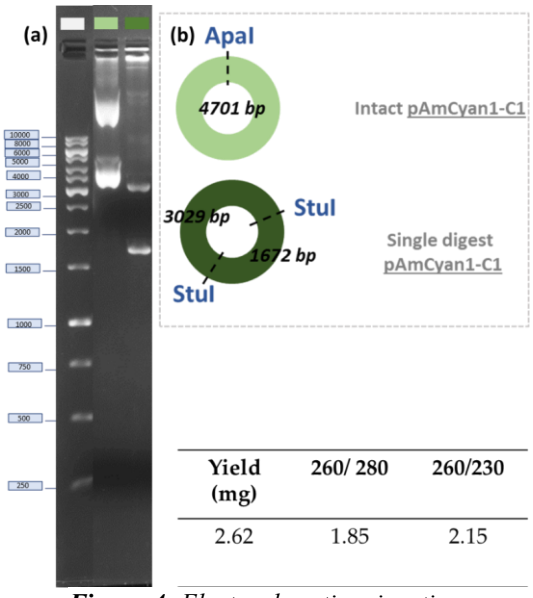

Figure 4. *Electrophoretic migration assay of in-house propagated pAmCyan1 using restriction enzyme mapping for product identification (a)Agarose gel migration assay of ApaI and StuI digested pAmCyan1 (b) expected digestion patterns of pAmCyan1 using ApaI and StuI*

data the following gelatin:pAmCyan1 mass ratios 100:1, 70:1, 50:1, 30:1, and 1:1 were selected for further screening using DLS for their capacity to form coacervates with a size below 250 nm, a PDI< 0.2, and overall negative zeta-potential.

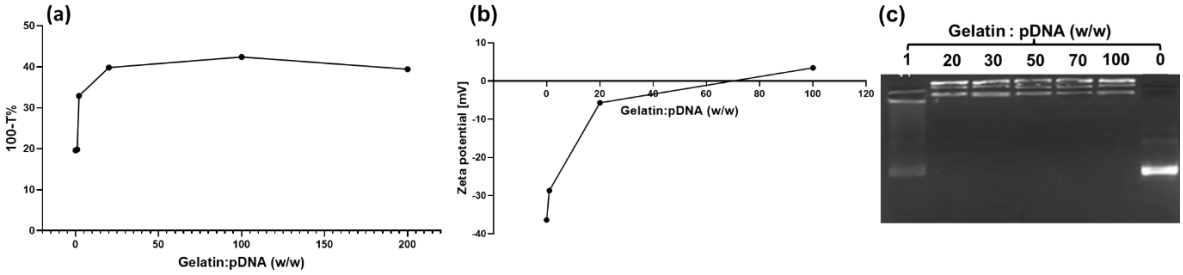

Figure 5. *(a)Turbidemtric Analysis, T% represents the percentage of transmitted light, y-axis depicting 100-T% represents % of scattered light (b)zeta-potential screening, and (c)gel retardation assay of gelatin-pAmCyan1 coacervate candidates at different mass ratios.*

2.4.3. optimal conditions for assembly of Gelatin-pDNA complex coacervation based particle core (CoAc)

Based on the preliminary screening of coacervation mass ratios, pAmCyan (pDNA) and gelatin were assembled into coacervates via electrostatic interaction in Milli-Q purified water. The gelatin to pDNA (pAmCyan1) mass ratios in these coacervates were varied between the five aforementioned ratios of 100:1, 70:1, 50:1, 30:1, 20:1, and 1:1 w/w, and the results of their particle size, PDI, and zeta-potential are shown in (**Figure 6).** Gelatin to pDNA mass ratios of 30:1 ($CoAc_{30}$) or 70:1 ($CoAc_{70}$) formed significantly smaller coacervates possessing diameters of (170 nm and 151 nm, respectively) as well as smaller PDIs (0.17 and 0.21, respectively) in comparison to higher or lower mass ratios **(Figure 6-c, d)**. $CoAc_{30}$ and $CoAc_{70}$ also showed either slightly negative (-5.5 mV) or positive (1.8 mV) zeta-potentials, respectively.

Meanwhile, $CoAc_{50}$ showed a zeta-potential of almost zero (**Figure 6-b)**. Interestingly, the intermediate-mass ratio of 50:1 ($CoAc_{50}$) displayed the largest particle diameter (1772 nm) and a PDI of 0.52 (**Figure 6-c, d)** with a zeta-potential approaching zero.

The coacervation conditions (MQ water, pH=6.2, 37°C) that were used for gelatin type A (Bloom number 228) and pAmCyan1 (4.7 kbp) assembly, were provided the three coacervates with the smallest zeta-potentials at gelatin to pDNA mass ratios of 30:1, 50:1, and 70:1. Above and below these ratios, coacervates of higher zeta-potential were obtained. This could be resorted to the presence of a surplus of the positively charged gelatin or negatively charged pDNA in the coacervates, and hence the existence of repulsive forces between the similarly charged predominant polyion molecules. These repulsive forces within the coacervate lead to a reduction in its packing density of storage modulus, which also accounts for the observed increase in particle size and PDI $CoAc_1$, $CoAc_{20}$, and $CoAc_{100}$ compared to $CoAc_{30}$ and $CoAc_{70}$.This data agrees with previous reports by Arfin *et al.* [249]. $CoAc_{30}$ and $CoAc_{70}$, being slightly overcharged coacervates, despite not having lower packing densities and storage moduli, remain more kinetically stable by their higher

surface charge than perfect coacervates formed at the point of absolute charge neutralization ($CoAc_{50}$). Such absolute or perfect coacervates, on the other hand, are more liable to aggregation and colloidal instability simply due to their near-neutral surfaces[250]. This accounts for the acceptable particle sizes and PDIs of $CoAc_{30}$ and $CoAc_{70}$ compared to $CoAc_{50}$.

Upon attempting to mix gelatin and pDNA at different temperatures, a pronounced impact of gelatin-pDNA mixing temperature on the particle size and the PDI of the product could be observed. $CoAc_{100}$ assembled at 37°C showed a smaller particle diameter of 190 nm and PDI of 0.26 compared to $CoAc_{100}$ assembled at 55°C or 23°C **(Figure 6-c,d).** The observed impact of temperature on CoAc is relevant to the data previously presented by Burgress *et al.* [251]. Given the helical conformation possessed by both gelatin and pDNA in aqueous media below 40°C with persistence lengths of 10 nm and 50 nm, respectively[252,253], factors that can alter the proximity in persistence length values can also impact particle size and PDI. When two polyions undergo complexation, the smaller the persistence length, the higher the chain flexibility of the two polyions and hence the better interaction between them[253]. DNA's persistence length has been reported to be inversely proportional to solution temperature[254]. We thus assume that pDNA would have a smaller persistence length at 37°C than it does at 23°C, increasing the proximity between the persistence lengths of gelatin and pDNA chains and thus the proximity of their interaction at 37°C compared to 23°C. This could explain why $CoAc_{100}$ assembled at 37°C had a smaller size and PDI compared to that formed at 23°C. $CoAc_{100}$ assembled at 55°C possessed significantly higher PDI and much larger particle size than those assembled at 37°C and 23°C. At 55°C, which exceeds the helix-coil transition temperature of gelatin[255], gelatin loses its helical structure displaying a random coil conformation, leading to what we assume to be a simultaneous loss of the helical synonymity of gelatin and pDNA. Eventually, a coacervate formed between gelatin's random coil and pDNA's helix at 55°C was much less compact than the coacervates formed between pDNA's and gelatin's helices at 37°C and 23°C.

In conclusion, the CoAc assembly conditions were optimized at a gelatin to pDNA mass ratio of 30:1 and a mixing temperature of 37°C, as these conditions gave rise to the smallest particle size and PDI, as well as a slightly negative zeta-potential. Hence, such assembly conditions were adopted for all subsequent experiments. Such conditions were also successfully applied to varying plasmid sizes and could formulate successful CoAc and TS-CoAc with plasmids ranging in size from 2.6 to 7.2 Kbp (**Figure 7**).

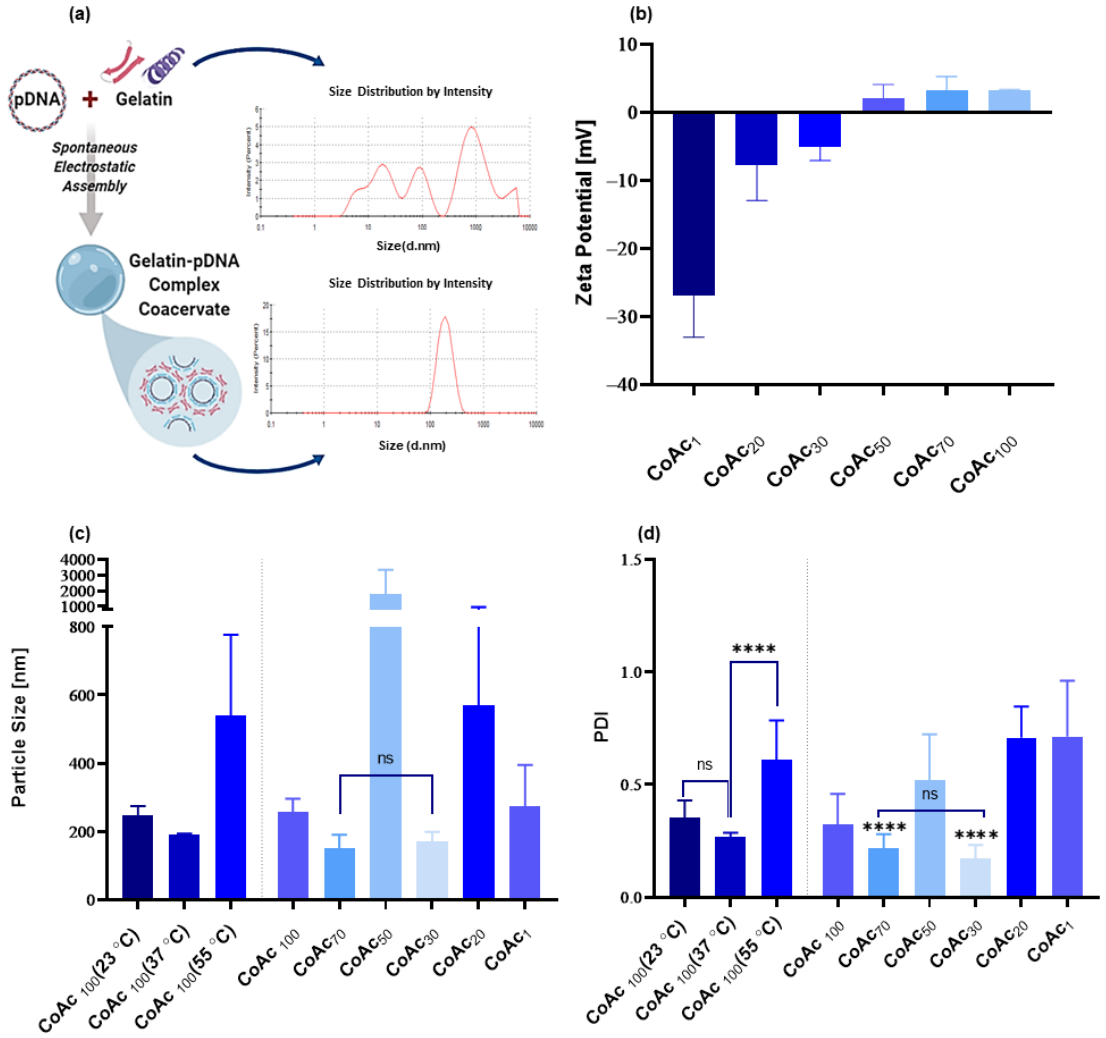

Figure 6. *Assessing the impact of gelatin: pAmCyan (a) coacervate assembly at mass ratios (of 100, 70, 50, 30, 20, and 1) on product's (b) zeta-potential(mV) (N=2, n=2), (c) particle size (nm) (N=3, n=3) and (d) PDI (N=3, n=3). Impact of assembly temperature (at 23, 37, and 55°C) was also assessed for (c) particle size (nm) (N=3, n=3) and (d) PDI (N=3, n=3). Data presented as mean with error bars indicating SD. Statistical significance indicates that present between CoAc $_{70}$ and CoAc $_{30}$ and other CoAcs. **** $p <$ 0.0001; ns = not significant.*

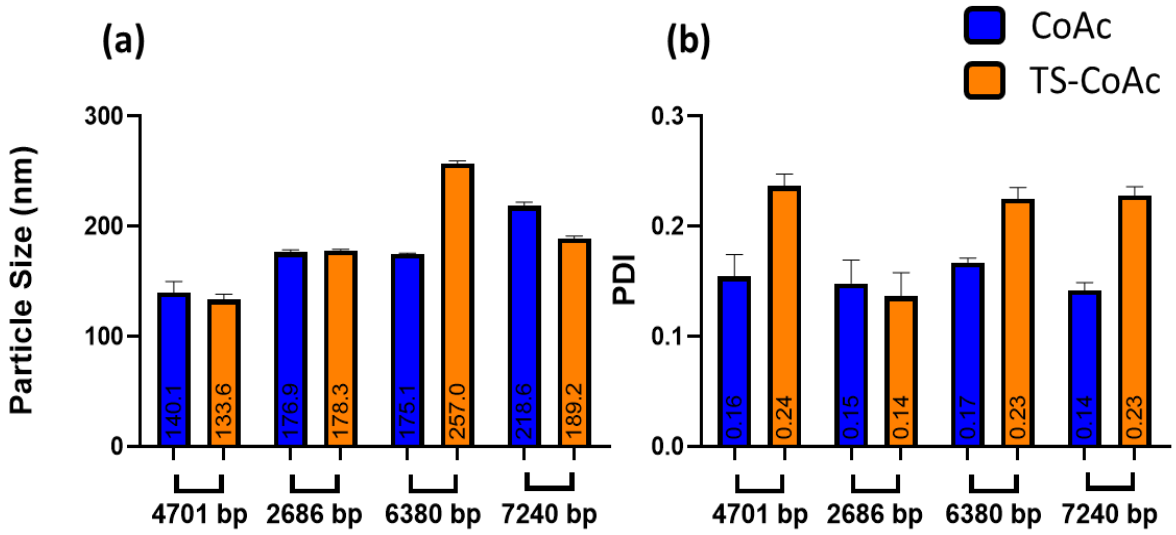

Figure 7. *DLS assessment of* ***(a)*** *particle size and* ***(b)*** *PDI of CoAc and TS-CoAc assembled using varying pDNA sizes at gelatin to pDNA mass ratio of 30:1.*

2.4.4. Impact of thermal stabilization of gelatin-pDNA coacervate system into anisotropic nanogel on its colloidal stability in cell culture medium

$CoAc_{30}$ was thermally stabilized via four subsequent heating-cooling cycles to form TS-CoAc, which led to a significant enhancement in the system's colloidal stability. Superior colloidal stability of TS-CoAc relative to CoAc could be demonstrated as a function of particle count (particle.mL^{-1}) using NTA **(Figure 8-a).** Both TS-CoAc and CoAc were incubated for 4h incubation in RPMI-1640, and their particle count was analyzed at 0h and 4h using NTA. CoAc dropped by one order of magnitude from 4.76 *10^{11} particles.mL^{-1} to 3.93 *10^{10} particles.mL^{-1}. Meanwhile, TS-CoAc dropped by 3-fold only from 2.9 *10^{11} particles.mL^{-1} to 1.1 *10^{11} particles.mL^{-1} **(Figure 8-b).**

A reduction in the negative ellipticity of gelatin's peak at 204 nm was observed in the circular dichroism data **(Figure 9)**, this peak is indicative of gelatin's random coil structure [256]. When measured at 37°C, The 204 nm peak intensity followed the rank order gelatin > CoAc > TS-CoAc. This may suggest that coacervation and thermal stabilization may have reduced the randomicity of the sample and promoted a more uniform arrangement of system components.

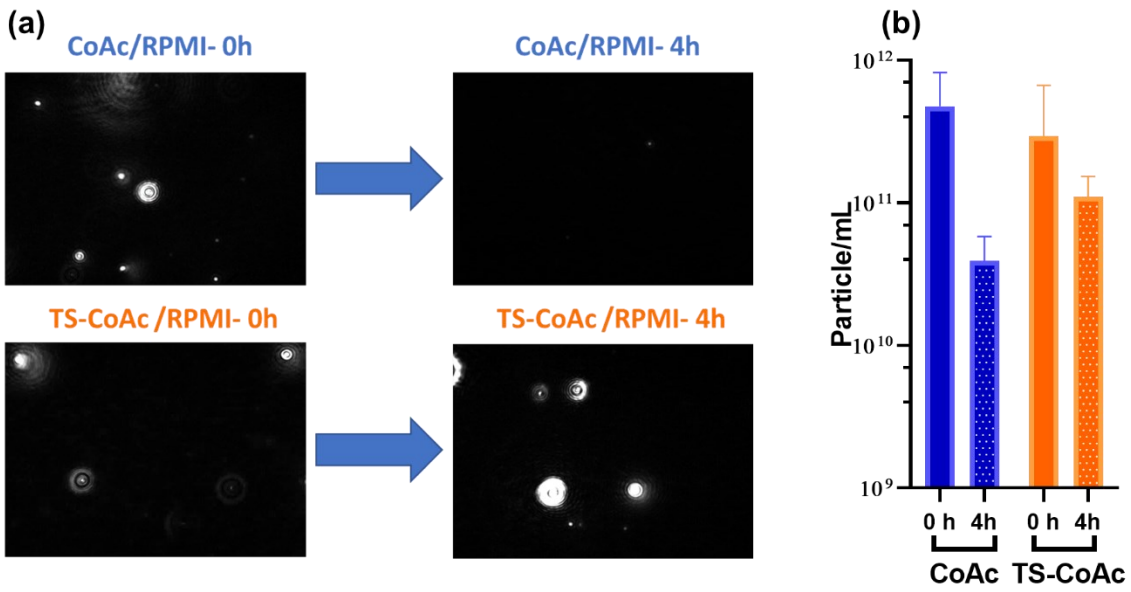

Figure 8. *(a) Still images from NTA videos of CoAc (top pannel) and TS-CoAc (bottom pannel) at 0h (left) and 4h(right) of incubation with RPMI-1640 at 37 °C (**b**) Colloidal stability as a function of particle count (particles.mL^{-1}) assessed using NTA for CoAc (blue columns) and TS-CoAc(orange columns) at 0h (solid columns) and 4h (dotted columns)of incubation in RPMI-1640 at 37 °C (N = 1, n = 3).*

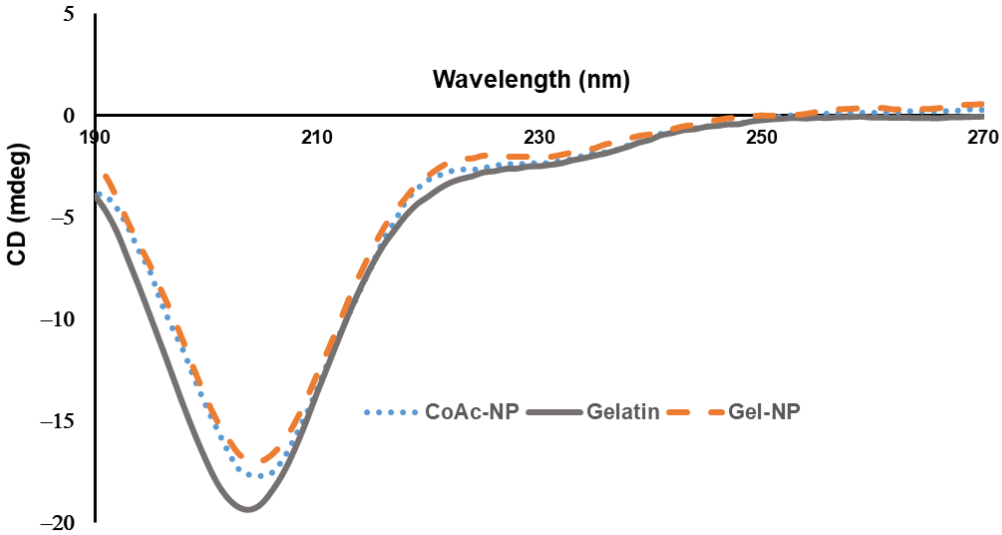

Figure 9. *Circular dichroism scans of gelatin, CoAc, and TS-CoAc in MQ water at 37 °C.*

2.4.5. Confirmation of protamine sulfate shell deposition

We selected a microfluidic system to coat either CoAc or TS-CoAc with protamine sulfate, in protamine sulfate to gelatin mass ratio of 1:5, under laminar flow conditions. The selected meander chip setting allowed the deposition of a homogenous coat on the cores that was best observed in the case of protamine coated thermally stabilized coacervates (P-TS-CoAc) rather than protamine coated non-thermally stabilized coacervates (P-CoAc) using TEM **(Figure 10)**. This observation was initial proof of the necessity of thermal stabilization of the coacervate core for the successful assembly of the eventual core-shell system.

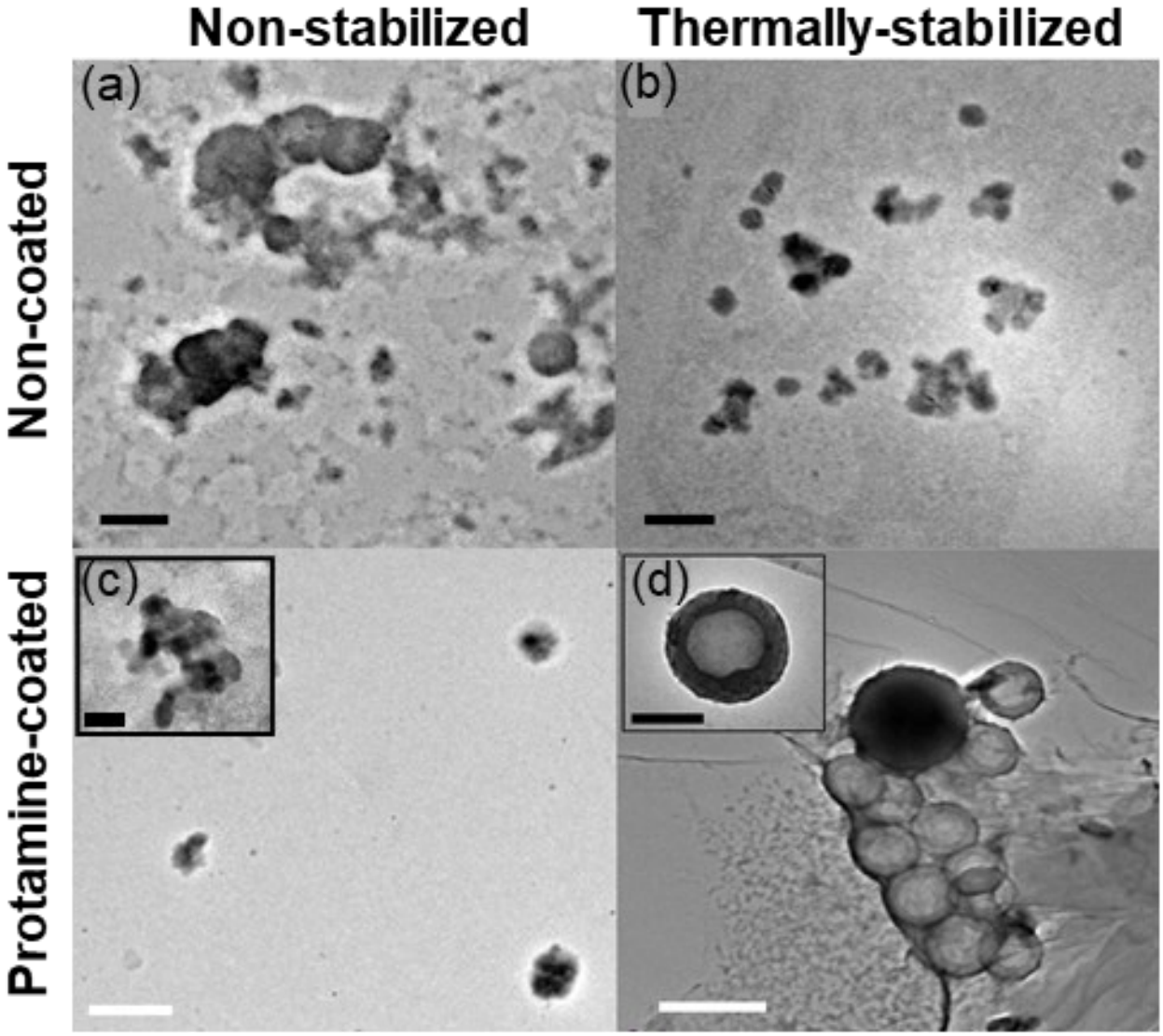

Figure 10. *Transmission electron microscopy of unstained (a) CoAc (b) TS-CoAc (c)P-CoAc, (d) P-TS-CoAc, black bar=200 nm, white bar= 500 nm*

The enhancement in colloidal stability of the system following thermal treatment was further confirmed by the progressive increase in particle diameter and PDI of the protamine-coated, non-stabilized coacervates (P-CoAc) in MQ water starting as early as 3

days post coating. Whereas the thermally stabilized protamine coated coacervates (P-TS-CoAc) resisted core disruption by the cationic protamine sulfate coat with no significant changes in particle diameter or PDI for 3 weeks **(Figure 11-a, b).**

A reduction in CoAc stability upon encountering a competing potent polycation like protamine sulfate could be expected in a liquid coacervate system, relying solely on electrostatic interactions to remain intact. In the absence of any chemical or physical stabilization techniques, protamine would simply displace the entity with lower charge density being gelatin from the CoAc, typically resulting in increased particle size and PDI as the heterogenous gelatin components are released from the nano-system (refer to **Figure 6-a** for DLS peak(s) pattern of free gelatin). This explains the exclusive observation of particle disruption in the case of P-CoAc rather than P-TS-CoAc.

A zeta-potential reversal from -3.9 mV in the case of TS-CoAc to 8.2 mV in the case of P-TS-CoAc, proved the successful deposition of protamine sulfate on the surface of TS-CoAc **(Figure 11-c).**

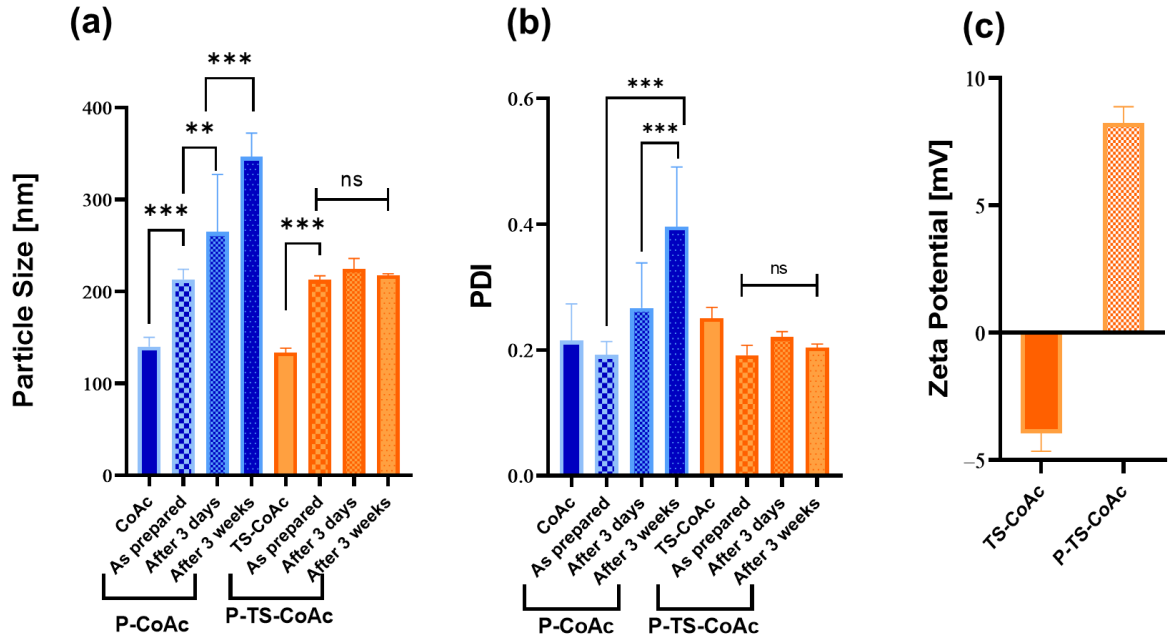

Figure 11. *DLS assessment of the impact of thermal stabilization on the colloidal stability of CoAc (blue columns) and TS-CoAc (orange columns) following protamine sulfate coating. (**a**) particle size (nm) and (**b**) PDI of CoAc (blue columns) and TS-CoAc (orange columns) before, as prepared immediately after protamine sulfate coating, after 3 days and 3 weeks of storage (N = 3, n = 3). (**c**) Zeta-potential of TS-CoAc before (solid column) and after (patterned column) protamine sulfate coating (N = 3, n = 3). Values are represented as means with standard deviation depicted as error bars, ** p < 0.01, *** p < 0.001, ns = not significant.*

2.4.6. NA cargo shielding effect exerted by P-TS-CoAc and P-CoAc assessed using agarose gel electrophoresis

P-TS-CoAc and P-CoAc were both subjected to DNase I/RNase A challenge followed by Gel migration assay. Results demonstrated that P-TS-CoAc possessed a higher pDNA shielding effect compared to P-CoAc. Yet both P-CoAc and P-TS-CoAc showed

comparable shielding capacity of their cargo mRNA which was in both cases superior to free mRNA **(Figure 12).**

It is also worth mentioning that this experiment explored the potential release mechanisms of the different NA cargos from the reported nanocarrier. Where a combination of proteolytic digestion (represented by the trypsinization of the system) and polyanion exchange (performed using HMWT Heparin) could be proposed as release mechanisms of these NA cargos.

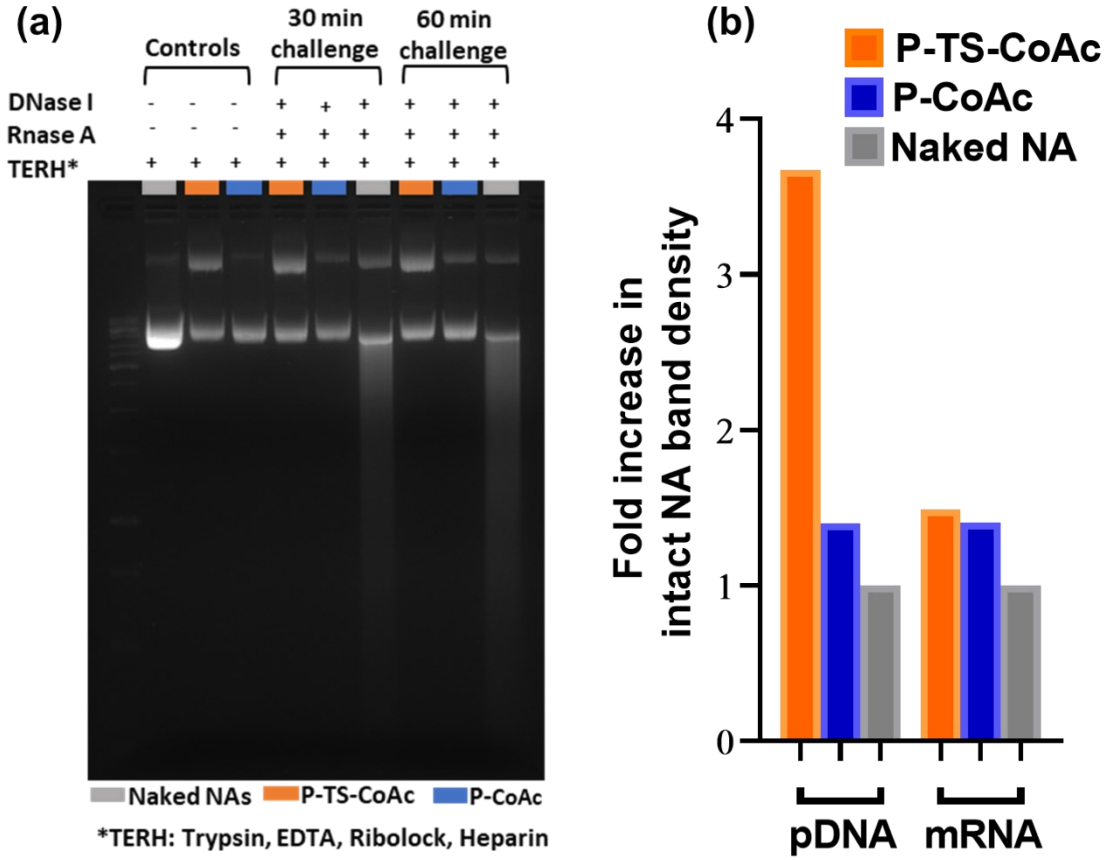

Figure 12. *(a) agarose gel electrophoresis migration assay of mCherry(lower bands' row) and pAmCyan(upper bands' row) either naked (grey-marked lanes), loaded on P-TS-CoAc (orange-marked lanes) or P-CoAc(blue-marked lanes), following either a 30 or 60 min incubation with DNase I/RNase A cocktail, (b) Densitometric analysis of NA bands at the 60 min incubation point of gel in (a)*

To simulate an even more physiologically relevant release and challenging medium, we challenged the uncoated particle cores in 10% FSC for 3h **(Figure 13)**. Here we observed enhanced protection of the pDNA observed as 31.9% of intact residual pDNA at the need of the incubation period in the case of TS-CoAc, compared to 17.4% in the case of CoAc particles.

Gelatin type A is the acidic denaturation product of collagen. Given its denatured structure, gelatin is minimally antigenic[257], making it an excellent candidate for multi-dosing within a vaccination context. Gelatin A is a weak cation of lower charge density than most cationic polymers and lipids typically used in transfection, which could be an advantage in terms of safety [258], but a disadvantage in terms of stability of its coacervates with nucleic acids. To the best of our knowledge, most techniques employing gelatin-based

nanocarriers for NA delivery were mainly stabilized via chemical cross-linking with or without gelatin cationization to form stable particles. The most commonly reported cross-linkers, in this case, are symmetrical bifunctional aldehydes such as glutaraldehyde and glyoxal [235], and EDC (1-ethyl-3-(3-dimethyl-aminopropyl) carbodiimide hydrochloride)[234]. Yet, in a nucleic acid delivery scenario, and taking into consideration the abundant amine groups content of gelatin itself the cargo NA could easily become covalently bound to the carrier gelatin matrix. Generally, covalent protein-NA interactions are unfavorable as they may hinder NA cargo release from the nanocarrier, as well as present a safety concern where covalently bound DNA-protein could interfere with the fidelity of gene expression in their host cell by interacting with the translation and transcription mechanisms of the cell via their DNA domain[236,259].

Given the aforementioned reasons, this study opted to explore an alternative physical stabilization technique when designing our nanocarrier to avoid chemical cross-linking. Gelatin-DNA coacervation relies mainly on easily reversible electrostatic assemblies, hydrophobic interactions, and hydrogen bonds between DNA and gelatin. These non-covalent interactions are more synonymous with physiological interactions between nucleic acids and proteins in the cell[237]. Yet DNA-Gelatin coacervates have been reported to possess an intrinsic capability to irreversibly transform to an anisotropic nanogel phase when heated and then cooled above and below gelatin's helix-coil transition, respectively [238,239]. This phenomenon has been reported by Rawat *et al*[239] but was not previously used as a DNA nano-delivery system assembly technique.

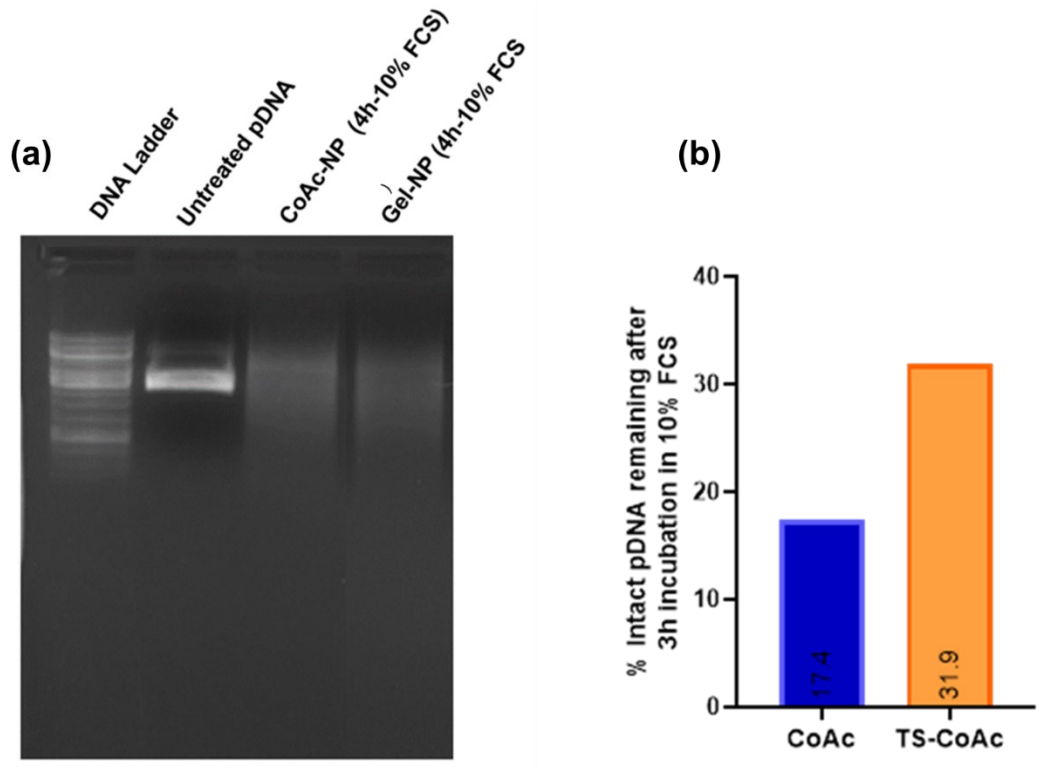

Figure 13. *(**a**) serum stability assessment of pAmCyan1 cargo in coacervate and TS-CoAc following 3 h incubation in 10 % fatal calf serum (FCS) using agarose gel electrophoresis. (**b**) Densitometric analysis of pAmCyan1 bands released from CoAc(blue column) and TS-CoAc(orange column) normalized to band*

intensity of the equivalent amount of free pAmCyan1 in TBE buffer; the pAmCyan1 cargo was released from CoAc or TS-CoAc using trypsin HMWT, following 3 h incubation with 10% FCS in HBSS.

We assume that when heated above its helix-coil transition temperature of 40°C, gelatin α-helices extend to assume predominantly random coil conformation, further extending across the matrix of the coacervate. By virtue of their relative lengths, a random coil can generally traverse and interact with more individual pDNA molecules along their length than a helix of equal molecular mass would. When suddenly cooled in their extended state while still in contact with pDNA, the immediate energy loss by the system is consumed in consolidating electrostatic and hydrogen bond interactions between pDNA and gelatin coils, rather than restoring the coils to their helix morphology. This physical method of cross-linking can be considered a safer option than most chemical cross-linkers commonly used for gelatin nanocarrier preparation, which could compromise the intrinsic biodegradability and biocompatibility of gelatin[260,261].

Protamine sulfate was our coat of choice for this core-shell nanocarrier system given its reported advantages within a vaccination context. Where it had been widely employed by CureVac AG in their RNactive® technology as an NA vaccine delivery and adjuvantation tool[244,245,262–264]. Protamine possesses comparable membrane translocating properties to the established cell-penetrating peptide HIV-1 tat[240]. Protamine-DNA coacervates can also bind to nuclear pore complex associated transport proteins (importins), which we assumed would allow the nuclear translocation of the pDNA component in the CoAc. nuclear translocation of pDNA[241,265]. In addition, protamine's safety and its established pharmaceutical application became our motivation to use it as a particle coating.

2.4.7. Colloidal properties of P-TS-CoAc following mRNA surface loading

mRNA was surface loaded on P-TS-CoAc simply via pipetting, and DLS was used to assess whether this may have led to system disruption. Yet, mRNA-loaded P-TS-CoAc showed no significant changes difference in particle size and PDI from unloaded P-TS, CoAc for up to one week. This could be a first indication that the dual-loaded nanocarrier remains intact and can be taken up as a unit by target cells, and that no mRNA-protamine sulfate coacervate sub-populations are formed **(Figure 14).**

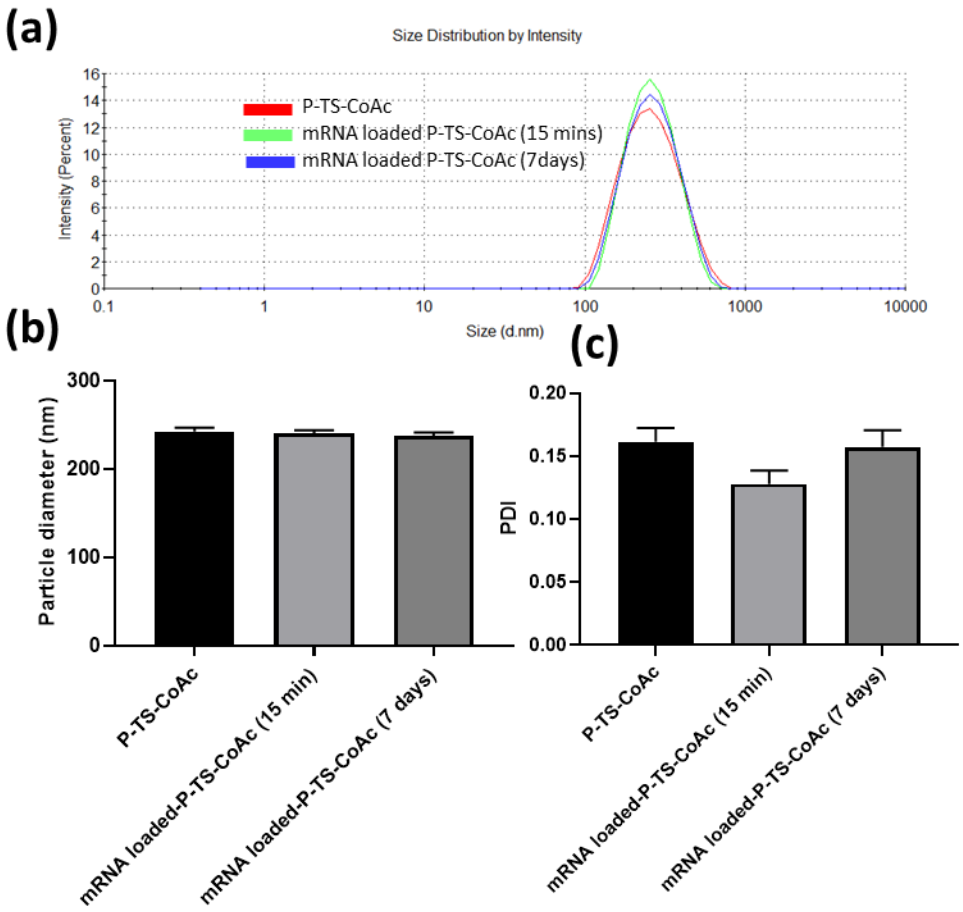

Figure 14. *(a) Particle size distribution by intensity was measured using DLS before (red), 15 min after(green), and 7 days(blue) after the surface loading of P-TS-CoAc with mCherry. (b) Particle sizes (nm) and (c) PDI of P-TS-CoAc before, 15 minutes after, and 7 days after loading with mCherry.*

2.4.8. Assessment of entrapment efficiency (EE%), loading efficiency (LE%), and numeric molecular capacity per nanocarrier using PicoGreen and RiboGreen Assays

PicoGreen assay was performed on the supernatant of either CoAc or TS-CoAc particle suspension following 2h of ultracentrifugation at 58,000× *g*, 4 °C to assess the systems' entrapment efficiency and drug loading. Results shown in **(Table 5)** demonstrated that at a gelatin: pDNA mass ratio as low as 30:1, pDNA was fully incorporated into both CoAc and TS-CoAc. A similarly performed RiboGreen assay on P-TS-CoAc showed an mRNA EE% of 97.81%. The selected NA, namely mCherry and pAmCyan1 existed in a molar ratio of 1.74:1 mCherry to pAmCyan1. Calibration curves of PicoGreen and RiboGreen assays are provided in **(Figure 15)**.

The carrier could deliver approximately $1.884 * 10^{12}$ mRNA molecules and $1.076 * 10^{12}$ pDNA molecules per 170 µg of particles (dose per well selected for subsequent transfection studies). Based on NTA-generated particle count, PicoGreen and RiboGreen generated

data, it was estimated that the carrier loaded approximately 5318 pDNA molecules and 9312 mRNA molecules per P-TS-CoAc particle.

Table 5. *The entrapment efficiency (EE%) of pAmCyan by P-CoAc and P-TS-CoAc assessed using PicoGreen assay, EE% of mCherry by P-TS-CoAc assessed using RiboGreen (N=1, n=3). The average number of pAmCyan1 or mCherry molecules per 170 µg particles as the dose used per well in a 24 well-plate format and the numbers of pAmCyan1 or mCherry molecules per particle was calculated based on the used amount of NAs and the particle count obtained by NTA.*

	pAmCyan			**mCherry**		
Sample	**EE [%]**	**molecules/dose**	**molecules/NP**	**EE [%]**	**molecules/ dose**	**molecules/NP**
CoAc	100.10±0.28%	$1.076*10^{12}$	5318	No colloidally stable coated P-CoAc for surface loading		
(P-)TS-CoAc	100.12± 0.39%	$1.076*10^{12}$	5318	97.81±1.06	$1.884*10^{12}$	9312
jetPrime*	$100.01±9*10^{-5}$ %	$1.076*10^{12}$	-	-	-	-
JetMessenger**	-	-	-	100.66±20.94 %	$1.884*10^{12}$	-

*,** For the transfection reagents JetPrime and JetMessenger, the particle count was not available to calculate the number of NA molecules/NP.

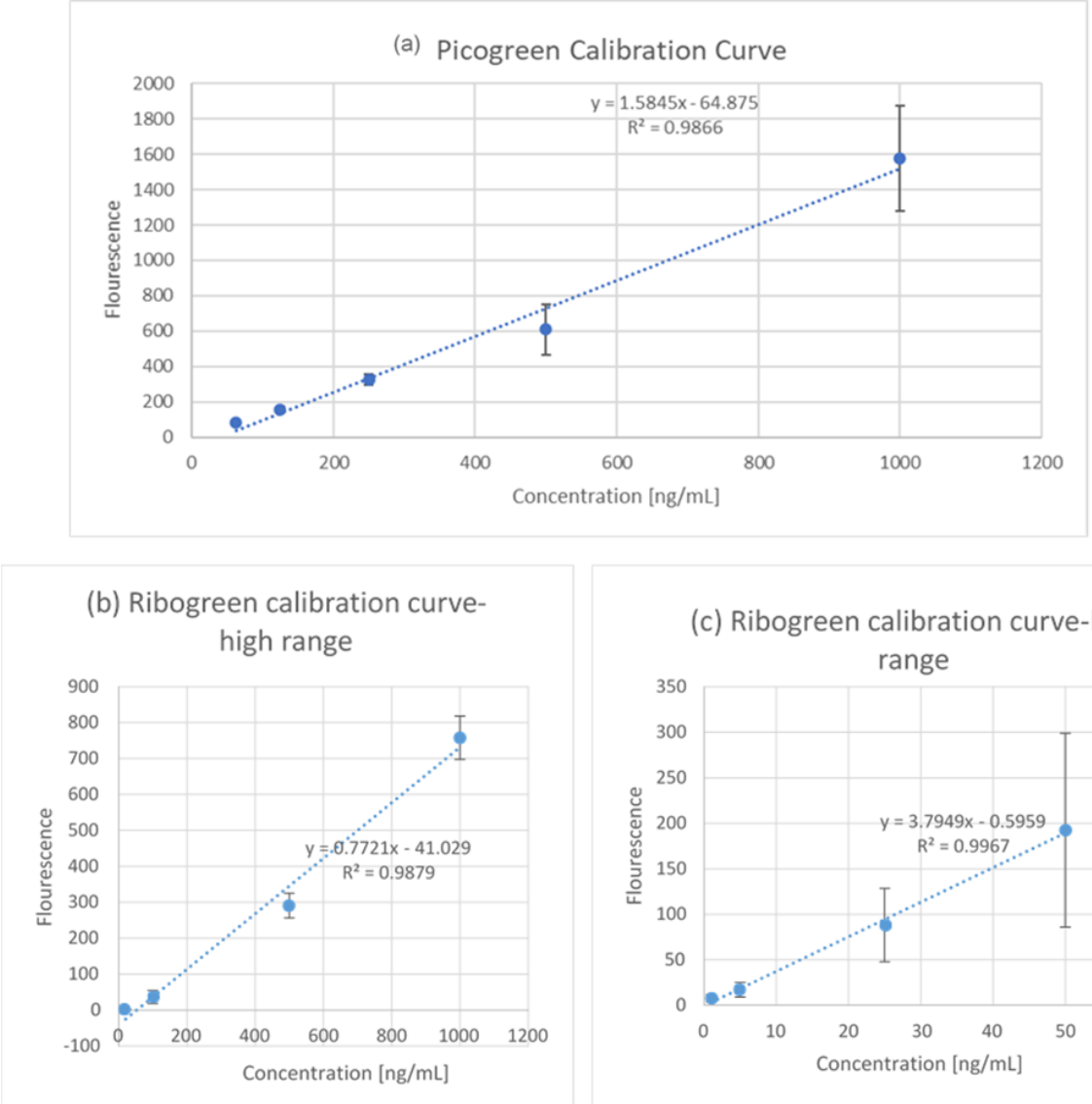

Figure 15. *(a) Picogreen assay calibration curve, pAmCyan1 concentration range from 31.5–1000 ng/mL (N = 3,n = 1) , Ribogreen assay calibration curves (b) high range with mCherry concentration range from 20–1000 ng/mL (c) low range with mCherry concentration range from 1–50 ng/mL (N = 3,n = 1).*

2.4.9. Cytotoxicity of P-TS-CoAc in murine dendritic cell line DC2.4

Murine dendritic cells (DC2.4) treated with 340,170 or 85 µg mL^{-1} P-TS-CoAc for 6h showed no statistically significant difference in viability from untreated cells with cell viabilities of 91.9%, 97.1%, and 97.7% respectively (**Figure 16**). A concentration of 170 µg/ml was further selected for an extended viability assay, where cells are incubated with P-TS-CoAc for 24h, yet cells still showed a viability of 87.4% at the end of this assay, indicating excellent system tolerability. This data aligns with the established biocompatibility of the two major nanocarrier components being gelatin and protamine sulfate[244,261]. For subsequent transfection efficiency studies, 170 µg/mL was the concentration of choice.

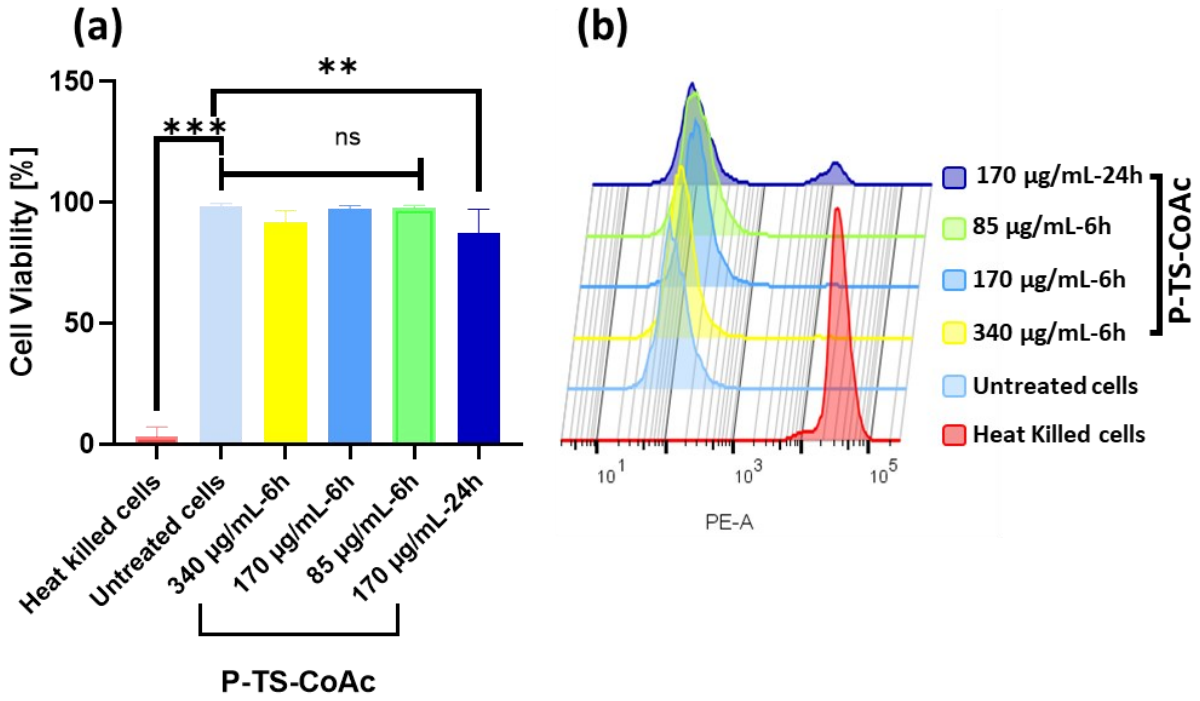

Figure 16. *Cytotoxicity assay of P-TS-CoAc in DC2.4 murine dendritic cell line using fixable dead stain (568/583) (a) % Cell viability following 6 h incubation of P-TS-CoAc (340,170 or 85 µg/mL) or 24h incubation of P-TS-CoAc (170 µg/mL) (N=3, n=3). Values are represented as mean with error bars representing standard deviation, *** $p < 0.001$, ns = not significant. (b) Fluorescence intensity (dead stain uptake) of cells following different treatments.*

2.4.10. Transfection performance of P-TS-CoAc and P-CoAc against established clinical, experimental, and commercial controls in murine dendritic cell line DC2.4

Following the application of mCherry (mRNA) surface loaded P-CoAc and P-TS-CoAc prepared using pAmCyan1(pDNA) to DC2.4, both particle systems could successfully and simultaneously transfect DC2.4 with both mRNA and pDNA (**Figure 17**). This co-transfectional capacity surpassed all other dual-transfection control groups in both transfection efficiency and level of protein expression of both pAmCyan1 and mCherry. Out of all the selected controls, only JetM and LNPs could show a comparable mRNA transfection efficiency to P-TS-CoAc and P-CoAc in case of dual-transfection, yet no success whatsoever for pDNA transfection.

Upon application of both protamine sulfate-coated and mRNA surface loaded P-CoAc and P-TS-CoAc to DC2.4, both P-CoAc and P-TS-CoAc showed successful, simultaneous transfection of the cells with both mRNA (mCherry) and pDNA (pAmCyan). The transfection efficiency and level of protein expression of both pAmCyan and mCherry significantly surpassed all other test groups except for the JetM single transfection of mCherry transfection. Both P-TS-CoAc and P-CoAc showed no significant differences in either transfection efficiencies or protein expression levels expressed as MFI for both

mRNA and pDNA. Yet, P-TS-CoAc displayed slightly higher transfection efficiencies and MFI compared to P-CoAc. Where P-TS-CoAc displayed a transfection efficiency and MFIs of 61.4%±21.6 and 909±253 as opposed to 53.8%±22.3 and 794±180 with P-CoAc for mRNA. The difference, though statistically insignificant, could be resorted to the overall higher system stability in the case of P-TS-CoAc allowing better binding and stabilization of the surface-loaded mRNA. A detailed gating strategy is provided in **(Figure 18).**

Protamine sulfate-NA coacervate was used as an internal control showing highly variable transfection of both NA cargos **(Figure 17-a).** As representatives of potent, widely used commercial controls JetMessenger was used for mRNA and JetPrime for pDNA. Yet upon their application as co-transfection reagents, both JetM and JetP gave negligible transfection for the NA they were not optimized to deliver, and a reduction in the transfection efficiency of the NA for which they were optimized. In contrast to all the aforementioned controls, P-TS-CoAc and P-CoAc successfully co-transfected DC2.4 with pAmCyna1 and mCherry.

We assume that the unique co-transfectional ability of our system is due to protamine's compound ability to both promote cytoplasmic delivery of mRNA, as well as nuclear translocation of pDNA. pDNA nuclear translocation can be achieved via four specialized nuclear localization signal-like sequences in protamine's structure[242,266]. But also, a protamine coacervate was assembled at the same protamine:mRNA:pDNA mass ratios as P-TS-CoAc did not perform as well as the P-TS-CoAc system which could be largely resorted to a trojan horse-like effect exerted by gelatin-pDNA coacervate core. In that arrangement, a large fraction of the pDNA's negative charges could be occluded inside the gel core, only the surface-displayed negative charge fraction would be interacting with the cationic protamine coat. In that case, a considerable fraction of protamine's cationic groups are spared to participate in cell-surface interaction, endosomal escape, and nuclear membrane association. This nanocarrier configuration could thus be allowing its protamine content to function at an apparently higher NP ratio despite the lower actual protamine dose.

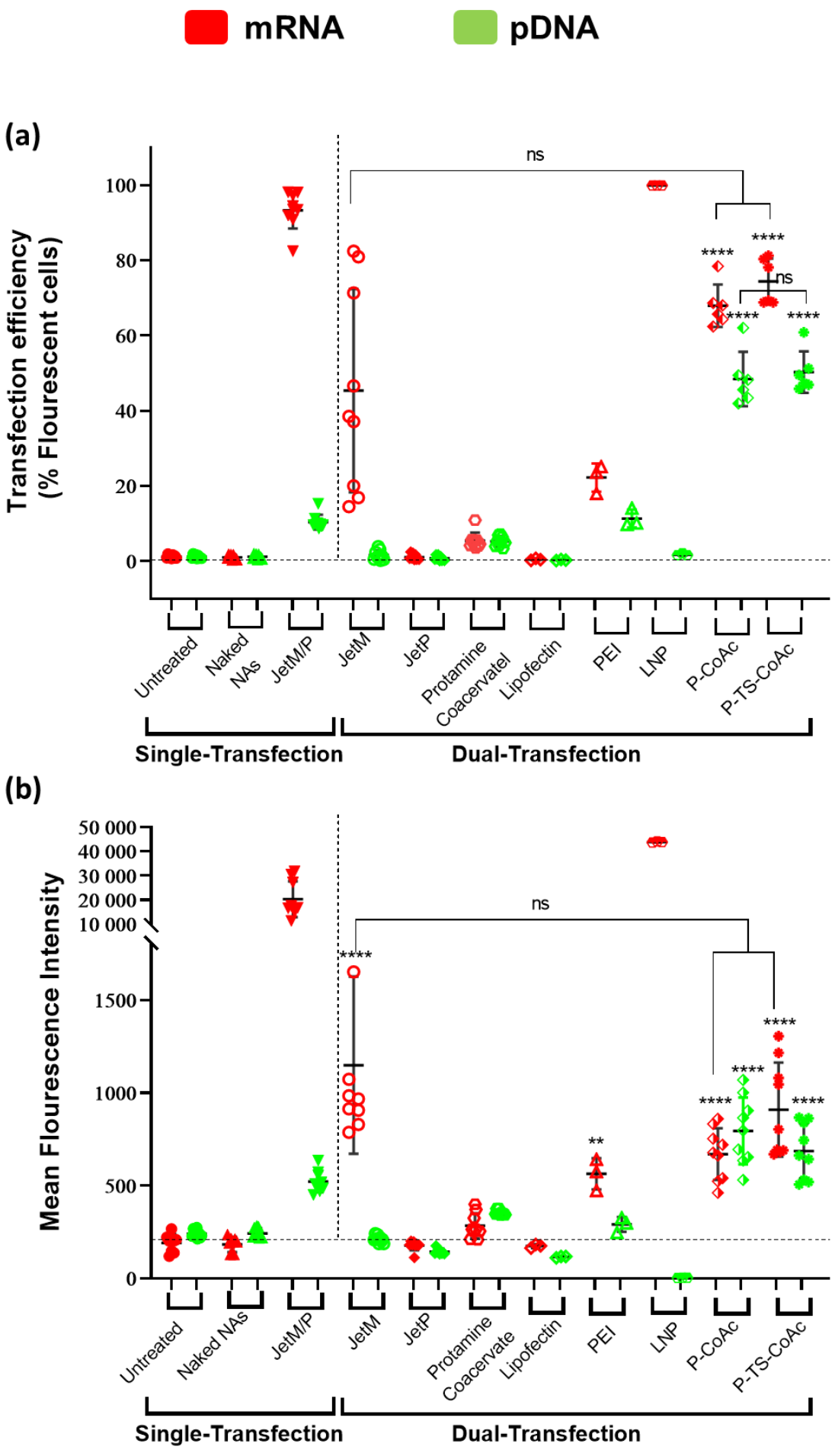
mRNA
pDNA
(a)
Transfection efficiency
(% Flourescent cells)
100
80
60
40
20
0
ns
****
****
ns
****
****
Untreated
Naked NAs
JetM/P
JetM
JetP
Protamine Coacervate
Lipofectin
PEI
LNP
P-CoAc
P-TS-CoAc
Single-Transfection
Dual-Transfection
(b)
Mean Flourescence Intensity
50 000
40 000
30 000
20 000
10 000
1500
1000
500
0
ns
****
**
****
****
****
Untreated
Naked NAs
JetM/P
JetM
JetP
Protamine Coacervate
Lipofectin
PEI
LNP
P-CoAc
P-TS-CoAc
Single-Transfection
Dual-Transfection

Figure 17. *Flow-cytometric assessment of (a) transfection efficiency and (b) level of ürotein expression expressed as Mean fluorescence intensity (MFI) of pAmCyan (green) and mCherry (red) loaded on P-CoAc and P-TS-CoAc, compared to single transfection with JetMessenger for mCherry or JetPrime for pAmCyan1or double transfection using both mCherry and pAmCyan1 with either JetMessenger, JetPrime, protamine sulfate coacervate in murine dendritic cell line DC2.4 (N=3, n=3), Lipofectin, PEI, LNP (N=1, n=3). Values are represented as means with standard deviation depicted as error bars, levels of significance indicated in comparison to untreated controls, ** $p < 0.01$, **** $p < 0.0001$, ns = not significant.*

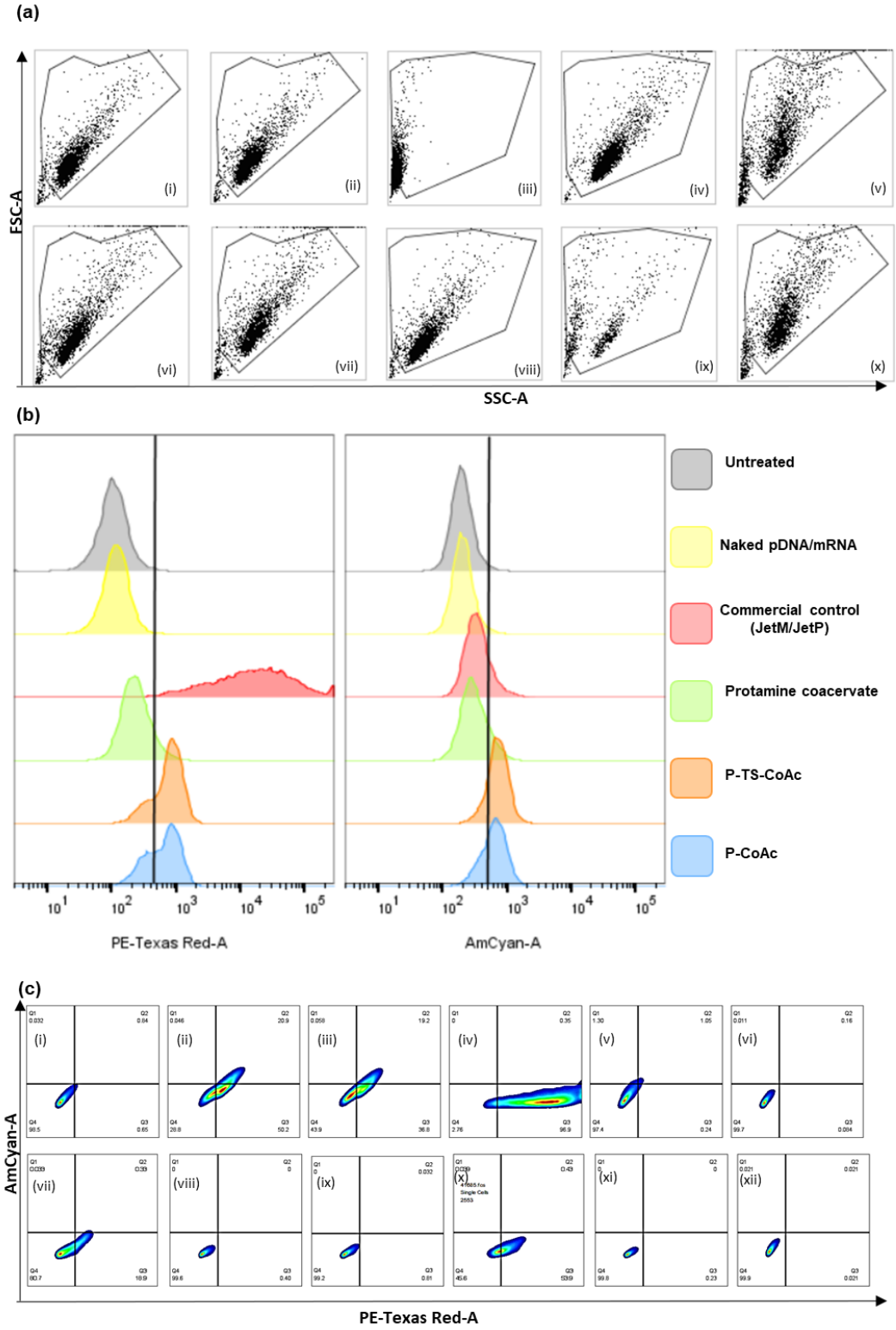

Figure 18. *(a) Dot plots and gating of DC2.4 with different treatments (i) untreated, (ii) protamine coacervate, (iii) JetM-single transfection, (iv) JetP-single transfection, (v) JetM-dual transection, (vi) JetP-dual transfection, (vii) Lipofectamine-dual transfection, (viii) PEI dual transfection, (ix) P- Co-Ac, and (x) P-TS-CoAc. (b) Histograms of DC2.4 with different traetements showing shift in flourscence intensity along the PE-Texas Red-A and AmCyan-A channel. (c) Quadrant gating of DC2.4 with different treatemnets (i) untreated cells, (ii) P-TS-CoAc, (iii) P-CoAc, (iv) JetM-single transfection, (v) JetP-single transfection, (vi) naked pAmCyan1 and mCherry, (vii) PEI-double transfection, (viii) Lipofectamine double transfection, (ix)*

protamine coacervate-double transfection, (x) JetM-double transfection, (xi) JetP-double transfection, and (xii) LNPs-double transfection.

2.4.11. Confocal Laser Scanning Microscopic assessment of co-transfection using P-TS-CoAc and P-CoAc

Confocal Laser Scanning Microscopy of the selected highest performing treatments from flow-cytometric assessment showed that DC2.4 treated with P-TS-CoAc had visibly more consistent transfection patterns for both mCherry and pmCyan1A **(Figure 19-b,f)** than cells treated with the P-CoAc (**Figure 19-c,g).** This could be an indication of the enhanced colloidal stability of the system by thermal stabilization, which provided superior protection to the core-loaded pAmCyan1 and a more stable surface for mCherry loading, allowing P-TS-CoAc to stay intact longer during transfection and deliver its dual NA cargo as a unit to the target cells. Such a feature could be rather valuable within a vaccination context of antigen-adjuvant co-delivery. Cells treated with commercial transfection reagent displayed a strong expression of mCherry in the case of JetM (**Figure 19-d**) and a weaker yet more diffuse expression of AmCyan in the case of JetP (**Figure 19-h**).

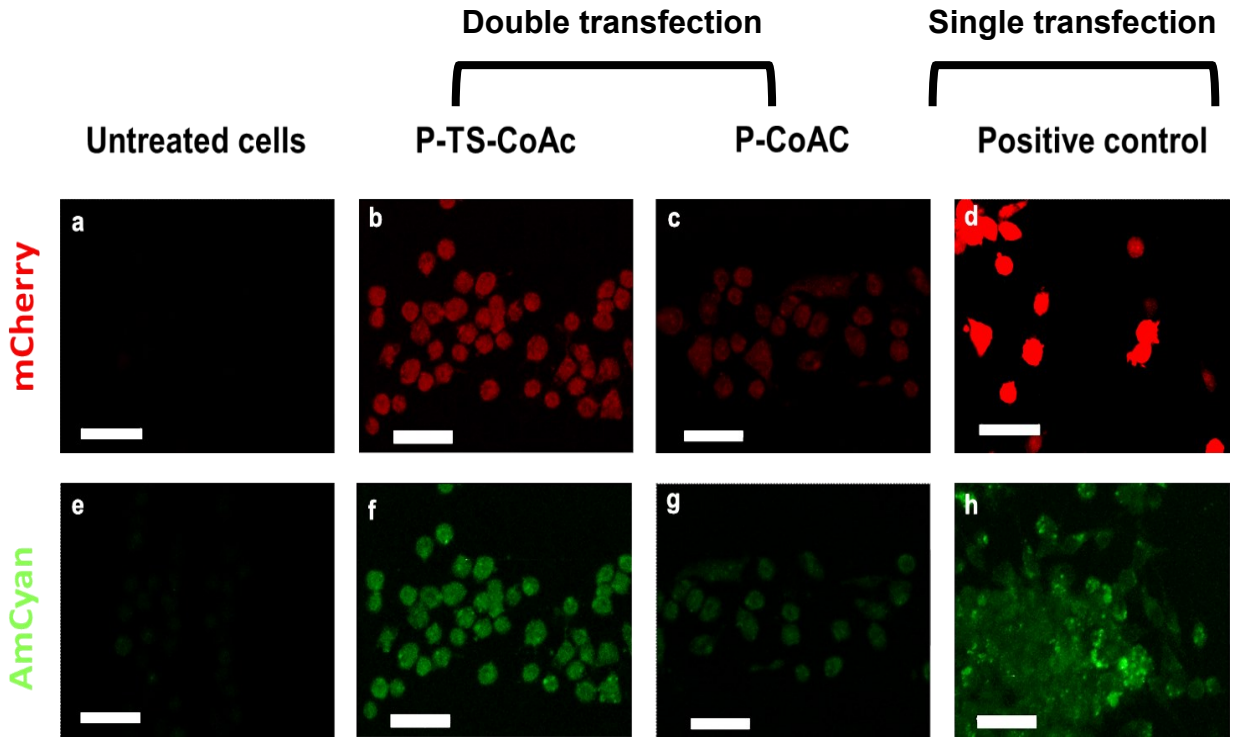

Figure 19. *Assessment of transfection efficiency and gene expression of mCherry (red fluorescent reporter) and pAmCyan (green fluorescent reporter) in DC2.4 after 6 h of treatment of samples or controls followed by 48 h incubation (a) confocal laser scan microscopy showing expression of mCherry (red) and AmCyan(green) in DC2.4 cells treated with (ii, vi) P-TS-CoAc, (iii, vii) P-CoAc, (iv) JetMessenger, (viii) JetPrime compared to (i,v) untreated cells, the white bar=39.64 µm. CLSM images are shown with 40% increased brightness from the original images (obtained with identical laser intensity settings for all samples).*

2.5. Conclusion

This study demonstrated a novel NA nanocarrier design approach, in which gelatin, a biocompatible, pharmaceutically established biopolymer, was employed as a matrix former along with plasmid DNA. A straightforward and mild preparation technique, based on an intrinsic property of the complex coacervate of the two core components, gelatin, and pDNA, being their ability to form an irreversible anisotropic nanogel when heated together. The thermal stabilization of this gelatin-pDNA coacervate allowed its use as a core that can be stably coated with a stronger cationic peptide, namely protamine sulfate. We then surface-loaded mRNA on the protamine coat, while pDNA remained in the core.

Given the biocompatibility of its different components, the system was very well tolerated in the concentration range selected for transfection. Successful transfection of both mRNA and pDNA cargos was observed with comparable transfection efficiencies when used in a pDNA to mRNA mass ratio of 5:1. In contrast, clinical, experimental, and commercial transfection reagents, could not successfully co-transfect DC2.4 with mRNA and pDNA. I thus report a proto-type NA carrier with unique co-transfectional capabilities. A wide range of applications can be expanded on the concept, both in the areas of vaccine delivery, as well as protein replacement therapies. Using selected combinations of nucleotides, we think the interesting possibility of time-resolved gene expression could be achievable. Apart from clinical applications, this nanocarrier could serve as a research tool to study differences in expression kinetics between more than one NA species delivered on a single carrier in parallel.

Chapter III: Impact of varying assembly conditions of TS-CoAc based core-shell nanocarriers on transfection performance and expression kinetics of co-delivered mRNA and pDNA cargos in-vitro

3.1. Abstract

Co-delivery of different protein-encoding polynucleotide species with varying expression kinetics to achieve a temporally- resolved expression of their therapeutic proteins or peptides can become a prominent requirement in the upcoming years, as nucleic acid-based therapies expand in their application. The current study explores such a possibility by employing a biodegradable, biocompatible core-shell, nano-carrier co-loaded with pDNA at the core and mRNA on the shell. The system's core is based on a gelatin Type A-pDNA coacervate, thermally stabilized to form a stable gel, eligible for deposition of cationic coats. The coating is attempted with either protamine sulfate or a lipid mixture of Dlin-DMA-MC3, DSPC, Cholesterol, DMG-PEG2000. Both protamine and lipid-coated core-shell particles display acceptable particle size and PDI, and a zeta-potential reversal from -3.6 ±0.8 for uncoated particles to either 14.9 ±0.6 and 8.3 ±0.5 for lipid and protamine sulfate coated particles, respectively. Yet only the protamine coated nanocarriers successfully co-transfect murine dendritic cell line DC2.4 with mRNA(mCherry) and pDNA (pAmCyan1), at 84.3±5.8 and 42.2±1.2 transfection efficiencies, respectively. Meanwhile, the lipid-coated nanocarrier and LNPs of equivalent lipid content and NP ratio only transfect DC2.4 with mCherry at 88.7±9.9 and 99.9 ± 0.0 transfection efficiencies, respectively, following 36h of incubation with DC2.4.

A factorial assessment of the impact of varying thermal stabilization cycles number and gelatin: protamine sulfate mass ratio on nanocarriers' colloidal properties and transfection performance is performed. Both factors display a statistically significant impact on particle size, PDI, transfection efficiency, and level of protein expression from pDNA and mRNA, yet neither results in a dramatic improvement of protein expression levels for either mRNA or pDNA.

Transfection efficiency and levels of protein expression are assessed over 33h in DC2.4. The onset of expression occurred at 3h and 6h for mRNA and pDNA respectively. While mRNA expression peaked at 24h, followed by a slight decrease at 33h, pDNA expression continued to gradually increase between 24h and 33h.

The investigated nanocarriers in this study, capable of co-delivery of mRNA and pDNA can provide promising platforms to achieve multi-dosing or sustained expression of nucleic acid-based therapeutics with minimal administration frequencies which can be useful in both protein replacement and vaccination scenarios.

3.2. Introduction

Following the outbreak of the Covid-19 pandemic, the approval of mRNA-based vaccines and their mass administration with high efficiency[56,63,267] and safety margin in the general population[96,268–270], is currently helping accelerate the advancement of NA-based therapeutic moieties towards mainstream therapeutics[271]. Now it is expected that the application of such NA-based therapeutics would expand within the infectious diseases [63,91,219,272–274]and cancer vaccination[245,275–278] milieu but also beyond to encompass more hereditary, chronic, and acute health concerns[271,279,280]. This pending shift in the clinical application may probably give rise to stronger demand for control over the expression kinetics of such nucleic acids to generate expression patterns synonymous with controlled-release patterns that have been addressed for many conventional therapeutics.

To generate sustained or sequential expression patterns emulating depot or multi-dosing drug delivery systems using NA-based therapies, several modifications will have to be considered. The required modifications may not be exclusive to the nucleic acid cargos' structures, but will most probably extend to their delivery systems as well, given the now proven instrumental role of nanocarriers to the functionality of therapeutic NAs[224,281,282].With regards to NA vaccines, nanocarriers capable of providing sustained antigen expression have been shown to augment and prolong the protective immunity rendered by the vaccine[184]. Also, as several initiatives now advance towards the co-delivery of immunomodulator encoding NA cocktails or combinations of NA encoded immuno-modulators and antigens[197,204,283], the kinetics and temporal resolution of expression of such immunomodulator combinations or the antigen-immunomodulator/adjuvant combination can prove to be detrimental to the efficacy and safety of such vaccines[284].

To date, several studies have already compared the expression kinetics of different NA species including plasmid DNA (pDNA), Self-amplifying mRNA (sa-mRNA), modified-base mRNA, and unmodified mRNA. Where Huysmans *et al.* demonstrated that following in-vivo skin electroporation in mice with equivalent masses of the aforementioned NA species, sa-mRNA displayed the highest level of expression of luciferase over 4 weeks, yet pDNA was the NA species that maintained the highest level of luciferase expression during the fourth week compared to equivalent doses of 1 and 5 µg of sa-mRNA. pDNA also demonstrated much lower immunogenicity compared to all the other mRNA species[200]. Leyman *et al.* have also demonstrated similar results in pigs[201]. These data indicate the potential value of pDNA in sustained-release scenarios where minimal immune stimulation is required. Another situation where such a feature of pDNA may prove valuable is in situations where a wash-out period is required between repeated doses of therapeutic moieties to avoid receptor oversaturation and downregulation[285,286]. In such a situation using sa-mRNA may not be applicable due to the sustained high level of expression that could extend from days to weeks. In such a case combining non-replicating mRNA with pDNA can provide a transient loading dose followed by lower delayed expression from pDNA as a maintenance dose, thus establishing a multi-dosing scenario through a single administration.

mRNA is structurally less stable than pDNA, yet, when it successfully escapes the endo-lysosomal compartment and reaches the cytoplasm intact, mRNA can be rapidly translated in the cytoplasm[287]. As opposed to pDNA, which requires nuclear translocation, mRNA can give early onset and transient expression of the encoded protein/peptide, and also cell cycle independent transfection efficiency. Conversely, Plasmid DNA, despite its more challenging delivery[288], possesses a longer half-life than mRNA. pDNA can also present more options for manipulation and control over the rate, duration, and cellular target of the encoded protein/peptide expression[289,290]. For instance, promoter manipulation can alter pDNA expression kinetics[291] Such temporal tuning of expression is much more difficult to achieve using mRNA as it requires discrete optimization of the tRNA frequency of each codon on the ORF [292], thus within a multi-dosing context, co-delivery mRNA and pDNA on a single nanocarrier can thus benefit from the rapid and transient expression pattern of mRNA, and the adjustable, delayed yet sustained expression of pDNA, creating temporally-resolved expression patterns for one or more transgenes.

Until now, only a very limited number of studies have been dedicated to the development of NA delivery systems capable of successful co-transfection with different species of protein-encoding NA polynucleotides such as mRNA and pDNA[293–295]. From such studies even fewer focus on the kinetics of expression of the different NA species from such systems. Carriers dedicated to mRNA delivery, most famously LNPs, may not be eligible for pDNA delivery, as they lack nuclear translocation capabilities and would hence produce a transfection pattern highly aberrant and reliant on the target cell cycle[296].

In the current study, we tried to optimize our previously described system for the co-delivery of pDNA and mRNA, we explore exchanging the protamine coat for a lipid-based coat featuring the lipid composition of Onpattro's LNPs. Following an initial transfection scanning that demonstrates the superiority of protamine coated to the lipid-coated system, the impact of varying number of thermal stabilization cycles or coat to core mass ratio on particle properties and in-vitro transfection is assessed. Eventually, the capability of the protamine-coated system to temporally resolve the expression of fluorescent reporter proteins encoded by the co-loaded NA moieties.

3.3. Methodology

3.3.1. Materials

Gelatin GELITA® MedellaPro® <=100, porcine gelatin, 228g Bloom, pharmaceutical-grade was purchased from GELITA® Deutschland GmbH, Eberbach, Germany. Protamine sulfate was purchased from Sigma-Aldrich, Darmstadt, Germany. Plasmid DNA encoding AmCyan fluorescent protein (pAmCyan1-C1) was purchased from Clontech Laboratories Inc., Mountain View, CA, USA. Subcloning Efficiency™ DH5α E. coli competent cells were purchased from Invitrogen, Thermo Fisher Scientific, Darmstadt, Germany, Qiagen EndoFree Plasmid Mega Kit was purchased from Qiagen, Hildesheim, Germany.

CleanCap® mCherry mRNA was purchased from Tri-Link BioTechnologies LLC, CA, USA. Purified water was obtained from a Milli-Q water purification system (Merck, Millipore) and is referred to as MQ water.

JetMessenger (JetM) and JetPrime (JetP) were purchased from Polyplus-transfection®, Illkirch, France. Cholesterol was purchased from Sigma-Aldrich Darmstadt, Germany. DLin-MC3-DMA was purchased from MedChemExpress (New Jersey, USA), DMG-PEG2000 was purchased from and DSPC was a kind gift from Lipoid GmbH (Ludwigshafen, Germany).

Murine dendritic cell line DC2.4 was purchased from Millipore Corporation, California, USA. Cells RMPI-1640, Fetal Calf Serum (FCS), non-essential amino acids (NEAA,100X), HBSS 1X, and HEPES buffer solution(1M) were all purchased from Gibco, Thermo Fisher Scientific, Darmstadt, Germany. β-mercaptoethanol 100X was purchased from Merck, Darmstadt, Germany

3.3.2. Preparation of Protamine coated thermally stabilized gelatin-pDNA coacervates (P-TS-CoAc) and Lipid coated gelatin-pDNA coacervates (L-TS-CoAc)

Gelatin-pDNA coacervate-based cores (CoAc) were prepared as previously reported[297]. Briefly, 3 mg mL^{-1} gelatin type A was dissolved in MQ water at 55˚C. The gelatin solution was then mixed with 100 µg mL^{-1} pAmCyan1 at a ratio of 1:1 v/v at 37˚C by vortexing to final gelatin to pAmCyan1 mass ratio of 30:1 w/w. The cores were then thermally stabilized via four cycles of heating at 55±0.5 ˚C for 30 minutes followed by cooling at 0±0.5 ˚C for 5 minutes to form thermally-stabilized gelatin-pDNA coacervates (TS-CoAc) in the form of anisotropic nanogels. TS-CoAc were then coated with either protamine sulfate or a lipid cocktail composed of Dlin-MC3-DMA: DSPC: Cholesterol: DMG-PEG2000 in the following molar ratios (50%:10.5%:38.5%:1.5%)**(Table 6).**

For the protamine coating of TS-CoAc to produce (P-TS-CoAc), a protamine sulfate solution in MQ water was used, at final gelatin to protamine mass ratio of 4:1 w/w. A staggered herringbone micromixer was used at a mixing ratio of 1:1 v/v and a total flow rate of 2 $mL.min^{-1}$.

For lipid coating, ethanolic solutions of either Dlin-MC3-DMA, DSPC, Cholesterol, DMG-PEG2000 were mixed in the aforementioned molar ratios to a final total lipid concentration of 3.56 mg mL^{-1}. The ethanolic lipid solution was mixed with TS-CoAc in sodium acetate buffer 10 mM, pH 4.2, at a final ratio of 0.3114:1 v/v via vortexing, and a final gelatin to lipid mass ratio of 0.69:1 w/w. For the preparation of LNP controls without TS-CoAc cores, an equivalent mass of the same lipid cocktail was used, yet was mixed

with pAmCyan1 and mCherry in sodium acetate buffer 10 mM, pH 4.2, directly via vortexing. For both L-TS-CoAc and LNP, the final NP ratio was 6, and before cell treatment particles were re-adjusted to physiological pH by mixing with HBSS to a final ratio of 2:5 v/v. mRNA surface loading to either L-TS-CoAc or P-TS-CoAc is performed 15 min before nanocarrier application to cells in transfection experiments, whereas no such step was required for LNPs as the mRNA was already core loaded during initial assembly.

Table 6. *Composition and assembly conditions of mCherry and pAmCyan1 co-loaded lipid or protamine coated thermally stabilized gelatin-pAmCyan1 coacervates*

Sample name	**Lipid coated TS-CoAc (L-TS-CoAc)**	**Protamine coated TS-CoAc**
Core composition	Thermally stabilized pDNA-Gelatin with 4 Heating cycles **(TS_4-CoAc)**	
Coat composition	Dlin-MC3-DMA:DSPC:Cholesterol:DMG-pEG2000 (50%:10.5%:38.5%:1.5%)*	Protamine sulfate (Protamine: Gelatin =1:4 w/w)
NP Ratio (excluding Gelatin Core)	6	na**
Assembly technique	Vortex mixing with lipids' solution	Coat deposition using microfluidic meander chip
pDNA/mRNA w/w	5:1	
Core-loaded NA Cargo	pAmCyan1	
Surface-loaded NA Cargo	mCherry	

*Molar ratios

**Given the heterogeneous molecular weight range of the protamine sulfate component, the calculation of NP ratio was not applicable.

3.3.3. Assessment of particle size, particle size distribution, and zeta-potential of different nanocarriers using Dynamic Light Scattering (DLS)

L-TS-CoAc, as well as different P-TS-CoAc, were assessed for particle size, PDI, and zeta-potential using DLS (Nano-ZS, Malvern Instruments, Worcestershire, U.K.), with 4 mW He−Ne laser at a wavelength of 633 nm and a backscattering angle of 173° at 25 °C using high-resolution mode. Before coating, TS-CoAc was analyzed at a concentration of 775 µg mL^{-1} in MQ water, whereas after lipid coating L-TS-CoAc was analyzed at a concentration of 1997 µg mL^{-1} and in sodium acetate buffer of 10 mM, pH=4.2, whereas P-TS-CoAc were analyzed at varying concentrations of 962.5, 1150 and 1550 µg mL^{-1} for P_4-$TS_{\#}$-CoAc, P_2-$TS_{\#}$-CoAc, P_1-$TS_{\#}$-CoAc, respectively, in MQ water, pH6.1. All P-TS-CoAc nanocarriers were further followed for their colloidal stability as a function of particle size and PDI over 3 weeks at 4˚C.

3.3.4. Comparative assessment of transfection efficiency of L-TS-CoAc, P-TS-CoAc, and LNPs in murine dendritic cell line (DC2.4)

This assessment was done to select the best performing candidate to be involved in the factorial assessment of nanocarrier performance. In brief, the transfection efficiency of P-TS-CoAc and L-TS-CoAc was assessed against LNPs in dendritic murine cell lines (DC2.4). Briefly, cells were initially seeded at a density of 50000 cell/well in 24 well plates and allowed 48h in RPMI-1640 supplemented with FCS (10% v/v), HEPES (1%), NEAA (1%), β-mercaptoethanol (0.0054%)- further referred to as DC2.4 culture medium- at 37°C and 5 % CO_2 to reach approximately 80% confluence. The cells were then incubated with either L-TS-CoAc, P-TS-CoAc, or LNPs in (what? Buffer? Medium without or with FCS?) at concentrations equivalent to 5 µg pAmCyan1 and 1 µg mCherry per well, under shaking at 250 RPM and 37°C for 6h. Following which particle samples were removed, cells were washed twice with HBSS, fed with fresh full medium, and further incubated for 36h at 37°C and 5 % CO_2. Either JetMessenger or JetPrime commercial transfection reagents specialized for mRNA and pDNA, respectively, were used as dual transfection tools for comparison. Where either JetM or JetP was combined with both pDNA and mRNA as per the manufacturer's protocol at final NA doses equivalent to L-TS-CoAC, P-TS-CoAc, and LNPs (5 µg pDNA, 1µg mRNA). Eventually, cells were detached using Trypsin/EDTA, washed twice in HBSS, fixed using 4% paraformaldehyde, and flowcytometrically analyzed (BD LSRFortessaTM Cell Analyzer Biosciences, Heidelberg, Germany) for pAmCyan1 and mCherry transfection efficiency on AmCyan1 and PE-Texas red channels, respectively. Data were analyzed using Flowjo version 10.8.0.

3.3.5. Preparation of P-TS-CoAc for factorial assessment of the impact of varying the number of thermal stabilization cycles and gelatin:protamine mass ratio on particle properties

A design of experiment (DOE) approach was adopted to systematically assess the impact of a varying number of thermal stabilization cycles, and mass ratio of gelatin (core): protamine (coat) content on the particle size, PDI as well as transfection efficiency and level of protein expression in DC2.4. Hence a full factorial design (2^3) was implemented, where CoAc were prepared as previously described and then subjected to either 4, 8, or 12 heating-cooling cycles to obtain TS_4-CoAc, TS_8-CoAc, or TS_{12}-CoAc, respectively. Each of the aforementioned TS-CoAcs (775 µg mL-1) was coated with protamine sulfate at concentrations of either 187.5,375 or 750 µg. mL^{-1} using the previously described microfluidic assembly at final gelatin to protamine ratio of 4:1,2:1 or 1:1, respectively **(Table 7)**

All samples were prepared as singlets with triplicate center point repetitions at 8 thermal stabilization cycles and 2:1 gelatin: protamine (w/w), where the center point combined the intermediate levels of both test parameters. P-TS-CoAcs prepared under different conditions, and their nomenclature is detailed in **(Table 8)**.

Table 7. *Design of experiment (DOE) for assessment of varying assembly conditions on colloidal properties and transfection performance of P-TS-CoAc*

variables	Design levels		
	High	**Intermediate**	**Low**
Number of thermal stabilization cycles	12	8	4
Gelatin: protamine (w/w)	4:1	2:1	1:1

Table 8*. Preparation conditions and nomenclature of P-TS-CoAc series included in the DOE for factorial analysis of the impact of varying number of thermal stabilization cycles and gelatin to protamine ratio on the colloidal properties na d transfection performance of the nanosystem.*

Sample name*	Gelatin: Protamine mass ratio (w/w)	Number of thermal stabilization cycles
P_4-TS_8-CoAc**,***	4:1	8
P_1-TS_{12}-CoAc	1:1	12
P_4-TS_4-CoAc	4:1	4
P_2-TS_4-CoAc	2:1	4
P_4-TS_{12}-CoAc	4:1	12

P_1-TS_4-CoAc	1:1	4
P_2-TS_{12}-CoAc	2:1	12
P_2-TS_8-CoAc	2:1	8
P_1-TS_8-CoAc	1:1	8

*Samples are listed in run order of the model
**$P_{\#}$, (#) is equivalent to gelatin to protamine mass ratio
*** $TS_{\#}$, (#) is equivalent to the number of thermal stabilization cycles

3.3.6. Flow cytometric assessment of the transfection performance of P-TS-CoAc nanocarriers included in the factorial design

Further assessment of the impact of varying P-TS-CoAc preparation parameters on transfection efficiency and protein expression level following different P-TS-CoAc treatments was performed as previously described in section 3.3.5. using DC2.4, with a post-treatment incubation of 48h, following which cells were similarly detached and analyzed.

3.3.7. Flow-cytometric assessment of the kinetics of expression of pDNA and mRNA following DC2.4 treatment with P_4-TS_4-CoAc

To assess the kinetics of mCherry and pAmCyan1 expression in DC2.4 following P-TS-CoAc treatment, P_4-TS_4-CoAc was selected based on its transfection performance in the factorial assessment. Cells were cultured as previously described and then treated with the P_4-TS_4-CoAc at t=0h ,and up to 6h. Five predetermined time points were selected for sample collection and assessment of transfection at 1h,3h,6h, and 24h,33h post particle treatment. As for sample collection at time points of 6h or less, the particle treatment was removed and cells detached and analyzed either at 1h, 3h, or 6h post initial treatment. Meanwhile, for samples remaining in culture past 6h, the particle treatment was removed, samples washed, further incubated in DC2.4 medium then harvested for analysis at 24 or 33h. all samples were harvested and flowcytometrically analyzed as previously described.

3.3.8. Statistical analysis of data

Graph Pad Prism 8 for Windows (Version 8.01, GraphPad Software Inc.) was used for data analysis. Data were generally presented as the mean of individual values, with standard deviation indicated by the error bars. (N) equals the number of experiments, (n) equals the number of technical replicates o per sample in a single experiment. For

longitudinal experiments, two-way ANOVA followed by Tukey's post hoc test was used. For fixed time point experiments one-way ANOVA was followed by Tukey's post hoc test was used. Data were considered statistically significant at a level of significance of $p < 0.05$ (* $p < 0.05$, ** $p < 0.01$, *** $p < 0.001$ and **** $p < 0.0001$).

Design of experiment for factorial assessment of the impact of varying assembly conditions on P-TS-CoAc performance as well as analysis of the designs was performed using Minitab 20.1 (JMP, Buckinghamshire, UK).

3.4. Results and Discussion

3.4.1. Particle characteristics of protamine coated thermally stabilized gelatin-pDNA coacervates (P-TS-CoAc) and Lipid coated gelatin-pDNA coacervates (L-TS-CoAc)

DLS results provided first evidence for successful coating of TS-CoAc with either protamine sulfate (P-TS-CoAc) or the lipid mixture (L-TS-CoAc). Both P-TS-CoAc and L-TS-CoAc displayed increased particle diameters of 257.3±3.3 nm and 273.3±3.2 nm, respectively in comparison to the non-coated TS-CoAc (168±5.8 nm) **(Figure 20-a).** The PDI of both L-TS-CoAc and P-TS-CoAc was higher than TS-CoAc, yet this increase was statistically insignificant in the case L-TS-CoAc which when combined with the particle size results provides a further positive indication of the successful deposition of a lipid coat on TS-CoAc in L-TS-CoAc **(Figure 20-b).** For P-TS-CoAc the core-shell structure was previously confirmed using TEM[297] **(Figure 10-d).** A reversal in zeta-potential from a slightly negative value of -3.6 ±0.8 for TS-CoAc to either 14.9 ±0.6 For L-TS-CoAc or 8.3 ±0.5 for P-TS-CoAc **(Figure 20-c)** could also be a further indication of the successful cationic coat deposition for both nanocarriers**.** Both particle size distributions **(Figure 20-e)**, as well as zeta-potential **(Figure 20-f),** showed monophasic peaks for all particles in high-resolution measurement mode, further indicating a homogenous population of coated TS-CoAc.

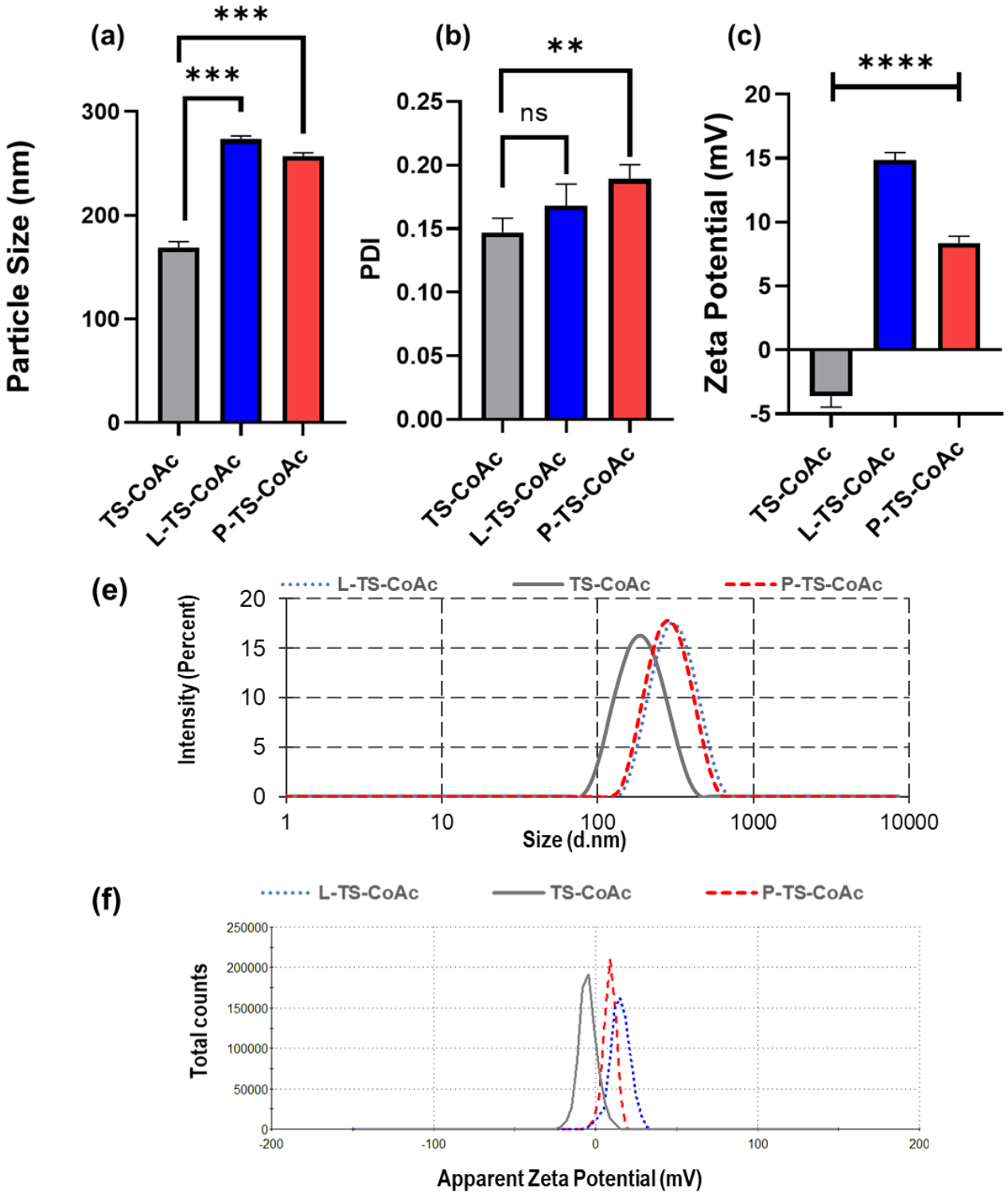

Figure 20. *Dynamic light scattering assessment of (a) particle size(nm) (b) PDI and (c)zeta-potential(mV) of either protamine sulfate coated(P-TS-CoAc), Lipid coated (L-TS-CoAc), and uncoated (TS-CoAc) thermally stabilized gelatin-pAmCyan1 coacervate. (e) Particle size distribution by the intensity of TS-CoAc, P-TS-CoAc, and L-TS-CoAc. (f) Apparent zeta-potential distribution of TS-CoAc, P-TS-CoAc, and L-TS-CoAc.*

3.4.2. In-vitro transfection performance of L-TS-CoAc, P-TS-CoAc, and LNPs in murine dendritic cell line (DC2.4)

In this experiment, the aim was to assess the comparative performance of a lipid coat compared to a protamine coat in the contest of the previously reported core-shell structure in Chapter. II. Where P-TS-CoAc had already displayed superior co-transfectional capacities of fluorescent reporters mCherry and pAmCyan1 compared to an equivalent mass of protamine alone, simply complexed with equivalent doses of the fluorescent reporters. That experiment indicated some degree of merit of the core-shell arrangement to the desired co-transfection. Hence, given the established superiority of ionizable lipid, helper lipid, cholesterol, and pegylated lipid combinations in siRNA and mRNA transfection, I aimed to further explore the capacity of a lipid-coated against a protamine-coated system.

Results demonstrated that in terms of transfection efficiency, 36h following treatment application to DC2.4, JetM, JetP LNPs, L-TS-CoAc, and P-TS-CoAc could all achieve a statistically significant enhancement in % of cells expressing mCherry (%transfection efficiency) **(Figure 21-b)** as well as, the protein expression level (MFI) **(Figure 21-c)** compared to untreated control. While no statistically significant difference in mCherry transfection efficiency between P-TS-CoAc, L-TS-CoAc, and JetM could be observed, LNP demonstrated significantly higher transfection efficiency of mCherry compared to both P-TS-CoAc and JetM. regarding the levels of mCherry expression, all the applied treatments resulted in a statistically significant enhancement in mCherry expression level compared to untreated control. LNP demonstrated a statistically higher expression level of mCherry compared to JetM, L-TS-CoAc, and P-TS-CoAc.

On the other hand, L-TS-CoAc and P-TS-CoAc showed no statistically significant difference in mCherry expression levels from one another. This could indicate comparable endosomal escape capabilities of protamine for P-TS-CoAc[298], and the ionizable[101,104] and helper lipid[122] components of L-TS-CoAc[63], since endosomal escape is the rate-limiting step of mRNA expression[299–301].

As for pAmCyan1 transfection efficiency, none of the treatments except for P-TS-CoAc demonstrated any statistically significant improvement in pAmCyan1 transfection compared to untreated control. As for levels of pAmCyan1 expression, P-TS-CoAc was the only treatment that produced a statistically significant pAmCyan1 expression level compared to untreated control, with 3.4 fold increase in MFI, thus making P-TS-CoAc the only successful system for simultaneous transfection with mRNA and pDNA, highlighting the unique co-transfectional capacity of this nanosystem.

Neither L-TS-CoAc nor LNP could produce an effective expression of their pDNA cargos. The data is in line with what has been previously demonstrated by Kulkarni *et al*. for Dlin-MC3-DMA and DSPC-based LNPs for pDNA delivery [302]. In general, for LNPs, pDNA and mRNA transfection can be improved by using unsaturated helper lipids[302], which have also been reported as more efficient for mRNA transfection[123]. Eventually, however, DSPC was incorporated in all the commercial mRNA transfection systems, possibly due to outperforming unsaturated counterparts in this particular LNP formulations[63]. Both LNPs and L-TS-CoAc also lack any nuclear translocation sequences, which is not the case for protamine. Hence, P-TS-CoAc on the other hand was uniquely capable of the successful co-transfection with pDNA- alongside mRNA- mainly due to the nuclear translocation properties of protamine rendered by four nuclear translocation-like signals present in its structure possesses[240,265].

To conclude, upon comparing the co-transfectional capacity of P-TS-CoAc to either L-TS-CoAc, LNPs, JetM, or JetP, P-TS-CoAc showed a unique potential for incurring successful simultaneous transfection of DC2.4 with both the pDNA and mRNA cargos **(Figure 21-a)**.

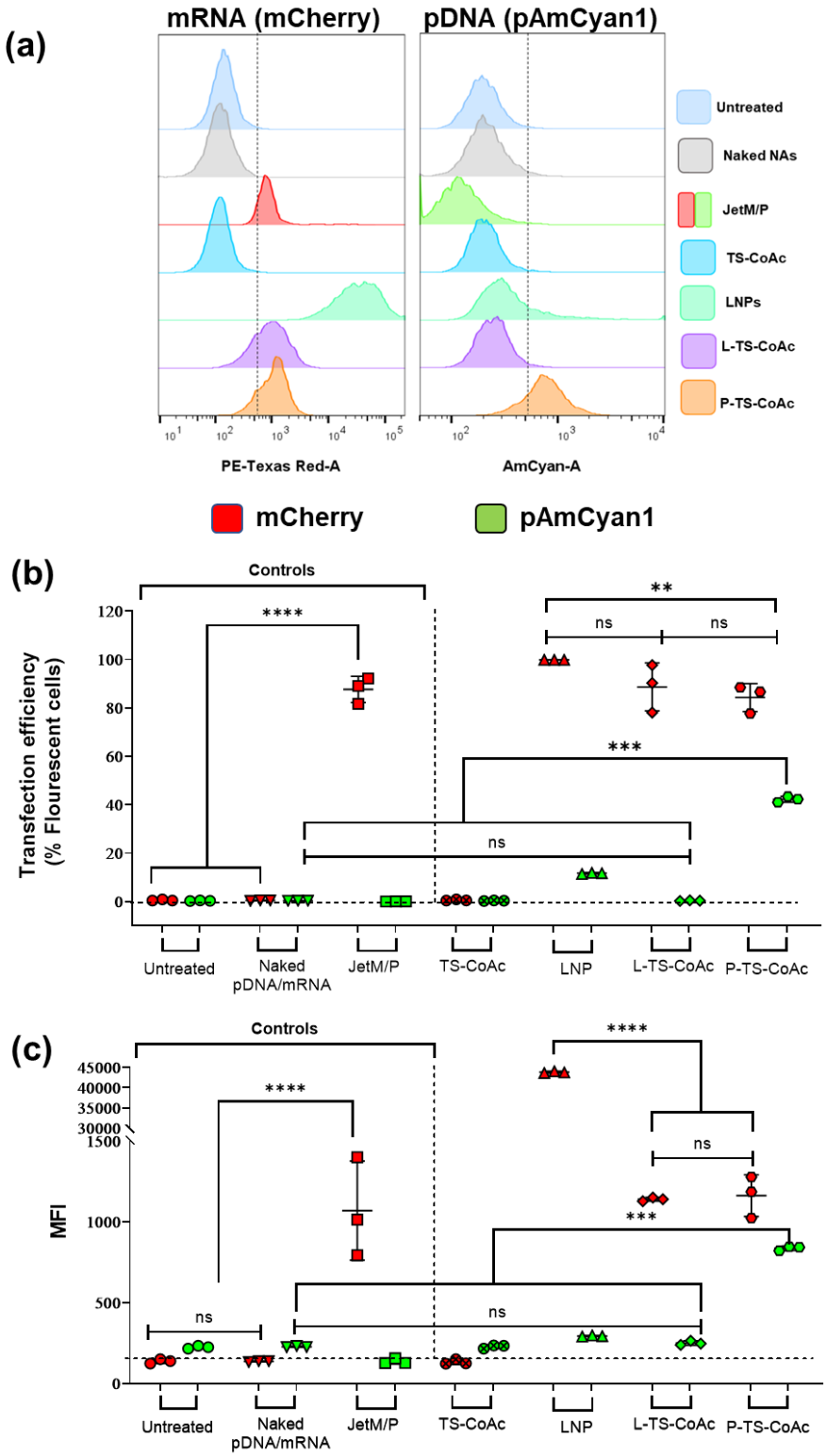

Figure 21. *Flow-cytometric analysis of the impact of varying coat structure on the co-transfectional performnace of TS-CoAc for pDNA (pAmCyan1) and mRNA(mCherry). (a) shift in flourescence intenstity of DC2.4 36h following treatement with different samples and controls on PE-Texas red channel for mCherry treatment(left) and AmCyan channel for pAmCyan1 (right). (b) Transfection efficiency of DC2.4 with either mCherry (red) or pAmCyan1 (green) 36h following treatement with different samples with equivalent doses of 5µg pAmCyan1 and 1µg mRNA, data is displayed as mean±SD (N=1,n=3), dotted line represents background signal of untreated control. (c) Mean flourescence intensity (MFI) of mCherry (red) or pAmCyan1 (green) by DC2.4 following treatement with different samples with equivalent doses of 5µg pAmCyan1 and 1µg mRNA, Data are displayed as mean±SD (N=1,n=3), dotted line represents background MFI of untreated control. **** p < 0.0001; *** p < 0.001; ** p < 0.01; ns = not significant.*

3.4.3. Factorial assessment of the impact of varying P-TS-CoAc assembly conditions on colloidal properties of the nanosystem using DLS

Factorial assessment of the impact of varying the number of thermal stabilization cycles and gelatin to protamine mass ratio revealed that, for the different conditions tested, particles remained within an acceptable and narrow particle size and PDI range as can be observed in (**Figure 22-a**). The PDI values across all P-TS-CoAcs particles featuring the different number of heating cycles and gelatin: protamine mass ratios ranged between 0.105-01.3, whereas particle size ranged between 200-224 nm. Overall varying both the number of heating cycles or gelatin to protamine mass ratio had more or less a negligible impact on the colloidal properties of the system.

Yet when examining the contour plot of particle size (**Figure 22-a**), despite the narrow range of particle size variation, particle size slightly increased at higher gelatin to protamine ratio, which can be resorted to the progressive decrease in the zeta-potential of the system with declining protamine content, and hence lower repulsive forces acting to minimize particles' aggregation overtime.

P-TS-CoAc prepared under different conditions of number of stabilization cycles and protamine: gelatin ratios also predominantly showed good colloidal stability over 2 weeks of storage at 4˚C (**Figure 22-b,c,d,e,f,g**). Except for P2-TS12-CoAc (**Figure 22-d,g**), all the other particle systems showed little change in particle size and PDI during storage. Even the particles that displayed statistically significant changes in either size or PDI did so within a small numerical range and remained within acceptable size and PDI ranges.

3.4.4. Impact of varying nanosystem assembly conditions on its transfection performance

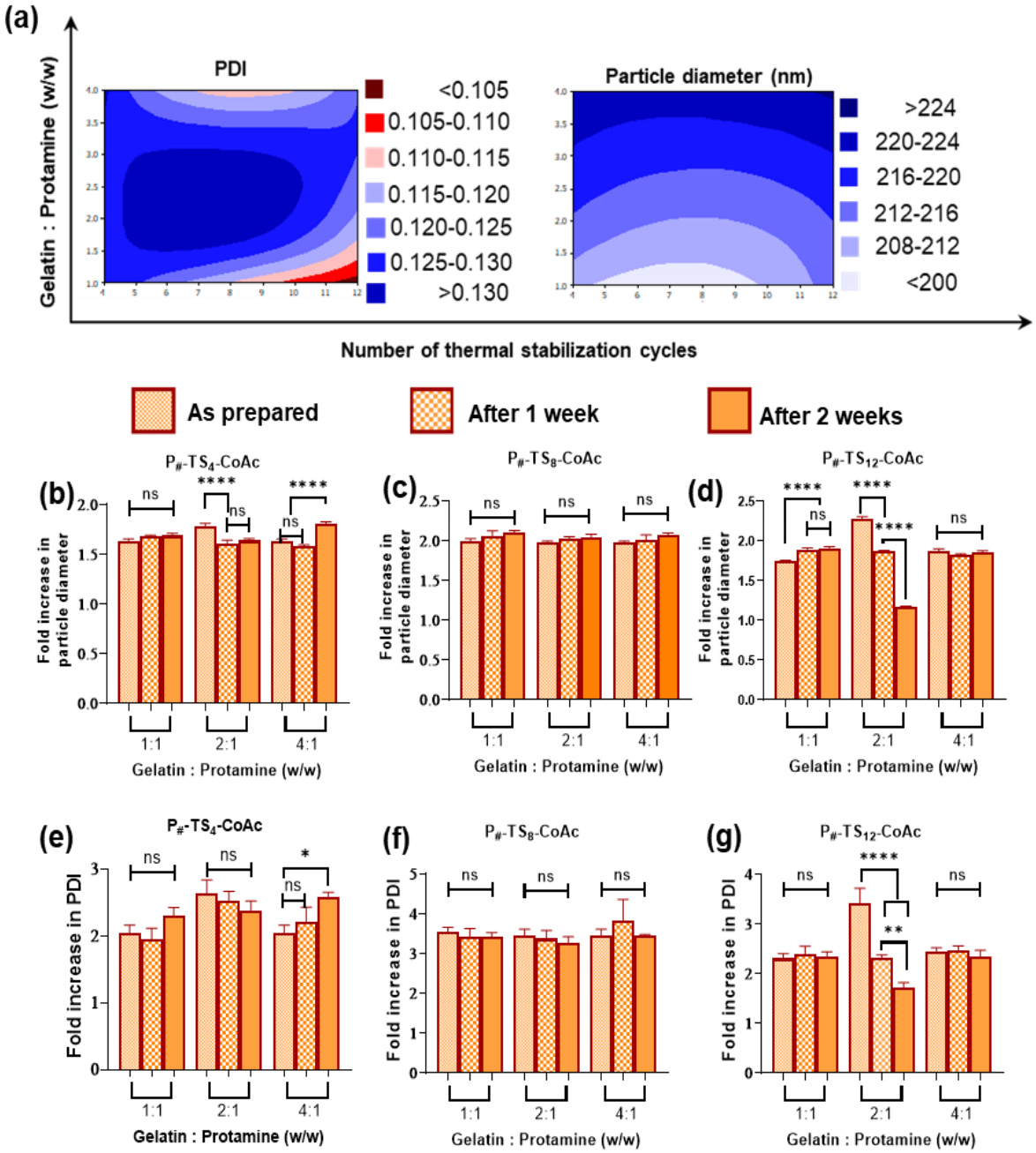

Figure 22. *Factorial assessment of impact of varying number of thermal stabilization cycles or gelatin: protamine mass ratio on particle size and PDI of P-TS-CoAc using DLS. (a) Contour plot of impact of number thermal stabilization cycle(x-axis) and gelatin: protamine ratio (w/w) (y-axis) on PDI (left) and particle diameter (nm) (right) of P-TS-CoAc. (b-d) Fold increase in particle diameter of P-TS-CoAc compared to uncoated TS-CoAc at either 4 (b), 8 (c) or 12 (d) thermal stabilization cycles and varying gelatin:protamine (w/w) ratio (x-axis).(e-f) Fold increase in PDI of protamine coated TS-CoAc compared to*

Factorial assessment of transfection performance of P-TS-CoAc prepared using a varying number of thermal stabilization cycles and gelatin to protamine mass ratios showed mostly higher transfection efficiency of mCherry at lower gelatin to protamine ratio as observed in the top left panel of **(Figure 23-a)**. This could be expected since, at higher protamine concentration, particle uptake as well as endosomal escape, are expected to increase, given the enhanced interaction of the cationic particle component, protamine, with cellular and endosomal membranes, respectively. Whereas the impact of the number of thermal stabilization cycles is less pronounced on mRNA since it is surface-loaded.

While for pAmCyan1, the highest transfection efficiency could be achieved either at higher gelatin to protamine ratio and an intermediate number of thermal stabilization cycles or at a higher number of thermal stabilization cycles as well as lower gelatin to protamine ratio. A lower number of thermal stabilization cycles lead to lower pAmCyan transfection efficiency across the different gelatin to protamine ratios **(Figure 23-a bottom left panel).** These trends were also largely maintained for levels of AmCyan1 expression **(Figure 23-a, bottom right panel).** We hypothesize that the increase in the number of thermal stabilization cycles may be accompanied by an increase in the frequency of electrostatic and hydrogen bonding interaction points between gelatin and pDNA. This delays pDNA release from the core and its availability for nuclear translocation in conjunction with protamine. Simultaneously, the protamine content of the system is being continually depleted following cellular uptake via proteolytic digestion whether before or following the endosomal escape. Thus at a lower number of thermal stabilization cycles, the rapid pDNA release from the system still allows high transfection efficiency as it coincides with less protamine degradation time, and hence more abundant protamine for pDNA sequestration and nuclear translocation. Whereas at a higher number of thermal stabilization cycles, the delayed pDNA release may require to be coupled with higher protamine content in the particle, to allow enough residual protamine at that late time, for mediating pDNA transfection still. As for lower thermal stabilization cycle number, the reduced transfection efficiency across different gelatin to protamine mass ratios may be due to early pDNA release prior to endosomal escape.

Generally, the highest expression of levels of both mCherry and pAmCyan1 were observed at the highest number of thermal stabilization cycles and lowest gelatin to protamine ratio. This can largely be resorted to the higher NP ratio incurred by the higher protamine content for both NAs, as well as the superior shielding effect against nucleases in the case of the more stabilized pDNA. P_1-TS_{12}-CoAc showed the highest levels of both transfection efficiency and protein expression for both mCherry and pAmCyan1 among all P-TS-CoAc. Yet, the range across which the particle performance was varied was rather narrow ranging from 98.5-99.5% for mCherry transfection efficiency, 82%-96% for pAmCyan transfection efficiency, as well as for MFI which ranged from 2550-2800 for mCherry expression and 580-660 for pAmCyan1 expression. Taking such ranges into account alongside the time and material consumption required for either P_4-TS_4-CoAc and P_1-TS_{12}-CoAc, we opted for P_4-TS_4-CoAc for subsequent experiments.

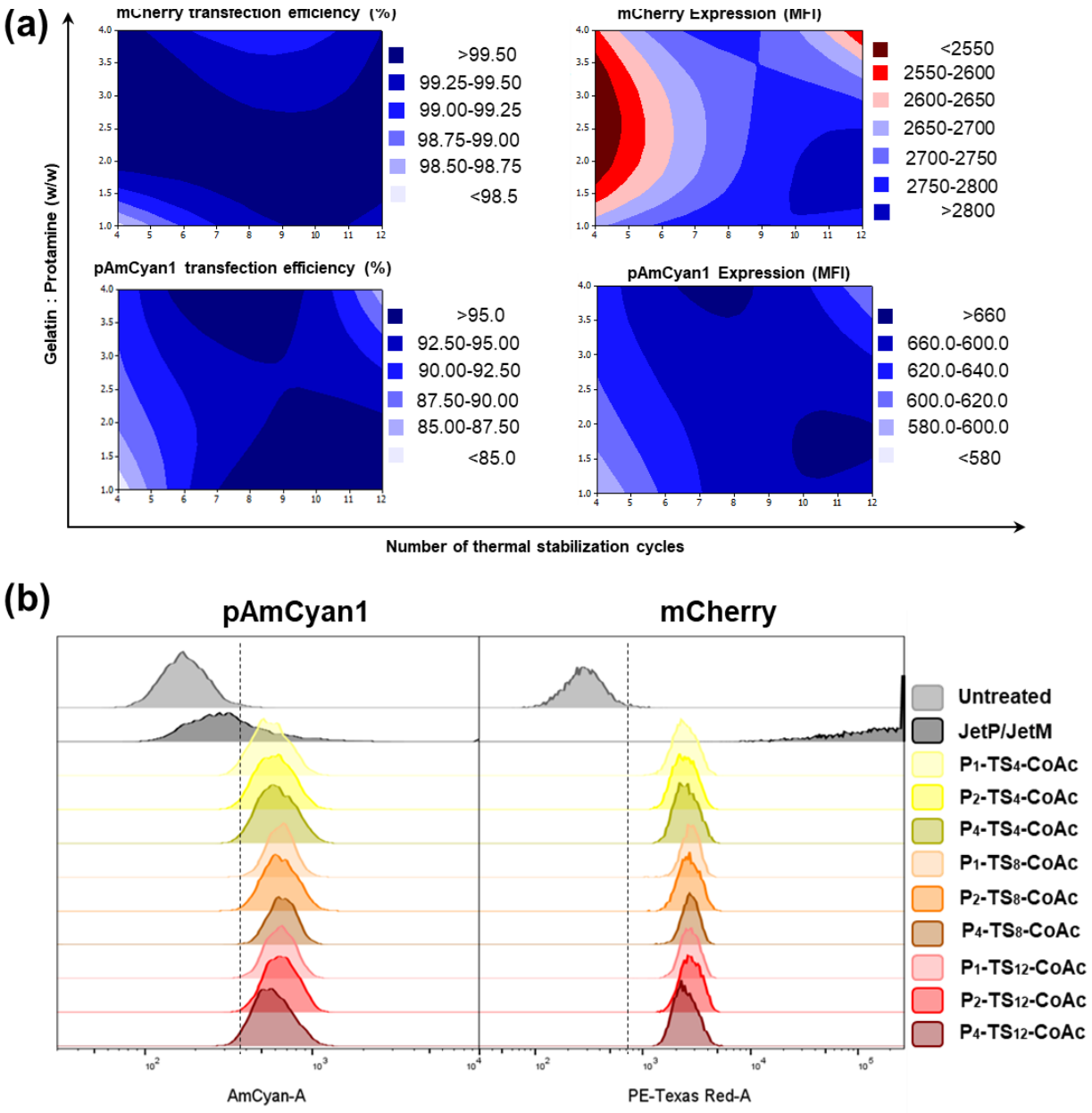

Figure 23. *Factorial assessment of impact of varying number of thermal stabilization cycles or gelatin: protamine mass ratio on the co-transfectional performance of different P-TS-CoAc for 5µg pDNA (pAmCyan1) and 1µg mRNA(mCherry) in DC2.4. (a) contour plot of impact of number thermal stabilization cycle(x-axis) and gelatin: protamine ratio (w/w) (y-axis) on mCherry transfection efficiency (top-left), mCherry MFI (top-right) pAmCyan transfection efficiency (bottom left), AmCyan1 MFI (bottom right) (b) Shifts in flourescence intenstity of DC2.4 48h following treatment with commercial control JetM and JetP and with different P-TS-CoAc samples on AmCyan channel for pAmCyan1 and PE-Texas red channel for mCherry treatment (right).*

3.4.5. Assessment of the kinetics of expression of pDNA and mRNA following DC2.4 treatment with P_4-TS_4-CoAc

Following the factorial assessment of the impact of varying P-TS-CoAc assembly conditions on transfection efficiency and level of protein expression in DC2.4, we proceeded to assess the time-resolved expression of mCherry and pAmCyan1 in DC2.4 over 33h **(Figure 24-a).** P_4-TS_4-CoAc was selected for this experiment given its favorable assembly conditions as well as high pAmCyan1 and mCherry transfection efficiencies of 90.1% and 99.7%, respectively in DC2.4 48h following original particle treatment (**Figure 21**).

During the first 6h following P-TS-CoAc application, no statistically significant increase in transfection efficiency could be detected for either mCherry or pAmCyan1 (**Figure 24**-b). Yet, in terms of protein expression levels, a time-resolved expression of the two nucleic acid cargos mCherry and pAmCyan1 could be observed in DC2.4 **(Figure 24-c).** A detectable statistically significant increase in the level of mCherry expression could be detected as early as 3h after P-TS-CoAc application, while no such detectable expression could still yet be observed for pAmCyan1 at the same time point. The first discernible expression of AmCyan1 was yet to follow at 6h. This was hence the first detectable difference in expression kinetics of the co-delivered mRNA and pDNA observed as an earlier expression onset from mRNA and a later one from pDNA.

After 24h, the transfection efficiency of mRNA in terms of the percentage of fluorescent cells had already reached a maximum of 91.9%±1.15, and later decreased slightly to 89.3% ±2.5 at 33h **(Figure 24-b)**; a similar trend was observed for the total level of mCherry protein expression as indicated by the overall mean fluorescence intensity (MFI) **(Figure 24-c).** Conversely, pDNA expression was delayed and only reached approximately half the transfection efficiency of mRNA at 24h with 42.5±2.5%, and even continued to increase to 54.63±2.95 at 33h, indicating some both delayed and prolonged expression-time profile relative to its mRNA co-cargo.

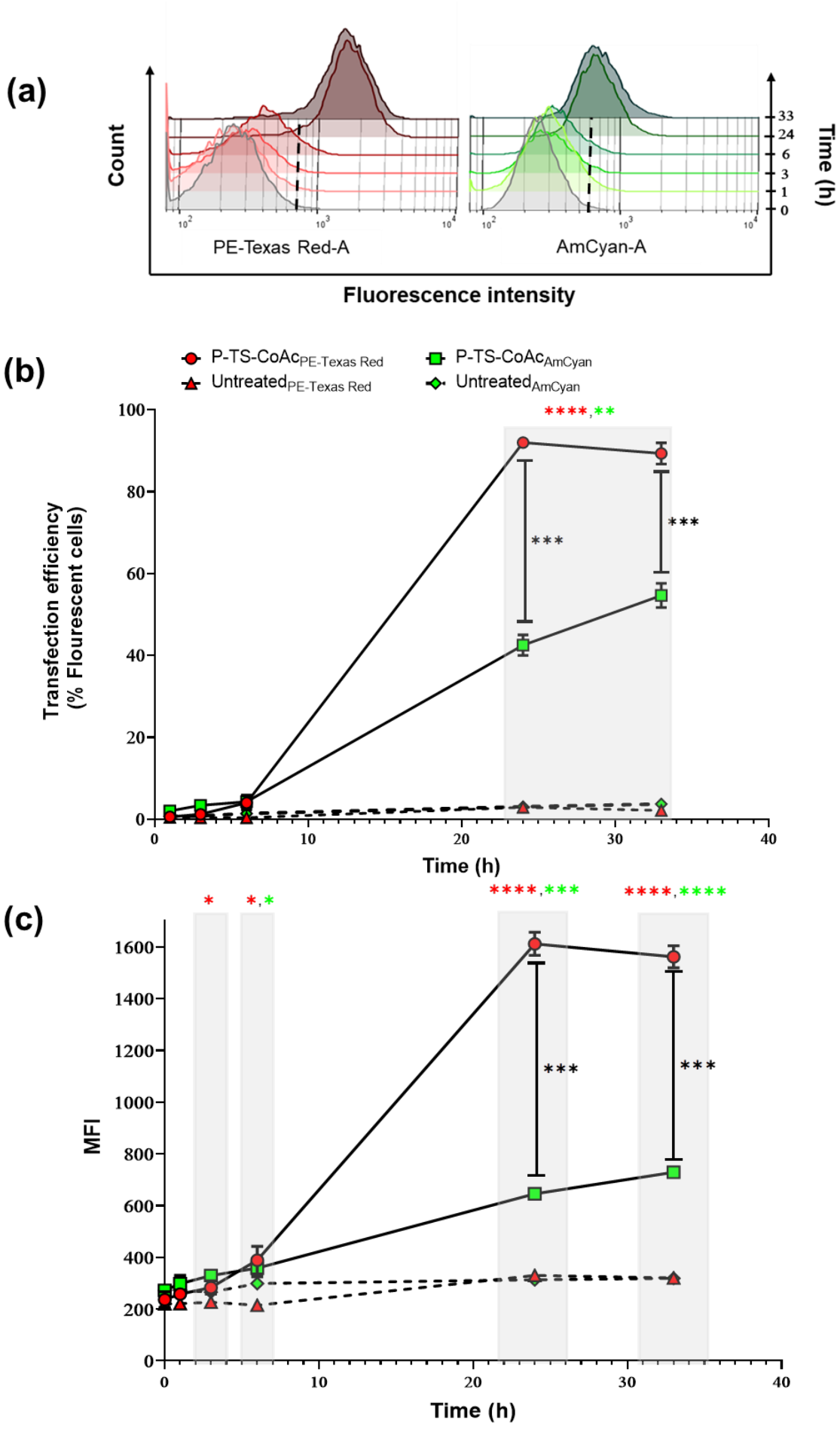
(a)
Count
PE-Texas Red-A
AmCyan-A
Time (h)
33
24
6
3
1
0
Fluorescence intensity
(b)
P-TS-CoAcPE-Texas Red
Untreated PE-Texas Red
P-TS-CoAcAmCyan
Untreated AmCyan
Transfection efficiency (% Flourescent cells)
****,**
***
***
Time (h)
(c)
*
,
****,***
****,****
MFI
***
***
Time (h)

Figure 24. *Expression kinetics of mCherry (mRNA, 1µg) and pAmCyan1 (pDNA,5 µg) in DC.4 over 33h, following P_4-TS_4-CoAc application. (a) The shifts in fluorescence intensity of DC2.4 at 0,1,3,6,24, and 33h following P_4-TS_4-CoAc application on PE-Texas red channel for mCherry treatment (left) and AmCyan channel for pAmCyan1(right). (b) % cells expressing fluorescent reporter protein from mCherry (red) and pAmcyan1(green) in DC2.4 over time up to 33h following P_4-TS_4-CoAc application (solid lines) compared to untreated control (dotted lines). (c) Level of mCherry or AmCyan expression mCherry (red) and pAmcyan1(green) in DC2.4 over time up to 33h following P_4-TS_4-CoAc application (solid lines) compared to untreated control (dotted lines). Shaded areas indicate time-points where a significant difference existed between P_4-TS_4-CoAc treatment and untreated controls, with levels of significance indicated with either red (*) for mCherry or green (*) for pAmCyan1. Levels of significance of the statistical difference between mCherry and pAmCyan-1 expression from P-TS-CoAc at similar time points are indicated by black (*). Data are displayed as mean±SD (N=1,n=3), and the dotted line represents the background MFI of untreated control. **** $p < 0.0001$; *** $p < 0.001$; ** $p < 0.01$, * $p < 0.05$; ns = not significant.*

3.5. Conclusion

The aim of this study was to investigate thermally stabilized gelatin-pDNA complex coacervate (TS-CoAc), as a suitable core structure for cationic coating and consequent surface loading with mRNA, as a co-transfectional tool for pDNA and mRNA. We could demonstrate the superiority of nuclear-translocating signal containing protamine coat which resulted in a unique co-transfection capacity for this system which remained unattainable by neither LNPs nor lipid-coated TS-CoAc. In contrast, LNPs or lipid-coated TS-CoAc co-loaded with mRNA and pDNA and featuring a lipid mixture comprising ionizable lipid Dlin-MC3-DMA, DSPC, DMG-PEG2000, and cholesterol could only cause mRNA transfection, whereas none was detected for pDNA. Protamine-coated TS-CoAc on the other hand displayed high pAmCyan1 and mCherry transfection efficiencies of 90.1% and 99.7%, respectively in DC2.4 48h following original particle treatment.

A factorial assessment of the impact of varying the two main assembly conditions of P-TS-CoAc, namely; the number of thermal stabilization cycles of the gelatin-pDNA core and the mass ratio between gelatin core content and protamine coat content revealed that neither factor could dramatically impact the transfection performance of the nanosystem.

The most interesting feature of the system remains to be its ability to instigate a different time course of protein expression from its dual nucleic acid cargos, where mRNA produces an early, strong, and transient expression, while pDNA produces a delayed yet prolonged-expression. The possibility to realize different expression kinetics for protein-encoding polynucleotides could become useful within an NA-based vaccination context, for example, optimizing the co-delivery of NA-based antigens and adjuvants, where time resolution between antigen and adjuvant expression can strongly affect vaccine safety and efficacy.

Chapter IV: In-house Preparation, Quality, and In-vitro Performance assessment of pDNA and mRNA Encoding CCL4 and CCR7 as NA-based Adjuvant Candidates

4.1 Abstract

As vaccination is undergoing a paradigm shift from conventional to nucleic acid (NA) based vaccines, a similar approach may be extended to adjuvantation strategies. Hence, the current study aims to investigate the possibility of delivering pDNA or mRNA encoding Chemokine Receptor 7 (CCR7) or Chemokine Ligand 4 (CCL4) using the previously described P-TS-CoAc nanocarrier system.

At first, mRNA encoding for either CCR7 (mCCR7) or CCl4 (mCCL4) was transcribed in-vitro from linearized plasmid templates of CCR7(pCCR7) and CCL4(pCCL4), respectively. Product quality and purity were investigated using agarose gel electrophoresis which demonstrated successful production of mCCL4, while mCCR7 production was not feasible. In-vitro transfection of pCCR7 and mCCR7 in murine dendritic cell line DC2.4 was investigated using fluorescently labeled anti-CCR7 staining followed by flow cytometric analysis, where only DC2.4 electroporated with pCCR7 showed successful CCR7 expression on DC2.4 at approximately 10% transfection efficiency 24h post-treatment, whereas DC2.4 treated with pCCR7 or mCCR7 delivered using either commercial controls or P-TS-CoAc failed to express any detectable CCR7 expression. CCL4 In-vitro expression was investigated in DC2.4 as well as A549 cell lines. Flow-cytometric assessment of CCL4 content in the supernatant of cells electroporated with either pCCL4 or mCCL4 showed successful expression of CCL4 after 6h in DC2.4, while expression in A549 was negligible. DC2.4 treated with the NAs delivered using either commercial controls or P-TS-CoAc showed successful mCCL4 and pCCL4 expression with commercial transfection reagents at 3h and 22h post-treatment, respectively, whereas no discernible expression was achieved using either mCCR7 or pCCR7 loaded on P-TS-CoAc.

To follow, chemotactic migration studies were performed using a combination of microfluidic and live-cell imaging techniques to assess the chemoattractive potential of pCCL4 and mCCL4 electroporated DC2.4 to untreated immature DC2.4, yet no chemoattractive effect could be detected using this setting. In conclusion, this study could be a stepping stone for the endogenous-adjuvantation concept where NA-encoded antigens and adjuvants can be co-delivered on a singular nanocarrier and possibly expressed in a time-resolved manner, but further optimization is still required for the nanocarrier to realize such application.

4.2. Introduction

The quest for effective co-delivery of antigens and adjuvants in the realm of vaccination is now gaining more momentum than ever[303], where the COVID-19 Pandemic brought issues such as maximizing single vaccine dose safety, efficacy, and vaccine dose sparing to the center stage of public and scientific debate. For decades, adjuvantation has been an integral approach to achieving such objectives[1]. Three adjuvantation strategies are currently in focus;(i) the use of nanocarriers with immunostimulatory components such as MF59, AS03, AS04, and LNPs featuring ionizable or cationic lipids[304,305], (ii) antigen-adjuvant conjugation[306], and (iii) co-delivery of NA-encoded immunomodulators[204] in combination with NA-encoded antigens. In this study, we investigate the capacity of a recently reported nanocarrier (P-TS-CoAc)[297] for co-delivery of surface-loaded mRNA and core-loaded pDNA to deliver mRNA or pDNA encoded Chemokine Ligand 4 (CCL4/MIP-1ß) or Chemokine receptor 7 (CCR7) **(Figure 25).**

Chemokine Ligand 4 (CCL4) also referred to as Macrophage Inflammatory Protein-1ß (MIP-1ß), is a chemokine capable of mobilizing a range of innate and adaptive immune effector cells to inflammation sites, and hence we believe could be valuable adjuvant candidate[307]. Originally secreted by macrophages it can attract natural killer cells, monocytes, neutrophils, immature DCs (as part of the innate immune component), but also B and T lymophocytes[308–310].

CCR7 is G-protein coupled receptor expressed mainly by mature and semi-mature DCs, naïve T-cells, and B-cells, as well as central memory T-cells. It plays a central role in mobilizing these key players in the adaptive immune response along the chemotactic gradient of CCR7's two ligands CCL19 and CCL21 towards primary lymphatic organs[311]. This major role played by CCR7 in DC mobilization has been repeatedly confirmed by the inability of dermal CCr7 knockout DCs to migrate from their original tissue to the draining lymph nodes following in-vivo mobilization induced by fluorescein isothiocyanate (FITC) skin staining[312]. Also, BMDCs of CCR7-deficient mice failed to migrate to the draining lymph nodes upon their intra-tracheal instillation or subcutaneous injection[313,314]. Upon being activated by CCL19, CCR7 expressed by licensed or semi-mature DCs can allow their full maturation by enhancing their cytokine production of IL-3, IL-6, and TNF, so that they reach T-cells in the lymph node fully ready for their activation [315]. Another role for it, during the later stages of adaptive immune response in secondary lymphoid organs, is the ability of CCR7 to mediate the exchange of B-cells and CD4+ T-helper cells between the B and T-cell regions, thus promoting their interaction and hence resulting in more efficient humoral immunity[316].

The hypothesis for adjuvant action in the case of CCL4 expressed either by or in the vicinity of antigen-expressing APCs, is that CCL4 can attract larger numbers of CD8+, CD4+ among other adaptive immune effectors ready to interact with the APCs and propagate a stronger adaptive immune response. For CCR7 on the other hand, its overexpression on antigen primed DCs can promote higher sensitivity to the chemotactic

gradients of its ligand and promote faster migration to lymphatic sites and the ensuing immuno-synapsing, thus again promoting potentially faster and stronger immune response. From the aforementioned roles of CCL4 and CCR7, it is evident in theory, that both candidates if co-delivered as NA-encoded formats with an NA-encoded antigen, on a single carrier that would allow the delayed expression of the adjuvant (from a core loaded pDNA) to the antigen (from a surface loaded mRNA), can promote and improve the quality of the resulting adaptive immune response. Hence, we opted to investigate the potential of delivery of NA-encoding CCR7 and CCL4 on P-TS-CoAc.

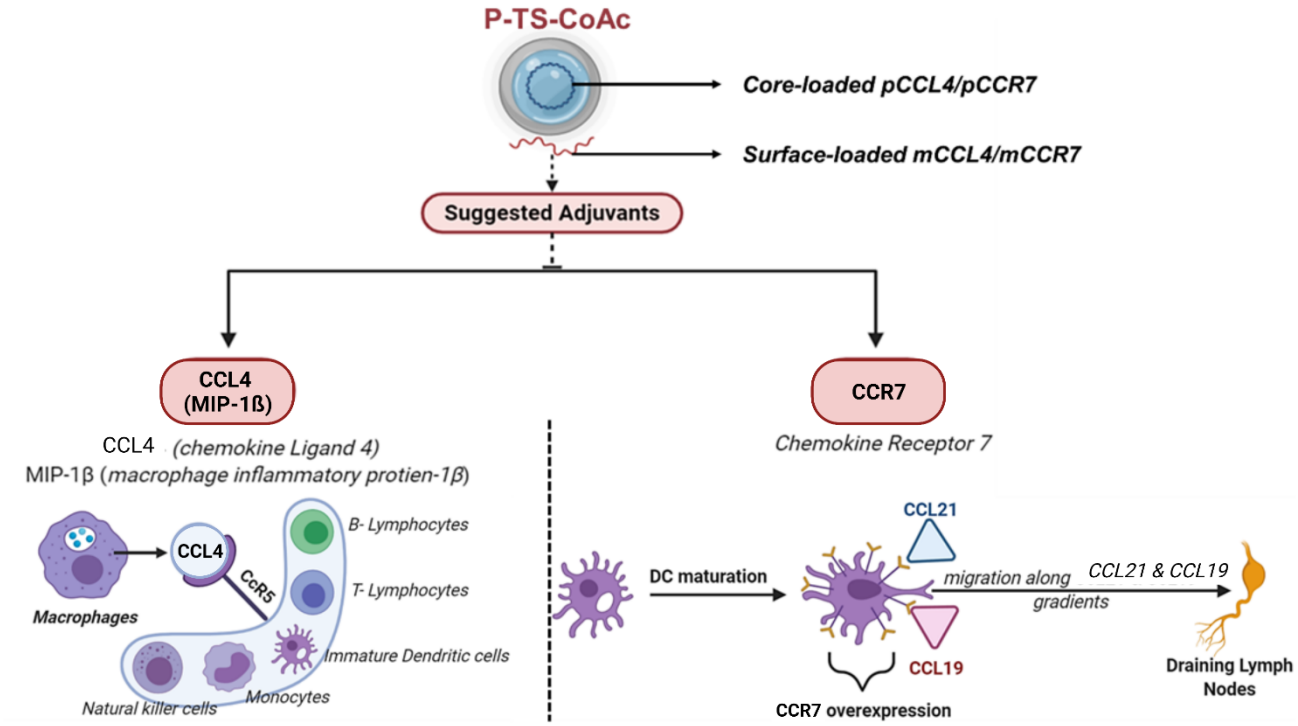

***Figure 25**. Graphic illustration of the modes of action of the selected adjuvant candidates Chemokine Ligand 4 (CCL4) and Chemokine Receptor 7 (CCR7), the NA-formats coding for them and their loading location on P-TS-CoAc.*

4.3. Methodology

4.3.1. Materials

Gelatin GELITA® MedellaPro® <=100, 228g Bloom, porcine gelatin of pharmaceutical-grade was obtained from GELITA® (Deutschland GmbH, Eberbach, Germany). Protamine sulfate was obtained from Sigma-Aldrich (Darmstadt, Germany). DNA plasmids encoding for murine CCL4 (pCMV3-mCCL4-untagged) and CCR7 (pCMV3-mCCR7-untagged) were purchased from Sino Biological Europe GmbH (Eschborn, Germany). DH5α E. coli competent cells of subcloning efficiency were obtained from Invitrogen, Thermo Fisher Scientific (Darmstadt, Germany). Qiagen EndoFree Plasmid Mega Kit was obtained from Qiagen (Hildesheim, Germany). CleanCap® mCherry mRNA was obtained from Tri-Link BioTechnologies LLC (CA, USA). Purified water was supplied by a Milli-Q water purification system (Merck,

Millipore) and will be referred to as MQ water. Commercial transfection reagents JetMessenger (JetM) for mRNA and JetPrime (JetP) for pDNA were obtained from Polyplus-transfection® (Illkirch, France). HiScribe™ T7 Quick High Yield RNA Synthesis Kit, Vaccinia capping system, mRNA Cap 2'-O-methyltransferase system, E. coli poly (A) polymerase tailing system, Monarch® RNA Cleanup Kit (50 µg) were all purchased from New England Biolabs GmbH (Frankfurt am Main, Germany). Restriction enzymes XbaI, PdiI, KpnI, SmaI (10 U/ µL) as well as their working buffers were all purchased from Thermo Fisher Scientific (Darmstadt, Germany).

Research-grade agarose was obtained from Serva® (Heidelberg, Germany). Disodium dihydrate ethylenediamine tetra-acetic acid (EDTA-Na_2) was obtained from Roth GmbH + Co. KG (Karlsruhe, Germany). DNA Ladder 250-10000 bp was obtained from PEQLAB Biotech GmbH (Erlangen, Germany). 1kb DNA ladder was obtained from Promega GmbH (Walldorf, Germany). Ethidium bromide 10 mg mL^{-1} was obtained from Sigma-Aldrich (Darmstadt, Germany). Bovine Serum Albumin (BSA), DNase I, DNase I buffer, 50 mM EDTA, DNA loading dye- SDS (6x), and Ribolock were obtained from Thermo Fisher Scientific (Darmstadt, Germany). Purecol (Bovine collagen type I solution, 3.1 mg/mL) was obtained from CellSystems (Troisdorf, Germany).

A549 cells (human lung carcinoma cell line, No. ACC 107) were supplied by DSMZ GmbH (Braunschweig, Germany). Murine dendritic cell line DC2.4 was obtained from Millipore Corporation (California, USA). RMPI-1640, Fetal Calf Serum (FCS), non-essential amino acids (NEAA,100X), Accutase, 10X MEM, 7.5% $NaHCO_3$, and HEPES buffer solution(1M) were all obtained from Gibco, Thermo Fisher Scientific (Darmstadt, Germany). β-mercaptoethanol 100X was purchased from Merck (Darmstadt, Germany). Recombinant Mouse CCL19 (MIP-3ß) was purchased from Tonbo Biosciences (San Diego, CA, USA). LEGENDplex™ Mouse CCL4 (MIP-1β) Capture Bead B5 (13X), LEGENDplex™ Mouse Proinflammatory Chemokine Detection Antibodies, LEGENDplex™ Mouse Proinflammatory Chemokine Standards, PE anti-mouse CD197 (CCR7) Antibody, TruStain FcX™ PLUS (anti-mouse CD16/32) Antibody, and PE Rat IgG2a, κ Isotype Ctrl antibody were all purchased from Biolegend (San Diego, CA, USA). µ-Slide Chemotaxis were obtained from Ibidi GmbH (Gräfelfing,Germany).

4.3.2. Plasmid propagation and extraction

pCMV3-mCCL4-untagged and pCMV3-mCCR7-untagged, briefly referred to as pCCL4 and pCCR7, respectively, as well as pUC19, were initially propagated in-house **(Figure 26).** Where 100 ng of each plasmid was transformed into Subcloning Efficiency™ DH5α E. coli competent cells by gentle mixing with 50 µL cell suspension. The mixture was left on ice for 30 min, after that the cells were heat-shocked at 42˚C for 30 sec then returned to the ice for 2 minutes. Antibiotic-free LB-Broth (950 µL), pre-warmed to 37 ˚C was used to dilute the transformed cells, and they were further incubated for 1hr at 37 ˚C, and 225 RPM shaking. The transformed cell suspension (20 µL) was streaked on Ampicillin containing LB Agar and further incubated at 37 ˚C, 5% CO_2 for 16h.

Discreet colonies were picked off the LB Agar and used to set pre-cultures in 1mL Ampicillin containing (50 µg/mL) LB-Broth containing. These pre-cultures were incubated for 1 h at 37 ˚C, 225 RPM. The pre-cultures with the highest optical density were then used to inoculate 500 mL of the same medium followed by overnight incubation at 37 ˚C, 5% CO_2, and shaking at 225 RPM. The plasmid containing bacteria was later collected from its suspension by centrifugation at 300 g for 20 min at 4 ˚C and pCCR7, pCCL4, or pUC19 were extracted from its expressing bacteria using EndoFree Plasmid Mega Kit (Qiagen, Hildesheim, Germany) as per the manufacturer's instructions.

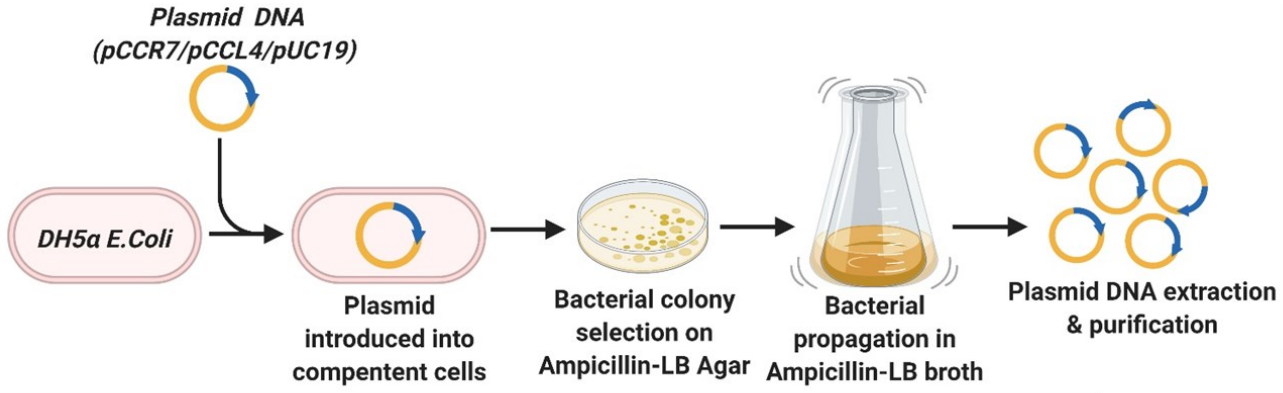

***Figure 26**. In-house preparation scheme of pCCR7, pCCL4 showing pCCR7, pCCL4, and pUC19 transformation in DH5α E. coli competent cells, propagation, and extraction*

4.3.3. pCCR7 and pCCL4 quality assessment

UV-Spectrophotometry

The resulting plasmids were assessed spectrophotometrically for both yield and purity using NanoDrop™ 2000 (Thermo Fisher Scientific, Darmstadt, Germany). Briefly, 1 µL of pDNA solution in TE buffer was exposed to UV light at λ= 260 nm and 280 nm. All measurements were blanked to TE buffer.

Agarose gel-electrophoresis based Restriction-enzyme mapping

Three restriction enzyme digests followed by agarose gel electrophoresis were performed on either pCCL4 or pCCR7 to map the plasmid digestion patterns and hence confirm its identity. The first digest was a single cut to linearize either pCCL4 or pCCR7 using XbaI to confirm the plasmid's full-length integrity. Briefly, 0.5 µg of pDNA was incubated for 1hr at 37 ˚C with 25 U XbaI, followed by XbaI inactivation via heating the reaction mixture at 80 ˚C for 10 min. The second digest aimed to confirm the integrity of the pCMV3-backbone of pCCL4 and pCCR7, hence 0.5 µg of pDNA was incubated for 1hr at 37 ˚C with 25 U PdiI, followed by restriction enzyme inactivation as previously described. The third digest aimed to confirm the identity of CCL4 and CCR7 gene inserts using double digestion of each 0.5 µg of pDNA using 25 U XbaI and 100 U KpnI, for 1hr at 37 ˚C, followed by restriction enzymes' inactivation as previously described. All reactions were performed in 1x Tango buffer (Thermo Fisher Scientific, Darmstadt,

Germany). pUC19 was also linearized and checked using XbaI in a similar procedure as pCCR7 and pCCL4.

Restriction enzyme(s) digests were then combined with DNA loading dye (1x) and run on a 1.3% Agarose gel, at 90 mV for 90 mins, against 250-10000 bp DNA Ladder, and later visualized under UV-light (Fusion FX7 imaging system, Peqlab, Erlangen, Germany).

4.3.4. In-vitro transcription (IVT) of mCCL4 and mCCR7

mCCR7 and mCCL4 were in-vitro transcribed in-house with sequential capping and tailing steps as indicated in **(Figure 27).**

pDNA template linearization

pCCL4 and pCCR7 were both linearized and used as templates for in-vitro transcription (IVT) of their respective mRNA open reading frame $mCCL4_{ORF}$ and $mCCR7_{ORF}$, respectively. Briefly, 10 µg of either plasmid were linearized with 50 U XbaI, the digestion was inactivated by heating at 65˚ C for 20 minutes.

IVT of Open Reading Frame (ORF)

After linearization, the linearized pDNA template was used to produce the respective ORF of mRNA using HiScribe™ T7 Quick High Yield RNA Synthesis Kit, as per the manufacturer's instructions. In-vitro transcription reaction proceeded for 4h at 37˚C, followed by pDNA template digestion using 1 U DNase I (Thermo Fisher Scientific, Darmstadt, Germany) and incubation at 37˚ C.

ORF Capping

A Cap 1 structure was added to the resulting $mRNA_{ORF}$, by incubating 50 µg $mRNA_{ORF}$ with 5 µL of 10mM GTP, 5 µL 4mM S-adenosylmethionine, 50 U Vaccinia capping enzyme, 250 U mRNA Cap 2'-O-Methyltransferase for 60 min at 37˚C.

ORF tailing

The capped $mRNA_{ORF}$ was then tailed in a post-transcription polyadenylation procedure, where the capped $mRNA_{ORF}$ was incubated with 50 U E.coli Poly(A) Polymerase and 10 µl 10mM Adenosine-5'-Triphosphate (ATP).

mRNA product purification

The capped and tailed $mRNA_{ORF}$ were eventually purified using Monarch® RNA Cleanup Kit (50 µg). Capped and tailed $mRNA_{ORF}$ would now be referred to as mCCL4 and mCCR7 throughout the text.

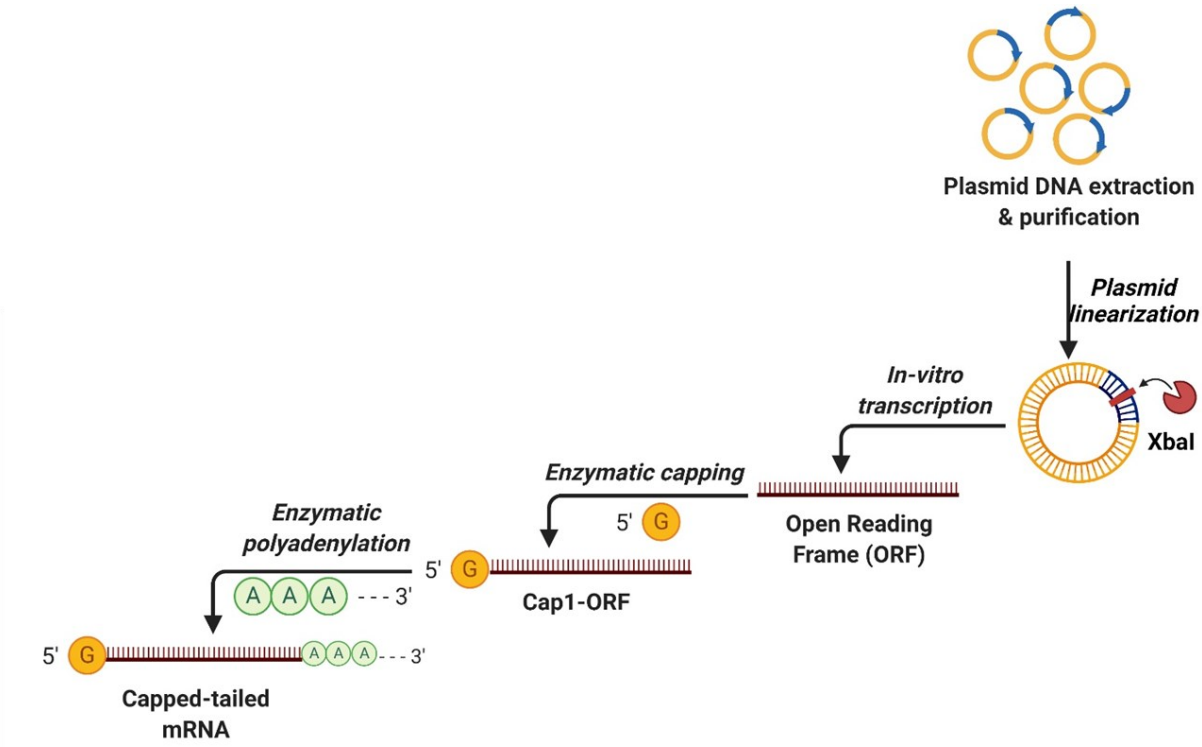

Figure 27. *In-vitro transcription of $mCCR7_{ORF}$ and $mCCL4_{ORF}$ from their corresponding linearized plasmid templates, followed by their capping (Cap1 structure) and tailing (polyadenylation).*

4.3.5. Assessment of mRNA product quality

The quality of the resulting mCCL4 and mCCR7 capped and tailed final product was spectrophotometrically assessed using NanoDrop™ 2000 (Thermo Fisher Scientific, Darmstadt, Germany) for concentration and purity. Also, agarose gel electrophoresis was run for both $mRNA_{ORF}$ on 2% agarose gel, at 90 mV for 90 minutes then the gel was visualized under UV light (Fusion FX7 imaging system, Peqlab, Erlangen, Germany).

4.3.6. Preparation of (P-TS-CoAc) for delivery of either mCCL4 or pCCL4

P-TS-CoAc were prepared as recently reported[297], briefly, gelatin A was electrostatically assembled with pCCR7, pCCL4, or pUC19, then thermally stabilized at 55˚C to form TS-CoAc, the sizes of coacervate cores before and after thermal stabilization were assessed using DLS. This was followed by protamine sulfate coating at gelatin: protamine 5:1 (w/w) and surface loading with mRNA. P-TS-CoAc was prepared using either a pCCL4 or pCCR7 core and no surface loaded mRNA or a non-coding pUC19 core on which mCCL4 or mCCR7 was surface loaded as indicated in **(Table 9).**

Table 9. *Composition of different P-TS-CoAc assembled using in-house prepared pCCL4, pCCR7, pUC19, mCCL4 or mCCR7 mRNA.*

Sample name	pDNA cargo (core-loaded)	mRNA cargo(surface-loaded)
P-TS-CoAc $_{pCCR7}$	pCCR7	_
P-TS-CoAc $_{mCCR7}$	pUC19*	mCCR7
P-TS-CoAc $_{pCCL4}$	pCCL4	_
P-TS-CoAc $_{mCCL4}$	pUC19	mCCL4

*pUC19 was used as a non-coding core-forming plasmid for P-TS-CoAc intended for surface loading of mCCL4 and mCCR7

4.3.7. In-vitro transfection efficiency and rate of in-house produced pCCR7, pCCL4, mCCR7, mCCL4

Electroporation

To assess the functionality of the in-house produced nucleic acids either DC2.4 was used in the case of pCCR7 or DC2.4 and A549 were used for pCCL4 and mCCL4. Cells were initially seeded in 24-well plates at a density of 50000 cells/ well in a medium consisting of RPMI-1640 supplemented with FCS (10% *v/v*) only in case of A549, or the same medium further supplemented with HEPES (1%), NEAA (1%), β-mercaptoethanol (0.0054%) in case of DC2.4. After 48 h incubation at 5% CO_2 and 37°C cells were approximately 80% confluent and ready for electroporation. Immediately before electroporation, cells were detached using 200 µL Accutase for 45 mins, then Accutase activity was quenched using 800 µL of the initial medium of cell growth according to cell type as previously described. Afterward, the cell pellet was collected via centrifugation at 300 g for 5 minutes and washed twice with HBSS. Following the final wash, cells were resuspended in 90 µL OptiMEM, then electroporated with a predetermined dose of either pCCL4 (5 µg), mCCL4(1 µg), pCCR7 (5 µg), or mCCR7(1 µg) at 200 mV for 25ms. Electoporated cells were afterward transferred to 500 µL of Pen-Strep containing A549 or DC2.4 culture medium and back into a 24-well plate to be further grown for 48h before analysis for CCL4 or CCR7 expression.

In-vitro transfection of DC2.4 with NAs encoding for CCL4 or CCR7 using commercial transfection reagents or P-TS-CoAc

DC2.4 were seeded in 24-well plates at a density of 50000 cells/ well in a medium consisting of RPMI-1640 supplemented with FCS (10% *v/v*), HEPES (1%), NEAA (1%),

β-mercaptoethanol (0.0054%). After 48 h incubation at 5% CO_2 and 37°C cells were approximately 80% confluent and were treated.

In the case of pCCR7, its attempted transfection was performed using 5µg pCCR7 loaded on P-TS-$CoAc_{pCCR7}$ against P-TS-$CoAC_{pUC19}$ as a negative control, respectively, applied to DC2.4 for 6h, following which P-TS-CoAc was removed, and replaced by cell culture medium in which cells were further incubated for 18h. Afterward, cells were detached and analyzed for CCR7 expression.

As for mCCL4 and pCCL4 cells were treated either: (i) With JetMessenger complexed mCCL4 or JetPrime complexed pCCL4 at a dose of 2 µg NA/ well for 3h in OptiMEM. The cell culture supernatant of DC2.4 was collected either 3h or 22h post-treatment and analyzed for CCL4 content to assess the time frame of CCL4 expression from either NAs in DC2.4. (iii) With P-TS-$CoAc_{pCCR7}$ or jetP-pCCL4 at a dose of 5 µg pCCL4/ well, or P-TS-$CoAC_{mCCL4}$ or jetM-mCCL4 at a dose of 1 µg/ well, and cell culture supernatant collected at 6h and 24 h pooled and assessed for CCL4 content to assess P-TS-CoAc transfection efficiency.

AB-staining assay for murine CCR7 expression in DC2.

Following electroporation or P-TS-CoAc application, cells were further incubated for 24h, then cells were detached using 200 µL Accutase for 45 min followed by the addition of 800 µL DC2.4 culture medium, cells were washed twice in HBSS. Following this Fc receptor blocking of the cells was performed by incubating cells with 50 µL 4µg/ mL TruStain FcX™ PLUS (anti-mouse CD16/32) Antibody, in 1% BSA in PBS. Cells were further incubated for 10 min on ice. Cells were then incubated with either 1µg, 2µg, or 4 PE labelled Anti-CCR7 or PE Rat IgG2a, κ Isotype Ctrl Antibody Per $1*10^6$ cells and further incubated for 120 min at 37°C. Afterward, cells were washed twice in 1% BSA in PBS, resuspended in HBSS, and flow cytometerically assessed for CCR7 expression on the PE-Channel (BD LSRFortessa™ Cell Analyzer Biosciences, Heidelberg, Germany).

Flow cytometric capture beads assay for murine CCL4 expression in DC2.4 and A549

CCL4 content in the cell culture supernatant was flow-cytometrically assessed using Legendplex murine CCL4 FACS capture beads (Biolegend, Amsterdam, The Netherlands). (BD LSRFortessa™ Cell Analyzer Biosciences, Heidelberg, Germany) on the PE-channel. The calibration curve **(Figure 32-a)** was established using LEGENDplex™ Mouse Proinflammatory Chemokine Standards, serially diluted 10000, 2500, 625,156.3,39.1,9.8, and 2.4 pg/mL CCL4.

Chemotaxis assay

DC2.4 were suspended at a concentration of $1.5*10^6$ c/mL in 300µL of 1.5 mg/mL collagen I, bovine (PureCol,CellSystems, Troisdorf, Germany), containing 0.75% $NaHCO_3$, 0.16X DC2.4 medium (100 I.U./mL penicillin and 100 µg/mL streptomycin), 0.6X MEM. The DC2.4 suspension was then seeded in the observation chamber of the µ-chemotaxis slide (Ibidi GmbH, Gräfelfing, Germany), and the collagen matrix was allowed

to solidify at 37 ˚C, 5% CO_2 for 45 min. Following which DC2.4 previously electroporated with 2 µg pCCL4, mCCL4 or nuclease-free water (NFW) as previously described were resuspended in DC2.4 medium containing Pen-strep at a density of $5*10^5$ cells/mL and dispensed in reservoirs 2 and 3 as indicated in **(Figure 33)** Following which cells were maintained at 37 ˚C, 5% CO_2 for 24 hr and monitored using live-cell microscopy (Lionheart FX Automated Microscope, Agilent, CA, USA). Data were processed using the FastTrack tool from Ibidi, mainly for changes in vector and magnitude of cell movement represented by changes in their center of mass (CoM).

Statistical analysis of data

Graph Pad Prism 8 for Windows (Version 8.01, GraphPad Software Inc.) was used for data analysis. Data were presented as the mean of individual values (generally 3–9 samples), and the standard deviation was indicated by the error bars. (N) refers to the number of experiments, (n) refers to the number of technical sample replicates per experiment. One-way ANOVA was performed for all test samples, and Tukey's post hoc test was used to assess inter-group differences. Data were considered statistically significant at a level of significance of $p < 0.05$ (* $p < 0.05$, ** $p < 0.01$, *** $p < 0.001$ and **** $p < 0.0001$).

4.4. Results and discussion

4.4.1. Product quality of in-house propagated plasmids (pCCL4,pCCR7,pUC19)

UV-Spectrophotometry

Spectrophotometric assessment of in-house propagated pCCR7 and pCCL4 **(Table 10)** showed good yields of 2.53 and 2.45 mg in compliance with the expected 2.5 mg outcome of the Qiagen EndoFree Plasmid Mega Kit. Both pCCR7 and pCCL4 also displayed acceptable 260/280 ratios of 1.88 and 1.85, respectively **(Table 10)**. The same was true for 260/230 ratios which were 2.27 for pCCR7 and 2.25 for pCCL4**,** thus indicating the absence of contaminants above the acceptable limits. The non-coding plasmid control, pUC19 showed a lower yield of 1.17 mg, yet had 260/280 and 260/230 ratios within the acceptable purity limits

Table 10. *Spectrophotometric assessment of pUC19, pCCL4, and pCCR7*

Plasmid name	Function	Selection antibiotic	Yield (mg)	260/280*	260/230**
pUC19	Non-coding	Ampicillin	1.17	1.88	2.16
pCCL4	Coding for murine Chemokine Receptor Ligand 4	Ampicillin	2.45	1.85	2.25
pCCR7	Coding for murine Chemokine Receptor 7	Ampicillin	2.53	1.88	2.27

*260/280 ratios lower than 1.8 may indicate the presence of protein, phenol, or other contaminants that absorb strongly at or near 280 nm.

**Expected 260/230 values are commonly in the range of 2.0-2.2. If the ratio is appreciably lower than expected, it may indicate the presence of contaminants that absorb at 230 nm (EDTA, Carbohydrates, Phenols, etc.)

Restriction-enzyme mapping of in-house propagated pCCL4, pCCR7, and pUC19

Restriction enzyme mapping assay **(Figure 28)** using XbaI confirmed the identity of the pUC19, with a band within the expected 2500-2700 bp range. As for pCCL4, the linearization product gave the expected band slightly above 6000 bp, the backbone check also conformed to expectations with two bands slightly above and below 4000 and 1800 bp, respectively. Yet for the gene digest, it was hard to detect the expected band at 280 bp on this gel. Regarding pCCR7, all mapping reactions conformed to expectations, with the linearization reaction giving a band in the middle of the 6000-8000 bp range, the backbone digest conforming to expectation, and bands at approximately 4000 and 1800 bp, and a gene band at 1400 bp between 1000-1500 bp as expected.

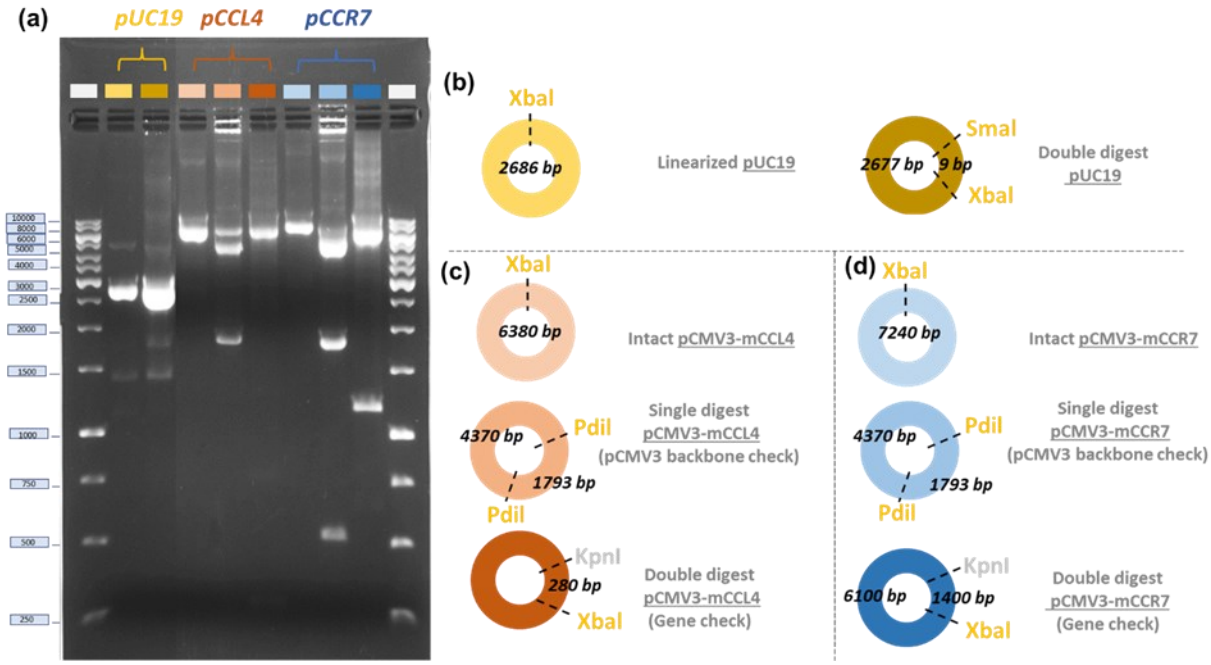

Figure 28. *(a) Electrophoretic migration assay of in-house propagated pUC19,pCCl4 and pCCR7 using restriction enzyme mapping for product identification (b,c,d) expected digestion patterns of pUC19, pCCl4, and pCCR7, respectively, using the indicated restriction enzymes.*

4.4.2. Product quality of in-vitro transcription (IVT) products (mCCL4 and mCCR7)

Spectrophotometric assessment **(Table 11)** confirmed the acceptable purity of the produced mCCL4 and mCCR7. Yet, agarose gel electrophoresis migration assay **(Figure 29**) of $mRNA_{ORF}$ data showed successful production of $mCCL4_{ORF}$ but not $mCCR7_{ORF}$. Where a compliant band was observed for $mCCL4_{ORF}$ at 280 b, yet the resulting band for $mCCR7_{ORF}$ in-vitro transcription reaction product primarily stood at approximately 600 b, which is far from the expected 1400 b for $mCCR7_{ORF}$, this could be resorted to the long gene and instability during the in-vitro transcription reaction. Both $mCCL4_{ORF}$ and $mCCR7_{ORF}$ showed detectable contamination with ds-RNA where the bands appeared at a base number double that of the $mRNA_{ORF}$ band.

Table 11. *Spectrophotometric assessment of mCCL4 and mCCR7*

Sample name	**mCCL4**	**mCCR7**
Yield	116 µg	212 µg
260/280	1.93	1.99
260/230	2.22	2.27

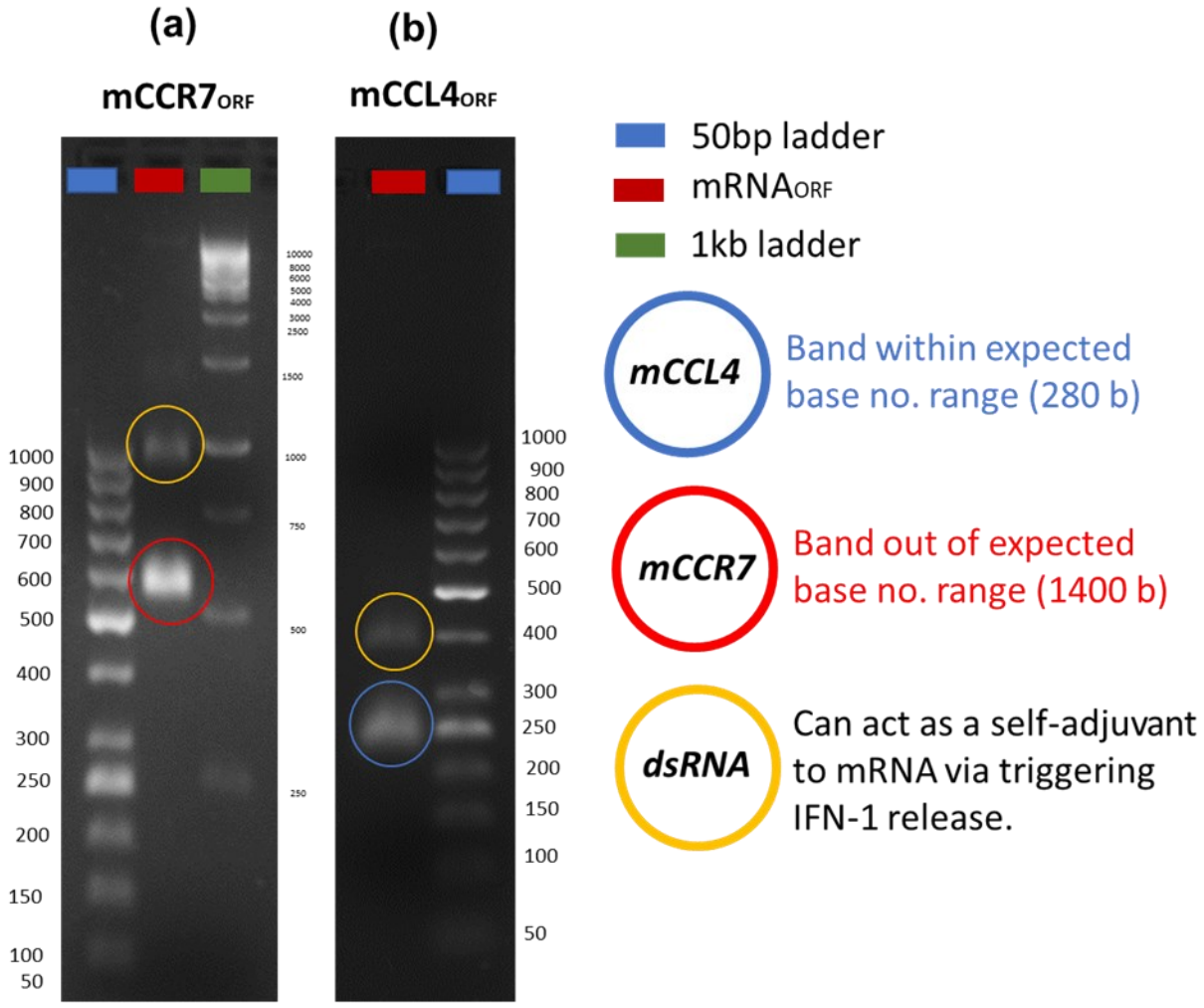

Figure 29. *Electrophoretic migration assay of in-vitro transcription product of (a) $mCCR7_{ORF}$ and (b) $mCCL4_{ORF}$.*

4.4.3. Particle properties of TS-CoAc prepared using pCCL4, pCCR7 or pUC19

CoAc and TS-CoAc of pCCL4, pCCR7, and pUC19 showed acceptable size and PDI **(Figure 30).**

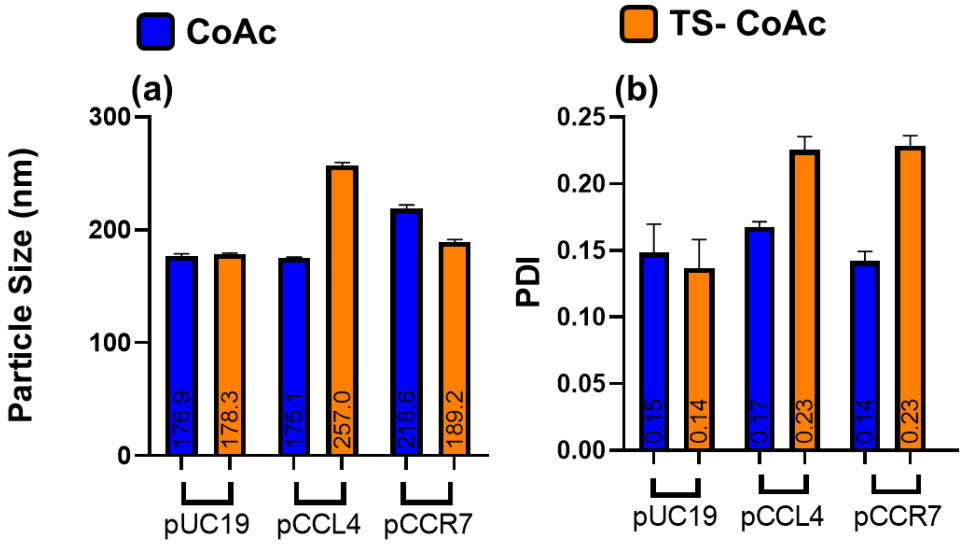

Figure 30. *(a) particle size and (b) PDI of CoAc and TS-CoAc nanocarriers assembled using pUC19, pCCR7, and pCCL4. Data values are expressed as means± SD. (N=1,n=3)*

4.4.4. In-vitro transfection performance of pCCR7 in DC2.4

CCR7 expression was assessed exclusively in DC2.4 since this is one of the cell lines of its native expression. To assess the functionality of in-house prepared pCCR7 and mCCR7, as well as, establish appropriate separation between the primary anti-CCR7 staining antibody and its isotype control **(Table 12, Equation 2, Figure 31-a)** DC2.4 were electroporated with either 5 µg pCCR7 or 1µg mCCR7 and assessed for receptor expression. The separation index (SI) between Anti-CCR7 and its isotype control was highest at 2 µg per $1*10^6$ and hence this concentration was adopted for all downstream experiments. No expression could be achieved following DC2.4 electroporation with 1µg mCCR7 which was already expected from the gel-migration assay results, depicting a non-compliant $mCCR7_{ORF}$ band, whereas 5µg pCCR7 produced a modest yet statistically significant transfection efficiency of 10.75% ±0.57 **(Figure 31-b)**. P-TS-$CoAc_{pCCR7}$ did not produce any discernible transfection compared to untreated control or non-coding nanocarrier control P-TS-$CoAc_{pUC19}$ **(Figure 31-c).**

Table 12. *Separation index (SI) of anti-CCR7 primary antibody against isotype control calculated using Equation 2.*

Mass Anti-CCR7 or Isotype Control antibody/1*10^6 cells	Separation Index
1 µg	0.09
2 µg	**0.18**
4 µg	0.03

$$SI = \frac{MFI_{AB} - MFI_{ISO}}{2 * SD_{ISO}}$$

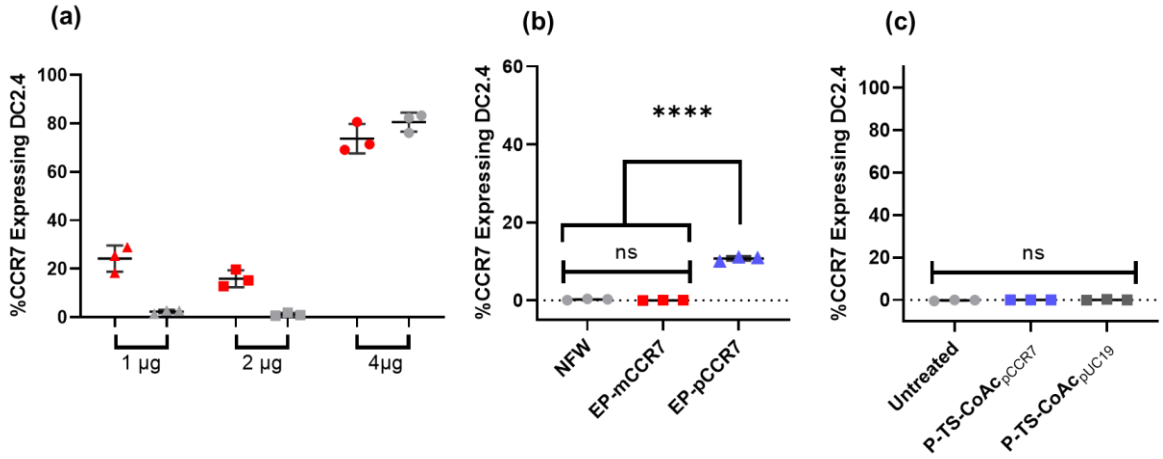

Figure 31. *Flow-cytometric assessment of CCR7 expression by DC2.4 24h following treatment with 5 µg pCCR7or 1µg mCCR7 (a) TruStain FcX™ PLUS (anti-mouse CD16/32) Antibody(red) vs PE Rat IgG2a, κ Isotype Ctrl Antibody(grey) dose titration for separation index calculation. (b) CCR7 expression by DC2.4 following electroporation with 5µg pCCR7 (blue) or 1µg mCCR7(red). (c) CCR7 expression by DC2.4 following treatment with P-TS-CoAc$_{pCCR7}$ (5µg pCCR7)(blue) or P-TS-CoAc$_{pUC19}$ (5µg pUC19)(dark grey). Data values are expressed as means± SD, (N = 1, n = 3), **** p < 0.0001, ns = not significant.*

4.4.5. In-vitro transfection efficiency of CCL4 encoding NA in DC2.4 and A549

Initial assessment of CCL4 expression using electroporation with either nuclease-free water (NFW), 1 µg mCCL4, or 5 µg pCCL4 (doses equivalent to those previously used in P-TS-CoAc for mCherry and pAmCyan1) showed exclusive success in DC2.4 murine dendritic cell line rather the human lung cell line A549 **(Figure 32-b)**. In the case of A549, no statistically significant difference in CCL4 expression was observed between cells electroporated with NFW, 1 µg mCCL4, and 5 µg pCCL4, whereas in the case of DC2.4 a significantly higher expression could be observed between NFW electroporated cells and both 1µg mCCL4 and 5 µg pCCL4 electroporated cells. Interestingly CCL4 expression from 5 µg pCCL4 was only slightly and not significantly higher than 1 µg mCCL4. This NFW electroporated control excludes the expression of CCL4 to be an artifact of the electroporation process themselves and the data obtained from DC2.4 confirmed the functionality of the in-house produced mCCL4 and pCCL4. The successful expression in DC2.4 rather than A549 could be resorted to the species specificity of the used pCCL4 and mCCL4, but may also be because dendritic cells and macrophages are generally more prone to secrete such chemokine across species. The kinetics of the expression were assessed from equivalent mCCL4 and pCCL4 doses of 2 µg delivered to DC2.4 using JetM and JetP, respectively, and CCL4 expression from those samples analyzed following 3h and 22h of treatment without pooling **(Figure 32-c).** It was observed that mCCL4 caused a discernible, yet non-statistically significant expression of CCL4 as early as 3h, yet after 22h CCL4 expressed from mCCL4 has declined to a level even lower than untreated cells, mCCL4 may thus induce an initially high, yet transient expression of CCL4 as expected. pCCL4 on the other hand showed no discernible expression of CCL4 at 3h post electroporation, yet a significantly higher expression could be observed 22h following treatment.

The CCL4 expression following DC2.4 treatment with P-TS-CoAcmCCL4 (equivalent to 1µg mCCL4) or P-TS-CoAcpCCL4 (equivalent to 5 µg pCCL4) compared to equivalent doses of mCCL4 and pCCL4 delivered using JetM and JetP, respectively. Transfection was assessed by pooling cell culture supernatant collected at 6h and 24h from individual wells **(Figure 32-d)** to assess overall expression at both time points, and then analyzed using the FACS capture beads as previously described. Data showed that only JetP-pCCL4 demonstrated successful CCL4 expression whereas all three other treatments showed no discernible difference from untreated cells. This could be correlated with the low levels of pAmCyan1 and mCherry expression in DC2.4 using P-TS-CoAc (**Figure 17-b).** The proposed carrier system P-TS-CoAc could hence benefit from further optimization to maximize levels of protein expression.

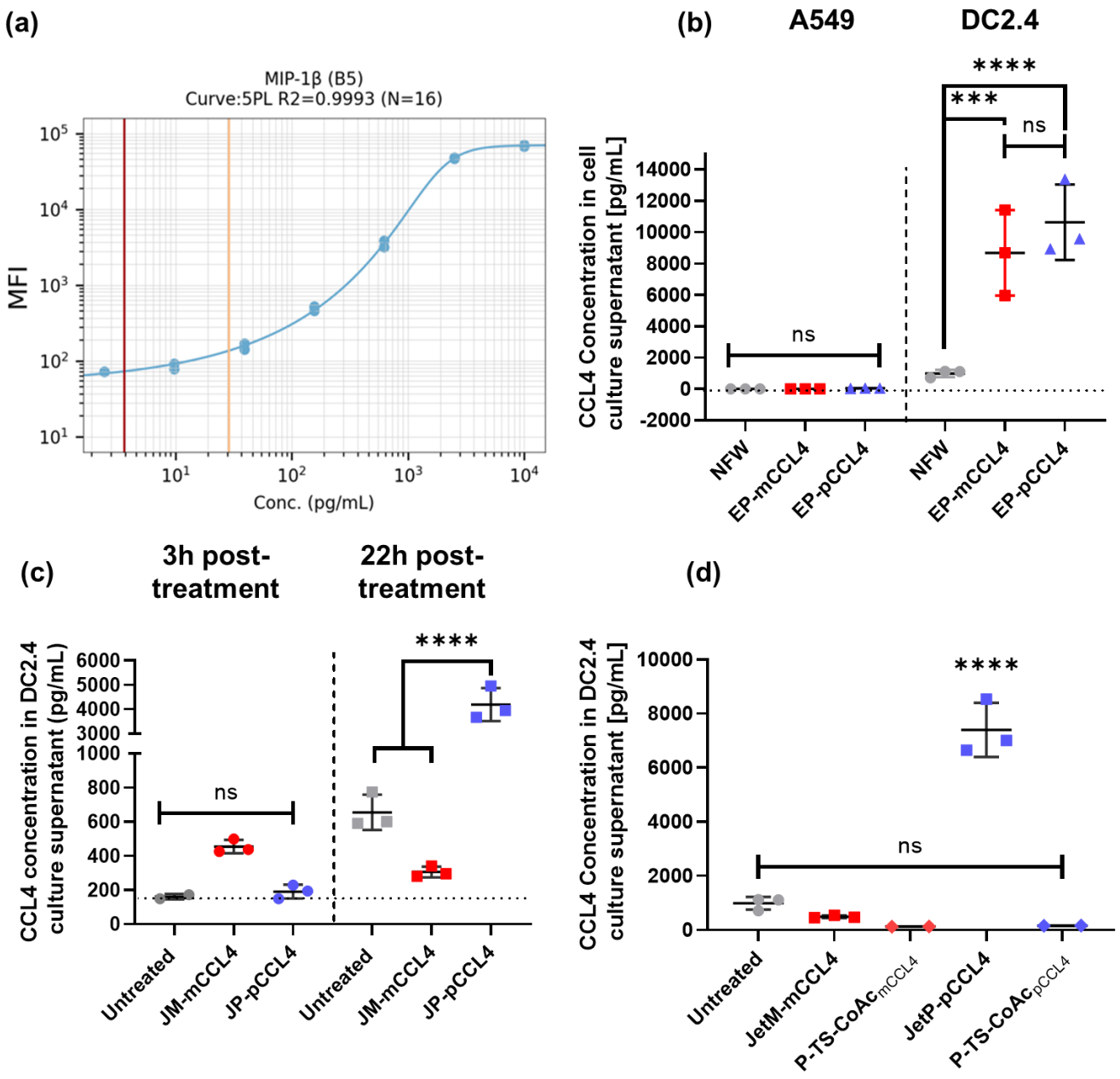

Figure 32. *Flow-cytometric assessment of in-vitro CCL4 expression (a) calibration curve of murine CCL4 FACS capture beads assay. (b) CCL4 expression in A549and DC2.4 following electroporation with nuclease-free water (NFW) (grey) 1µg of mCCL4(red) or 5 µg of pCCL4(blue), measurements were obtained by combining CCL4 content at 6h and 24h post-treatment from each well individually. (c) CCL4 expression by DC2.4 3h and 22h following treatment with 2 µg mCCL4 complexed with JetM (red) or 2µg pCCL4 complexed with JetP (blue)compared to untreated cells (grey) (d) CCL4 expression by DC2.4 treated with either 1µg of mCCL4 delivered using JetM (red square) or P-TS-CoAc$_{mCCL4}$ (red diamond) or 5µg pCCL4 delivered using JetP(blue square) or P-TS-CoAc$_{pCCL4}$ (blue diamond), measurements were obtained by combining CCL4 content at 6h and 24h post-treatment from each well individually. Data values are expressed as means± SD, (N = 1, n = 3). **** p < 0.0001, *** p < 0.001, ns = not significant.*

4.4.6. Chemotaxis assay

Chemotactic migration assay (**Figure 33**) showed no discernible difference in Center of mass (CoM) along the X-axis with a magnitude directed towards the right chamber for neither DC2.4 electroporated with mCCL4 nor pCCL4. Both populations appeared to have no discernible difference in chemotactic behavior from NFW electroporated cells (**Figure 33-c**). DC2.4 have been reported to express CCR5 among other receptors that would render them responsive to CCL4 expression. Yet the most responsive cell types are CD8+ and CD4+ T cells, respectively, as well as neutrophils in the case of mice[310].

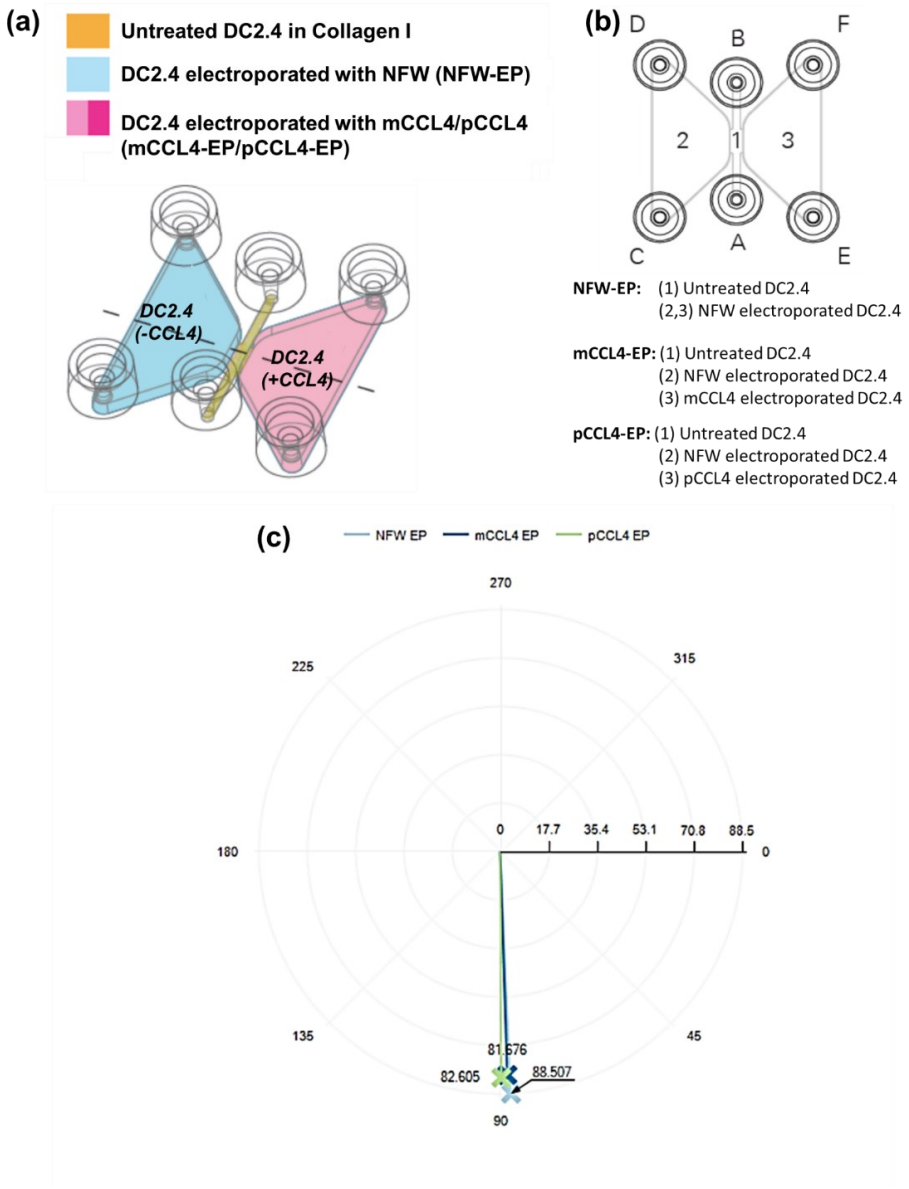

Figure 33. *Chemotactic migration assay using µ-chemotaxis slides (a) general experimental layout reproduced from www.Ibidi.com (b)Sample descriptions (C) Center of mass displacement (CoM) of untreated DC2.4 in observation chamber in response to different treatments.*

4.5. Conclusion

It was possible to produce mRNA encoding for CCL4 rather than CCR7, as indicated by successful expression by DC2.4 following electroporation, yet both pCCR7 and pCCL4 could produce successful transfection in DC2.4 following electroporation. The production and expression of mCRR7 on the other hand were not successful. As for mCCL4 and pCCL4 delivered using JetM and JetP to DC2.4 showed a time-resolved expression as expected, mCCL4 produced rapid transient expression while pCCL4 produced delayed and prolonged-expression. Such results when combined with the time-resolved expression observed from P-TS-CoAc in Chapter III, may be a step forward towards achieving time-resolved expression of antigen and adjuvant. Yet despite the previous success of P-TS-CoAc in co-delivery of fluorescent reporter pDNA and mRNA, the system needs further optimization to successfully deliver mCCL4 or pCCL4. Also, structural manipulation of pDNA and mRNA cargos to produce higher protein expression remains a viable option. If achieved this can allow future co-delivery of antigen and adjuvant encoding NAs which could become a useful adjuvantation approach.

Summary

In the current work, Chapter II demonstrated the design of a nanocarrier system capable of co-delivery and incurring successful co-transfection with pDNA and mRNA was feasible. The exploitation of the thermal-responsive property of spontaneously assembled Gelatin A- pDNA coacervates allowed the production of pDNA core-loaded nanogels (TS-CoAc). Such TS-CoAc were also exclusively liable to coating with densely the charged cationic peptide protamine sulfate in comparison to non-stabilized core variety. The nanocarrier design with pDNA in the core yet a cationic shell allowed further surface loading of mRNA on the nanocarrier system resulting in an elaborate core-shell system that can load two distinct NA-moieties in two distinct locations on the carrier, pDNA in the core,mRNA at the surface. Protamine coated TS-CoAc demonstrated a unique co-transfectional capacity of fluorescent reporter encoding mRNA and pDNA in dendritic murine cell lines (DC2.4), upon comparison to several well-established transfection controls (jetMessenger, JetPrime, Lipofectin, PEI) as well as, Onpattro's LNPs and Onpattro's lipid cocktail coated TS-CoAc.

In Chapter III, a factorial assessment of the impact of varying the number of thermal stabilization cycles as well as, gelatin: protamine mass ratio on the colloidal properties and the transfection performance of the nanocarrier was investigated. Yet the different variations of assembly conditions of the carrier seemed to have a very limited effect on the aforementioned factors. Another study exploring the kinetics of fluorescent reporter encoding mRNA and pDNA co-delivered by the nanocarrier to DC2.4 showed earlier expression onset of mRNA, a delayed yet more prolonged-expression from pDNA.

Eventually, the attempted in-house production of adjuvant encoding pDNA and mRNA was attempted for two adjuvant candidates namely CCL4 and CCR7. CCL4 showed more promising results in terms of feasibility of mRNA in-vitro transcription as well as, its in-vitro expression following electroporation into DC2.4 in comparison to CCR7. Yet so far optimizing the delivery of pDNA/mRNA encoding for CCL4 using P-TS-CoAc is still pending.

References

1. Rappuoli, R., Mandl, C. W., Black, S. & Gregorio, E. D. Vaccines for the twenty-first century society. *Nat Rev Immunol* 11, 865–872 (2011).

2. Rappuoli, R., Miller, H. I. & Falkow, S. The Intangible Value of Vaccination. *Science* 297, 937–939 (2002).

3. Hinman, A. ERADICATION OF VACCINE-PREVENTABLE DISEASES. *Annu Rev Publ Health* 20, 211–229 (1999).

4. Greenwood, B. The contribution of vaccination to global health: past, present and future. *Philosophical Transactions Royal Soc B Biological Sci* 369, 20130433 (2014).

5. Bell, C. & Lewis, M. Economic Implications of Epidemics Old and New. *Ssrn Electron J* (2005) doi:10.2139/ssrn.997387.

6. SHULMAN, S. T. The History of Pediatric Infectious Diseases. *Pediatr Res* 55, 163–176 (2004).

7. Crimmins, E. M. & Finch, C. E. Infection, inflammation, height, and longevity. *P Natl Acad Sci Usa* 103, 498–503 (2006).

8. Oeppen, J. & Vaupel, J. W. Demography. Broken limits to life expectancy. *Sci New York N Y* 296, 1029–31 (2002).

9. Kirkwood, T. B. L. A systematic look at an old problem. *Nature* 451, 644–647 (2008).

10. Coffman, R. L., Sher, A. & Seder, R. A. Vaccine Adjuvants: Putting Innate Immunity to Work. *Immunity* 33, 492–503 (2010).

11. Boyle, J. *et al.* The utility of ISCOMATRIX™ adjuvant for dose reduction of antigen for vaccines requiring antibody responses. *Vaccine* 25, 2541–2544 (2007).

12. Liu, H. *et al.* Preclinical evaluation of the saponin derivative GPI-0100 as an immunostimulating and dose-sparing adjuvant for pandemic influenza vaccines. *Vaccine* 29, 2037–2043 (2011).

13. Jiang, J. *et al.* Antigen sparing and enhanced protection using a novel rOv-ASP-1 adjuvant in aqueous formulation with influenza vaccines. *Vaccine* 32, 2696–2702 (2014).

14. Leroux-Roels, I. *et al.* Antigen sparing and cross-reactive immunity with an adjuvanted rH5N1 prototype pandemic influenza vaccine: a randomised controlled trial. *Lancet* 370, 580–589 (2007).

15. Schwarz, T. F. *et al.* Single dose vaccination with AS03-adjuvanted H5N1 vaccines in a randomized trial induces strong and broad immune responsiveness to booster vaccination in adults. *Vaccine* 27, 6284–6290 (2009).

16. Crooke, S. N., Ovsyannikova, I. G., Poland, G. A. & Kennedy, R. B. Immunosenescence and human vaccine immune responses. *Immun Ageing* 16, 25 (2019).

17. Goronzy, J. J. & Weyand, C. M. Understanding immunosenescence to improve responses to vaccines. *Nat Immunol* 14, 428–436 (2013).

18. Cox, L. S. *et al.* Tackling immunosenescence to improve COVID-19 outcomes and vaccine response in older adults. *Lancet Heal Longev* 1, e55–e57 (2020).

19. Lang, P. O., Govind, S., Michel, J. P., Aspinall, R. & Mitchell, W. A. Immunosenescence: Implications for vaccination programmes in adults. *Maturitas* 68, 322–330 (2011).

20. Pardi, N., Hogan, M. J., Porter, F. W. & Weissman, D. mRNA vaccines — a new era in vaccinology. *Nat Rev Drug Discov* 17, 261–279 (2018).

21. Awate, S., Babiuk, L. A. & Mutwiri, G. Mechanisms of Action of Adjuvants. *Front Immunol* 4, 114 (2013).

22. Podda, A. The adjuvanted influenza vaccines with novel adjuvants: experience with the MF59-adjuvanted vaccine. *Vaccine* 19, 2673–2680 (2001).

23. Pulendran, B., Arunachalam, P. S. & O'Hagan, D. T. Emerging concepts in the science of vaccine adjuvants. *Nat Rev Drug Discov* 20, 1–22 (2021).

24. Beran, J. Safety and immunogenicity of a new hepatitis B vaccine for the protection of patients with renal insufficiency including pre-haemodialysis and haemodialysis patients. *Expert Opin Biol Th* 8, 235–247 (2008).

25. Khurana, S. *et al.* AS03-adjuvanted H5N1 vaccine promotes antibody diversity and affinity maturation, NAI titers, cross-clade H5N1 neutralization, but not H1N1 cross-subtype neutralization. *Npj Vaccines* 3, 40 (2018).

26. Dose ranging of adjuvant and antigen in a cell culture H5N1 influenza vaccine: safety and immunogenicity of a phase 1/2 clinical trial. *Cochrane Central Register Control Trials Central* 2010, (2018).

27. Liu, H., Vries-Idema, J. de, Veer, W. ter, Wilschut, J. & Huckriede, A. Influenza virosomes supplemented with GPI-0100 adjuvant: a potent vaccine formulation for antigen dose sparing. *Med Microbiol Immun* 203, 47–55 (2014).

28. Keitel, W. *et al.* Dose ranging of adjuvant and antigen in a cell culture H5N1 influenza vaccine: Safety and immunogenicity of a phase 1/2 clinical trial. *Vaccine* 28, 840–848 (2010).

29. Huleatt, J. W. *et al.* Vaccination with recombinant fusion proteins incorporating Toll-like receptor ligands induces rapid cellular and humoral immunity. *Vaccine* 25, 763–775 (2007).

30. Galli, G. *et al.* Fast rise of broadly cross-reactive antibodies after boosting long-lived human memory B cells primed by an MF59 adjuvanted prepandemic vaccine. *Proc National Acad Sci* 106, 7962–7967 (2009).

31. Lefeber, D. J. *et al.* Th1-Directing Adjuvants Increase the Immunogenicity of Oligosaccharide-Protein Conjugate Vaccines Related to Streptococcus pneumoniae Type 3. *Infect Immun* 71, 6915–6920 (2003).

32. Vandepapelière, P. *et al.* Vaccine Adjuvant Systems containing monophosphoryl lipid A and QS21 induce strong and persistent humoral and T cell responses against hepatitis B surface antigen in healthy adult volunteers. *Vaccine* 26, 1375–1386 (2008).

33. Leroux-Roels, I. *et al.* Priming with AS03A-adjuvanted H5N1 influenza vaccine improves the kinetics, magnitude and durability of the immune response after a heterologous booster vaccination: An open non-randomised extension of a double-blind randomised primary study. *Vaccine* 28, 849–857 (2010).

34. Galli, G. *et al.* Adjuvanted H5N1 vaccine induces early CD4+ T cell response that predicts long-term persistence of protective antibody levels. *Proc National Acad Sci* 106, 3877–3882 (2009).

35. Li, Q. *et al.* Toll-Like Receptor 7 Activation Enhances CD8+ T Cell Effector Functions by Promoting Cellular Glycolysis. *Front Immunol* 10, 2191 (2019).

36. Lynn, G. M. *et al.* Impact of Polymer-TLR-7/8 Agonist (Adjuvant) Morphology on the Potency and Mechanism of CD8 T Cell Induction. *Biomacromolecules* 20, 854–870 (2019).

37. Kim, E. H. *et al.* Squalene emulsion-based vaccine adjuvants stimulate CD8 T cell, but not antibody responses, through a RIPK3-dependent pathway. *Elife* 9, e52687 (2020).

38. Oberhardt, V. *et al.* Rapid and stable mobilization of CD8+ T cells by SARS-CoV-2 mRNA vaccine. *Nature* 597, 268–273 (2021).

39. Gulck, E. V. *et al.* mRNA-based dendritic cell vaccination induces potent antiviral T-cell responses in HIV-1-infected patients. *Aids* 26, F1–F12 (2012).

40. Chahal, J. S. *et al.* An RNA nanoparticle vaccine against Zika virus elicits antibody and CD8+ T cell responses in a mouse model. *Sci Rep-uk* 7, 252 (2017).

41. Chung, Y. H., Beiss, V., Fiering, S. N. & Steinmetz, N. F. COVID-19 Vaccine Frontrunners and Their Nanotechnology Design. *Acs Nano* 14, 12522–12537 (2020).

42. Liljeroos, L., Malito, E., Ferlenghi, I. & Bottomley, M. J. Structural and Computational Biology in the Design of Immunogenic Vaccine Antigens. *J Immunol Res* 2015, 156241 (2015).

43. Seib, K. L., Zhao, X. & Rappuoli, R. Developing vaccines in the era of genomics: a decade of reverse vaccinology. *Clin Microbiol Infec* 18, 109–116 (2012).

44. Liu, L. *et al.* Potent neutralizing antibodies against multiple epitopes on SARS-CoV-2 spike. *Nature* 584, 450–456 (2020).

45. McDonald, I., Murray, S. M., Reynolds, C. J., Altmann, D. M. & Boyton, R. J. Comparative systematic review and meta-analysis of reactogenicity, immunogenicity and efficacy of vaccines against SARS-CoV-2. *Npj Vaccines* 6, 74 (2021).

46. Du, L. *et al.* The spike protein of SARS-CoV — a target for vaccine and therapeutic development. *Nat Rev Microbiol* 7, 226–236 (2009).

47. Peng, H. *et al.* Human memory T cell responses to SARS-CoV E protein. *Microbes Infect* 8, 2424–2431 (2006).

48. Dutta, N. K., Mazumdar, K. & Gordy, J. T. The Nucleocapsid Protein of SARS–CoV-2: a Target for Vaccine Development. *J Virol* 94, e00647-20 (2020).

49. Buchholz, U. J. *et al.* Contributions of the structural proteins of severe acute respiratory syndrome coronavirus to protective immunity. *P Natl Acad Sci Usa* 101, 9804–9809 (2004).

50. Grifoni, A. *et al.* Targets of T Cell Responses to SARS-CoV-2 Coronavirus in Humans with COVID-19 Disease and Unexposed Individuals. *Cell* 181, 1489-1501.e15 (2020).

51. Gordon, D. E. *et al.* A SARS-CoV-2 Protein Interaction Map Reveals Targets for Drug-Repurposing. *Nature* 583, 459–468 (2020).

52. Zhang, Y. *et al.* The ORF8 protein of SARS-CoV-2 mediates immune evasion through down-regulating MHC-I. *Proc National Acad Sci* 118, e2024202118 (2021).

53. Suthar, M. S. *et al.* Rapid Generation of Neutralizing Antibody Responses in COVID-19 Patients. *Cell Reports Medicine* 1, 100040 (2020).

54. Gao, Q. *et al.* Development of an inactivated vaccine candidate for SARS-CoV-2. *Sci New York N Y* 369, eabc1932 (2020).

55. Robbiani, D. F. *et al.* Convergent antibody responses to SARS-CoV-2 in convalescent individuals. *Nature* 584, 437–442 (2020).

56. Verbeke, R., Lentacker, I., Smedt, S. C. D. & Dewitte, H. The dawn of mRNA vaccines: The COVID-19 case. *J Control Release* 333, 511–520 (2021).

57. Dong, Y. *et al.* A systematic review of SARS-CoV-2 vaccine candidates. *Signal Transduct Target Ther* 5, 237 (2020).

58. Walsh, E. E. *et al.* Safety and Immunogenicity of Two RNA-Based Covid-19 Vaccine Candidates. *New Engl J Medicine* 383, NEJMoa2027906 (2020).

59. Corbett, K. S. *et al.* SARS-CoV-2 mRNA Vaccine Design Enabled by Prototype Pathogen Preparedness. *Nature* 586, 567–571 (2020).

60. Mallapaty, S. China's COVID vaccines have been crucial — now immunity is waning. *Nature* 598, 398–399 (2021).

61. Cobb, M. Who discovered messenger RNA? *Curr Biol* 25, R526–R532 (2015).

62. Verbeke, R., Lentacker, I., Smedt, S. C. D. & Dewitte, H. Three decades of messenger RNA vaccine development. *Nano Today* 28, 100766 (2019).

63. Chaudhary, N., Weissman, D. & Whitehead, K. A. mRNA vaccines for infectious diseases: principles, delivery and clinical translation. *Nat Rev Drug Discov* 20, 817–838 (2021).

64. Roche, P. A. & Furuta, K. The ins and outs of MHC class II-mediated antigen processing and presentation. *Nat Rev Immunol* 15, 203–216 (2015).

65. Beckert, B. & Masquida, B. RNA, Methods and Protocols. *Methods Mol Biology* 703, 29–41 (2010).

66. Miao, L., Zhang, Y. & Huang, L. mRNA vaccine for cancer immunotherapy. *Mol Cancer* 20, 41 (2021).

67. Paunovska, K., Loughrey, D. & Dahlman, J. E. Drug delivery systems for RNA therapeutics. *Nat Rev Genet* 1–16 (2022) doi:10.1038/s41576-021-00439-4.

68. Kumar, P. *et al.* Inhibition of translation by IFIT family members is determined by their ability to interact selectively with the 5′-terminal regions of cap0-, cap1- and 5′ppp-mRNAs. *Nucleic Acids Res* 42, 3228–3245 (2014).

69. Baiersdörfer, M. *et al.* A Facile Method for the Removal of dsRNA Contaminant from In Vitro-Transcribed mRNA. *Mol Ther - Nucleic Acids* 15, 26–35 (2019).

70. Linares-Fernández, S., Lacroix, C., Exposito, J.-Y. & Verrier, B. Tailoring mRNA Vaccine to Balance Innate/Adaptive Immune Response. *Trends Mol Med* 26, 311–323 (2019).

71. Margulis, L. & Chapman, M. J. Endosymbioses: cyclical and permanent in evolution. *Trends Microbiol* 6, 342–345 (1998).

72. Bokar, J. A. & Rottman, F. M. Biosynthesis and Functions of Modified Nucleosides in Eukaryotic mRNA. in *Modification and Editing of RNA* (eds. Grosjean, H. & Benne, R.) 183–200 (ASM Press).

73. Karikó, K., Buckstein, M., Ni, H. & Weissman, D. Suppression of RNA Recognition by Toll-like Receptors: The Impact of Nucleoside Modification and the Evolutionary Origin of RNA. *Immunity* 23, 165–175 (2005).

74. Verbeke, R. *et al.* Co-delivery of nucleoside-modified mRNA and TLR agonists for cancer immunotherapy: Restoring the immunogenicity of immunosilent mRNA. *J Control Release* 266, 287–300 (2017).

75. Martin, S., Paoletti, E. & Moss, B. Purification of mRNA guanylyltransferase and mRNA (guanine-7-) methyltransferase from vaccinia virions. *J Biol Chem* 250, 9322–9329 (1975).

76. Gallie, D. R. The cap and poly(A) tail function synergistically to regulate mRNA translational efficiency. *Gene Dev* 5, 2108–2116 (1991).

77. Jensen, S. & Thomsen, A. R. Sensing of RNA Viruses: a Review of Innate Immune Receptors Involved in Recognizing RNA Virus Invasion. *J Virol* 86, 2900–2910 (2012).

78. Muttach, F., Muthmann, N. & Rentmeister, A. Synthetic mRNA capping. *Beilstein J Org Chem* 13, 2819–2832 (2017).

79. Ross, J. & Sullivan, T. Half-lives of beta and gamma globin messenger RNAs and of protein synthetic capacity in cultured human reticulocytes. *Blood* 66, 1149–1154 (1985).

80. Holtkamp, S. *et al.* Modification of antigen-encoding RNA increases stability, translational efficacy, and T-cell stimulatory capacity of dendritic cells. *Blood* 108, 4009–4017 (2006).

81. Gustafsson, C., Govindarajan, S. & Minshull, J. Codon bias and heterologous protein expression. *Trends Biotechnol* 22, 346–353 (2004).

82. Thess, A. *et al.* Sequence-engineered mRNA Without Chemical Nucleoside Modifications Enables an Effective Protein Therapy in Large Animals. *Mol Ther* 23, 1456–1464 (2015).

83. Dobbs, C. *et al.* Strategies to Minimize Innate Immune Stimulation to Maximize Messenger RNA Bioavailability. https://www.trilinkbiotech.com/media/contentmanager/content/mRNA_OTS18.pdf.

84. Fleeton, M. N. *et al.* Self-Replicative RNA Vaccines Elicit Protection against Influenza A Virus, Respiratory Syncytial Virus, and a Tickborne Encephalitis Virus. *J Infect Dis* 183, 1395–1398 (2001).

85. Geall, A. J. *et al.* Nonviral delivery of self-amplifying RNA vaccines. *Proc National Acad Sci* 109, 14604–14609 (2012).

86. Bloom, K., Berg, F. van den & Arbuthnot, P. Self-amplifying RNA vaccines for infectious diseases. *Gene Ther* 28, 117–129 (2021).

87. Beissert, T. *et al.* A Trans-amplifying RNA Vaccine Strategy for Induction of Potent Protective Immunity. *Mol Ther* 28, 119–128 (2020).

88. Leitner, W. W., Ying, H. & Restifo, N. P. DNA and RNA-based vaccines: principles, progress and prospects. *Vaccine* 18, 765–777 (1999).

89. Prazeres, D. M. F. *et al.* Large-scale production of pharmaceutical-grade plasmid DNA for gene therapy: problems and bottlenecks. *Trends Biotechnol* 17, 169–174 (1999).

90. Williams, J. A. Vector Design for Improved DNA Vaccine Efficacy, Safety and Production. *Nato Adv Sci Inst Se* 1, 225–249 (2013).

91. Rauch, S., Jasny, E., Schmidt, K. E. & Petsch, B. New Vaccine Technologies to Combat Outbreak Situations. *Front Immunol* 9, 1963 (2018).

92. Lam, A. P. & Dean, D. A. Progress and prospects: nuclear import of nonviral vectors. *Gene Ther* 17, 439–447 (2010).

93. Grunwald, T. & Ulbert, S. Improvement of DNA vaccination by adjuvants and sophisticated delivery devices: vaccine-platforms for the battle against infectious diseases. *Clin Exp Vaccine Res* 4, 1–10 (2015).

94. Suschak, J. J., Williams, J. A. & Schmaljohn, C. S. Advancements in DNA vaccine vectors, non-mechanical delivery methods, and molecular adjuvants to increase immunogenicity. *Hum Vacc Immunother* 13, 00–00 (2017).

95. Gulce-Iz, S. & Saglam-Metiner, P. Current State of the Art in DNA Vaccine Delivery and Molecular Adjuvants: Bcl-xL Anti-Apoptotic Protein as a Molecular Adjuvant | IntechOpen. in *Immune Response Activation and Immunomodulation* (eds. Tyagi, R. K. & Bisen, P. S.) (2019).

96. Chen, M. *et al.* Safety of SARS-CoV-2 vaccines: a systematic review and meta-analysis of randomized controlled trials. *Infect Dis Poverty* 10, 94 (2021).

97. Kim, J., Eygeris, Y., Gupta, M. & Sahay, G. Self-assembled mRNA vaccines. *Adv Drug Deliver Rev* 170, 83–112 (2021).

98. Malone, R. W., Felgner, P. L. & Verma, I. M. Cationic liposome-mediated RNA transfection. *Proc National Acad Sci* 86, 6077–6081 (1989).

99. Cui, S. *et al.* Correlation of the cytotoxic effects of cationic lipids with their headgroups. *Toxicol Res-uk* 7, 473–479 (2018).

100. Lonez, C., Vandenbranden, M. & Ruysschaert, J.-M. Cationic lipids activate intracellular signaling pathways. *Adv Drug Deliver Rev* 64, 1749–1758 (2012).

101. Cullis, P. R. & Hope, M. J. Lipid Nanoparticle Systems for Enabling Gene Therapies. *Mol Ther* 25, 1467–1475 (2017).

102. Semple, S. C. *et al.* Efficient encapsulation of antisense oligonucleotides in lipid vesicles using ionizable aminolipids: formation of novel small multilamellar vesicle structures. *Biochimica Et Biophysica Acta Bba - Biomembr* 1510, 152–166 (2001).

103. Heyes, J., Palmer, L., Bremner, K. & MacLachlan, I. Cationic lipid saturation influences intracellular delivery of encapsulated nucleic acids. *J Control Release* 107, 276–287 (2005).

104. Sahay, G., Alakhova, D. Y. & Kabanov, A. V. Endocytosis of nanomedicines. *J Control Release* 145, 182–195 (2010).

105. Patel, S. *et al.* Brief update on endocytosis of nanomedicines. *Adv Drug Deliver Rev* 144, 90–111 (2019).

106. Alabi, C. A. *et al.* Multiparametric approach for the evaluation of lipid nanoparticles for siRNA delivery. *Proc National Acad Sci* 110, 12881–12886 (2013).

107. Miao, L. *et al.* Synergistic lipid compositions for albumin receptor mediated delivery of mRNA to the liver. *Nat Commun* 11, 2424 (2020).

108. Jayaraman, M. *et al.* Maximizing the Potency of siRNA Lipid Nanoparticles for Hepatic Gene Silencing In Vivo**. *Angewandte Chemie Int Ed Engl* 51, 8529–8533 (2012).

109. Love, K. T. *et al.* Lipid-like materials for low-dose, in vivo gene silencing. *Proc National Acad Sci* 107, 1864–1869 (2010).

110. Whitehead, K. A. *et al.* Degradable lipid nanoparticles with predictable in vivo siRNA delivery activity. *Nat Commun* 5, 4277 (2014).

111. Hajj, K. A. *et al.* A Potent Branched-Tail Lipid Nanoparticle Enables Multiplexed mRNA Delivery and Gene Editing In Vivo. *Nano Lett* 20, 5167–5175 (2020).

112. Fenton, O. S. *et al.* Bioinspired Alkenyl Amino Alcohol Ionizable Lipid Materials for Highly Potent In Vivo mRNA Delivery. *Adv Mater* 28, 2939–2943 (2016).

113. Li, B. *et al.* An Orthogonal Array Optimization of Lipid-like Nanoparticles for mRNA Delivery in Vivo. *Nano Lett* 15, 8099–8107 (2015).

114. Zhou, K. *et al.* Modular degradable dendrimers enable small RNAs to extend survival in an aggressive liver cancer model. *Proc National Acad Sci* 113, 520–525 (2016).

115. Wei, T., Cheng, Q., Min, Y.-L., Olson, E. N. & Siegwart, D. J. Systemic nanoparticle delivery of CRISPR-Cas9 ribonucleoproteins for effective tissue specific genome editing. *Nat Commun* 11, 3232 (2020).

116. Sabnis, S. *et al.* A Novel Amino Lipid Series for mRNA Delivery: Improved Endosomal Escape and Sustained Pharmacology and Safety in Non-human Primates. *Mol Ther* 26, 1509–1519 (2018).

117. Buschmann, M. D. *et al.* Nanomaterial Delivery Systems for mRNA Vaccines. *Nato Adv Sci Inst Se* 9, 65 (2021).

118. Hajj, K. A. *et al.* Branched-Tail Lipid Nanoparticles Potently Deliver mRNA In Vivo due to Enhanced Ionization at Endosomal pH. *Small* 15, 1805097 (2019).

119. Ding, W., Palaiokostas, M., Wang, W. & Orsi, M. Effects of Lipid Composition on Bilayer Membranes Quantified by All-Atom Molecular Dynamics. *J Phys Chem B* 119, 15263–15274 (2015).

120. Lokugamage, M. P., Sago, C. D., Gan, Z., Krupczak, B. R. & Dahlman, J. E. Constrained Nanoparticles Deliver siRNA and sgRNA to T Cells In Vivo without Targeting Ligands. *Adv Mater* 31, 1902251 (2019).

121. Zhao, X. *et al.* Imidazole-Based Synthetic Lipidoids for In Vivo mRNA Delivery into Primary T Lymphocytes. *Angew Chem-ger Edit* 132, 20258–20264 (2020).

122. Cheng, X. & Lee, R. J. The role of helper lipids in lipid nanoparticles (LNPs) designed for oligonucleotide delivery. *Adv Drug Deliver Rev* 99, 129–137 (2016).

123. Kauffman, K. J. *et al.* Optimization of Lipid Nanoparticle Formulations for mRNA Delivery in Vivo with Fractional Factorial and Definitive Screening Designs. *Nano Lett* 15, 7300–7306 (2015).

124. Ball, R. L., Hajj, K. A., Vizelman, J., Bajaj, P. & Whitehead, K. A. Lipid Nanoparticle Formulations for Enhanced Co-delivery of siRNA and mRNA. *Nano Lett* 18, 3814–3822 (2018).

125. Zhang, X., Barraza, K. M. & Beauchamp, J. L. Cholesterol provides nonsacrificial protection of membrane lipids from chemical damage at air–water interface. *Proc National Acad Sci* 115, 201722323 (2018).

126. Yang, S.-T., Kreutzberger, A. J. B., Lee, J., Kiessling, V. & Tamm, L. K. The role of cholesterol in membrane fusion. *Chem Phys Lipids* 199, 136–143 (2016).

127. Patel, S. *et al.* Naturally-occurring cholesterol analogues in lipid nanoparticles induce polymorphic shape and enhance intracellular delivery of mRNA. *Nat Commun* 11, 983 (2020).

128. Suk, J. S., Xu, Q., Kim, N., Hanes, J. & Ensign, L. M. PEGylation as a strategy for improving nanoparticle-based drug and gene delivery. *Adv Drug Deliver Rev* 99, 28–51 (2016).

129. Zukancic, D. *et al.* The Importance of Poly(ethylene glycol) and Lipid Structure in Targeted Gene Delivery to Lymph Nodes by Lipid Nanoparticles. *Pharm* 12, 1068 (2020).

130. Zhu, X. *et al.* Surface De-PEGylation Controls Nanoparticle-Mediated siRNA Delivery In Vitro and In Vivo. *Theranostics* 7, 1990–2002 (2017).

131. Akinc, A. *et al.* Development of Lipidoid–siRNA Formulations for Systemic Delivery to the Liver. *Mol Ther* 17, 872–879 (2009).

132. Oberli, M. A. *et al.* Lipid Nanoparticle Assisted mRNA Delivery for Potent Cancer Immunotherapy. *Nano Lett* 17, 1326–1335 (2017).

133. Ahn, J. *et al.* Microfluidics in nanoparticle drug delivery; From synthesis to pre-clinical screening. *Adv Drug Deliver Rev* 128, 29–53 (2018).

134. Maeki, M., Uno, S., Niwa, A., Okada, Y. & Tokeshi, M. Microfluidic technologies and devices for lipid nanoparticle-based RNA delivery. *J Control Release Official J Control Release Soc* 344, 80–96 (2022).

135. Kowalski, P. S., Rudra, A., Miao, L. & Anderson, D. G. Delivering the Messenger: Advances in Technologies for Therapeutic mRNA Delivery. *Mol Ther* 27, 710–728 (2019).

136. Bus, T., Traeger, A. & Schubert, U. S. The great escape: how cationic polyplexes overcome the endosomal barrier. *J Mater Chem B* 6, 6904–6918 (2018).

137. Moghimi, S. M. *et al.* A two-stage poly(ethylenimine)-mediated cytotoxicity: implications for gene transfer/therapy. *Mol Ther* 11, 990–995 (2005).

138. Ulkoski, D., Bak, A., Wilson, J. T. & Krishnamurthy, V. R. Recent advances in polymeric materials for the delivery of RNA therapeutics. *Expert Opin Drug Del* 16, 1–19 (2019).

139. Sabin, J., Alatorre-Meda, M., Miñones, J., Domínguez-Arca, V. & Prieto, G. New insights on the mechanism of polyethylenimine transfection and their implications on gene therapy and DNA vaccines. *Colloids Surfaces B Biointerfaces* 210, 112219 (2022).

140. González-Domínguez, I., Grimaldi, N., Cervera, L., Ventosa, N. & Gòdia, F. Impact of physicochemical properties of DNA/PEI complexes on transient transfection of mammalian cells. *New Biotechnol* 49, 88–97 (2019).

141. Ke, X. *et al.* Surface-Functionalized PEGylated Nanoparticles Deliver Messenger RNA to Pulmonary Immune Cells. *Acs Appl Mater Inter* 12, 35835–35844 (2020).

142. Li, M. *et al.* Engineering intranasal mRNA vaccines to enhance lymph node trafficking and immune responses. *Acta Biomater* 64, 237–248 (2017).

143. Li, M. *et al.* Enhanced intranasal delivery of mRNA vaccine by overcoming the nasal epithelial barrier via intra- and paracellular pathways. *J Control Release* 228, 9–19 (2016).

144. Tan, L. *et al.* Optimization of an mRNA vaccine assisted with cyclodextrin-polyethyleneimine conjugates. *Drug Deliv Transl Re* 10, 678–689 (2020).

145. Kaczmarek, J. C. *et al.* Optimization of a Degradable Polymer–Lipid Nanoparticle for Potent Systemic Delivery of mRNA to the Lung Endothelium and Immune Cells. *Nano Lett* 18, 6449–6454 (2018).

146. Kaczmarek, J. C. *et al.* Polymer–Lipid Nanoparticles for Systemic Delivery of mRNA to the Lungs. *Angewandte Chemie Int Ed* 55, 13808–13812 (2016).

147. Patel, A. K. *et al.* Inhaled Nanoformulated mRNA Polyplexes for Protein Production in Lung Epithelium. *Adv Mater* 31, 1805116 (2019).

148. Zeng, M. *et al.* Highly Branched Poly(β-amino ester)s for Gene Delivery in Hereditary Skin Diseases. *Adv Drug Deliver Rev* 176, 113842 (2021).

149. Zhou, D. *et al.* Highly branched poly(β-amino ester)s for skin gene therapy. *J Control Release* 244, 336–346 (2016).

150. Sunshine, J. C., Sunshine, S. B., Bhutto, I., Handa, J. T. & Green, J. J. Poly(β-Amino Ester)-Nanoparticle Mediated Transfection of Retinal Pigment Epithelial Cells In Vitro and In Vivo. *Plos One* 7, e37543 (2012).

151. Lynn, D. M. & Langer, R. Degradable Poly(β-amino esters): Synthesis, Characterization, and Self-Assembly with Plasmid DNA. *J Am Chem Soc* 122, 10761–10768 (2000).

152. Mintzer, M. A. & Simanek, E. E. Nonviral Vectors for Gene Delivery. *Chem Rev* 109, 259–302 (2009).

153. Kim, H. J. *et al.* Fine-Tuning of Hydrophobicity in Amphiphilic Polyaspartamide Derivatives for Rapid and Transient Expression of Messenger RNA Directed Toward Genome Engineering in Brain. *Acs Central Sci* 5, 1866–1875 (2019).

154. Lin, C.-Y. *et al.* Messenger RNA-based therapeutics for brain diseases: An animal study for augmenting clearance of beta-amyloid by intracerebral administration of neprilysin mRNA loaded in polyplex nanomicelles. *J Control Release* 235, 268–275 (2016).

155. Crowley, S. T., Fukushima, Y., Uchida, S., Kataoka, K. & Itaka, K. Enhancement of Motor Function Recovery after Spinal Cord Injury in Mice by Delivery of Brain-Derived Neurotrophic Factor mRNA. *Mol Ther - Nucleic Acids* 17, 465–476 (2019).

156. Aini, H. *et al.* Messenger RNA delivery of a cartilage-anabolic transcription factor as a disease-modifying strategy for osteoarthritis treatment. *Sci Rep-uk* 6, 18743 (2016).

157. Matsui, A., Uchida, S., Ishii, T., Itaka, K. & Kataoka, K. Messenger RNA-based therapeutics for the treatment of apoptosis-associated diseases. *Sci Rep-uk* 5, 15810 (2015).

158. Baba, M., Itaka, K., Kondo, K., Yamasoba, T. & Kataoka, K. Treatment of neurological disorders by introducing mRNA in vivo using polyplex nanomicelles. *J Control Release* 201, 41–48 (2015).

159. Lee, S., Loretz, B., Lehr, C.-M. & Hirsch, HK. H. A. POLYMER-CARGO-COMPLEXES COMPRISING CROSS-LINKED COPOLYMERS AND CARGO MOLECULES.

160. Haabeth, O. A. W. *et al.* mRNA vaccination with charge-altering releasable transporters elicits human T cell responses and cures established tumors in mice. *Proc National Acad Sci* 115, 201810002 (2018).

161. McKinlay, C. J. *et al.* Charge-altering releasable transporters (CARTs) for the delivery and release of mRNA in living animals. *Proc National Acad Sci* 114, E448–E456 (2017).

162. Guidotti, G., Brambilla, L. & Rossi, D. Cell-Penetrating Peptides: From Basic Research to Clinics. *Trends Pharmacol Sci* 38, 406–424 (2017).

163. Ziegler, A. & Seelig, J. Binding and Clustering of Glycosaminoglycans: A Common Property of Mono- and Multivalent Cell-Penetrating Compounds. *Biophys J* 94, 2142–2149 (2008).

164. Verdurmen, W. P. R. & Brock, R. Biological responses towards cationic peptides and drug carriers. *Trends Pharmacol Sci* 32, 116–124 (2011).

165. Udhayakumar, V. K. *et al.* Arginine-Rich Peptide-Based mRNA Nanocomplexes Efficiently Instigate Cytotoxic T Cell Immunity Dependent on the Amphipathic Organization of the Peptide. *Adv Healthc Mater* 6, 1601412 (2017).

166. Regberg, J., Vasconcelos, L., Madani, F., Langel, Ü. & Hällbrink, M. pH-responsive PepFect cell-penetrating peptides. *Int J Pharmaceut* 501, 32–38 (2016).

167. Sun, Y., Sun, Y., Zhao, R. & Gao, K. Intracellular delivery of messenger RNA by recombinant PP7 virus-like particles carrying low molecular weight protamine. *Bmc Biotechnol* 16, 46 (2016).

168. Sun, P. *et al.* Transcellular delivery of messenger RNA payloads by a cationic supramolecular MOF platform. *Chem Commun* 54, 11304–11307 (2018).

169. Kirchenbuechler, I., Kirchenbuechler, D. & Elbaum, M. Correlation between cationic lipid-based transfection and cell division. *Exp Cell Res* 345, 1–5 (2016).

170. Durymanov, M. O. *et al.* Subcellular trafficking and transfection efficacy of polyethylenimine–polyethylene glycol polyplex nanoparticles with a ligand to melanocortin receptor-1. *J Control Release* 163, 211–219 (2012).

171. Park, K. M. *et al.* All-trans-retinoic acid (ATRA)-grafted polymeric gene carriers for nuclear translocation and cell growth control. *Biomaterials* 30, 2642–2652 (2009).

172. Fan, Y. *et al.* Ternary Complexes with Core-Shell Bilayer for Double Level Targeted Gene Delivery: In Vitro and In Vivo Evaluation. *Pharmaceut Res* 30, 1215–1227 (2013).

173. Koyama, S. *et al.* Differential Role of TLR- and RLR-Signaling in the Immune Responses to Influenza A Virus Infection and Vaccination. *J Immunol* 179, 4711–4720 (2007).

174. Moliva, J. I., Turner, J. & Torrelles, J. B. Immune Responses to Bacillus Calmette–Guérin Vaccination: Why Do They Fail to Protect against Mycobacterium tuberculosis? *Front Immunol* 8, 407 (2017).

175. Tsuji, S. *et al.* Maturation of Human Dendritic Cells by Cell Wall Skeleton of Mycobacterium bovis Bacillus Calmette-Guérin: Involvement of Toll-Like Receptors. *Infect Immun* 68, 6883–6890 (2000).

176. Pulendran, B. & Ahmed, R. Immunological mechanisms of vaccination. *Nat Immunol* 12, 509–517 (2011).

177. Querec, T. D. *et al.* Systems biology approach predicts immunogenicity of the yellow fever vaccine in humans. *Nat Immunol* 10, 116–125 (2009).

178. Querec, T. *et al.* Yellow fever vaccine YF-17D activates multiple dendritic cell subsets via TLR2, 7, 8, and 9 to stimulate polyvalent immunity. *J Exp Medicine* 203, 413–424 (2006).

179. Tsai, T. F. Fluad®-MF59®-Adjuvanted Influenza Vaccine in Older Adults. *Infect Chemother* 45, 159–174 (2013).

180. Didierlaurent, A. M. *et al.* Adjuvant system AS01: helping to overcome the challenges of modern vaccines. *Expert Rev Vaccines* 16, 1–9 (2016).

181. Garçon, N., Chomez, P. & Mechelen, M. V. GlaxoSmithKline Adjuvant Systems in vaccines: concepts, achievements and perspectives. *Expert Rev Vaccines* 6, 723–739 (2014).

182. Garçon, N., Vaughn, D. W. & Didierlaurent, A. M. Development and evaluation of AS03, an Adjuvant System containing α-tocopherol and squalene in an oil-in-water emulsion. *Expert Rev Vaccines* 11, 349–366 (2014).

183. Didierlaurent, A. M. *et al.* AS04, an Aluminum Salt- and TLR4 Agonist-Based Adjuvant System, Induces a Transient Localized Innate Immune Response Leading to Enhanced Adaptive Immunity. *J Immunol* 183, 6186–6197 (2009).

184. Cirelli, K. M. *et al.* Slow Delivery Immunization Enhances HIV Neutralizing Antibody and Germinal Center Responses via Modulation of Immunodominance. *Cell* 177, 1153-1171.e28 (2019).

185. Kool, M. *et al.* Alum adjuvant boosts adaptive immunity by inducing uric acid and activating inflammatory dendritic cells. *J Exp Medicine* 205, 869–882 (2008).

186. Kasturi, S. P. *et al.* Programming the magnitude and persistence of antibody responses with innate immunity. *Nature* 470, 543–547 (2011).

187. Hou, B., Reizis, B. & DeFranco, A. L. Toll-like Receptors Activate Innate and Adaptive Immunity by using Dendritic Cell-Intrinsic and -Extrinsic Mechanisms. *Immunity* 29, 272–282 (2008).

188. Tian, M. *et al.* B Cell–Intrinsic MyD88 Signaling Promotes Initial Cell Proliferation and Differentiation To Enhance the Germinal Center Response to a Virus-like Particle. *J Immunol* 200, 937–948 (2018).

189. Akondy, R. S. *et al.* Initial viral load determines the magnitude of the human CD8 T cell response to yellow fever vaccination. *Proc National Acad Sci* 112, 3050–3055 (2015).

190. Gutjahr, A. *et al.* The STING ligand cGAMP potentiates the efficacy of vaccine-induced CD8+ T cells. *Jci Insight* 4, e125107 (2019).

191. Suthar, M. S. *et al.* The RIG-I-like Receptor LGP2 Controls CD8+ T Cell Survival and Fitness. *Immunity* 37, 235–248 (2012).

192. Kandasamy, M. *et al.* RIG-I Signaling Is Critical for Efficient Polyfunctional T Cell Responses during Influenza Virus Infection. *Plos Pathog* 12, e1005754 (2016).

193. Sinclair, C. *et al.* mTOR regulates metabolic adaptation of APCs in the lung and controls the outcome of allergic inflammation. *Science* 357, 1014–1021 (2017).

194. Ravindran, R. *et al.* Vaccine Activation of the Nutrient Sensor GCN2 in Dendritic Cells Enhances Antigen Presentation. *Science* 343, 313–317 (2014).

195. Gong, T., Liu, L., Jiang, W. & Zhou, R. DAMP-sensing receptors in sterile inflammation and inflammatory diseases. *Nat Rev Immunol* 20, 95–112 (2020).

196. Ndeupen, S. *et al.* The mRNA-LNP platform's lipid nanoparticle component used in preclinical vaccine studies is highly inflammatory. *Biorxiv* 2021.03.04.430128 (2021) doi:10.1101/2021.03.04.430128.

197. Yang, J. *et al.* Hybrid nanovaccine for the co-delivery of the mRNA antigen and adjuvant. *Nanoscale* 11, 21782–21789 (2019).

198. Moon, J. J. *et al.* Interbilayer-crosslinked multilamellar vesicles as synthetic vaccines for potent humoral and cellular immune responses. *Nat Mater* 10, 243–251 (2011).

199. Fischer, N. O. *et al.* Colocalized Delivery of Adjuvant and Antigen Using Nanolipoprotein Particles Enhances the Immune Response to Recombinant Antigens. *J Am Chem Soc* 135, 2044–2047 (2013).

200. Huysmans, H. *et al.* Expression Kinetics and Innate Immune Response after Electroporation and LNP-Mediated Delivery of a Self-Amplifying mRNA in the Skin. *Mol Ther Nucleic Acids* 17, 867–878 (2019).

201. Leyman, B. *et al.* Comparison of the Expression Kinetics and Immunostimulatory Activity of Replicating mRNA, Nonreplicating mRNA, and pDNA after Intradermal Electroporation in Pigs. *Mol Pharmaceut* 15, 377–384 (2018).

202. Tse, S.-W. *et al.* mRNA-encoded, constitutively active STINGV155M is a potent genetic adjuvant of antigen-specific CD8+ T cell response. *Mol Ther* 29, 2227–2238 (2021).

203. Hess, P. R., Boczkowski, D., Nair, S. K., Snyder, D. & Gilboa, E. Vaccination with mRNAs encoding tumor-associated antigens and granulocyte-macrophage colony-stimulating factor efficiently primes CTL responses, but is insufficient to overcome tolerance to a model tumor/self antigen. *Cancer Immunol Immunother* 55, 672–683 (2006).

204. Hotz, C. *et al.* Local delivery of mRNA-encoding cytokines promotes antitumor immunity and tumor eradication across multiple preclinical tumor models. *Sci Transl Med* 13, eabc7804 (2021).

205. Lint, S. V. *et al.* Intratumoral Delivery of TriMix mRNA Results in T-cell Activation by Cross-Presenting Dendritic Cells. *Cancer Immunol Res* 4, 146–156 (2016).

206. Nuffel, A. M. T. V. *et al.* Intravenous and intradermal TriMix-dendritic cell therapy results in a broad T-cell response and durable tumor response in a chemorefractory stage IV-M1c melanoma patient. *Cancer Immunol Immunother* 61, 1033–1043 (2012).

207. Guardo, A. C. *et al.* Preclinical evaluation of an mRNA HIV vaccine combining rationally selected antigenic sequences and adjuvant signals (HTI-TriMix). *Aids* 31, 321–332 (2017).

208. Dewitte, H. *et al.* The potential of antigen and TriMix sonoporation using mRNA-loaded microbubbles for ultrasound-triggered cancer immunotherapy. *J Control Release* 194, 28–36 (2014).

209. Wilgenhof, S. *et al.* Therapeutic Vaccination With an Autologous mRNA Electroporated Dendritic Cell Vaccine in Patients With Advanced Melanoma. *J Immunother* 34, 448–456 (2011).

210. Jong, W. de *et al.* Therapeutic Vaccine in Chronically HIV-1-Infected Patients: A Randomized, Double-Blind, Placebo-Controlled Phase IIa Trial with HTI-TriMix †. *Nato Adv Sci Inst Se* 7, 209 (2019).

211. Keersmaecker, B. D. *et al.* TriMix and tumor antigen mRNA electroporated dendritic cell vaccination plus ipilimumab: link between T-cell activation and clinical responses in advanced melanoma. *J Immunother Cancer* 8, e000329 (2020).

212. Pinzon-Charry, A., Maxwell, T. & López, J. A. Dendritic cell dysfunction in cancer: A mechanism for immunosuppression. *Immunol Cell Biol* 83, 451–461 (2005).

213. Janco, J. M. T., Lamichhane, P., Karyampudi, L. & Knutson, K. L. Tumor-Infiltrating Dendritic Cells in Cancer Pathogenesis. *J Immunol* 194, 2985–2991 (2015).

214. Nguyen-Hoai, T. *et al.* CCL4 as an adjuvant for DNA vaccination in a Her2/neu mouse tumor model. *Cancer Gene Ther* 23, 162–167 (2016).

215. Nguyen-Hoai, T. *et al.* CCL21 (SLC) improves tumor protection by a DNA vaccine in a Her2/neu mouse tumor model. *Cancer Gene Ther* 19, 69–76 (2012).

216. Westermann, J. *et al.* CCL19 (ELC) as an adjuvant for DNA vaccination: induction of a TH1-type T-cell response and enhancement of antitumor immunity. *Cancer Gene Ther* 14, 523–532 (2007).

217. Yamakawa, K., Nakano-Narusawa, Y., Hashimoto, N., Yokohira, M. & Matsuda, Y. Development and Clinical Trials of Nucleic Acid Medicines for Pancreatic Cancer Treatment. *Int J Mol Sci* 20, 4224 (2019).

218. Sridharan, K. & Gogtay, N. J. Therapeutic nucleic acids: current clinical status. *Brit J Clin Pharmaco* 82, 659–672 (2016).

219. Jackson, N. A. C., Kester, K. E., Casimiro, D., Gurunathan, S. & DeRosa, F. The promise of mRNA vaccines: a biotech and industrial perspective. *Npj Vaccines* 5, 11 (2020).

220. Redding, L. & Weiner, D. B. DNA vaccines in veterinary use. *Expert Rev Vaccines* 8, 1251–1276 (2014).

221. Spikevax and Moderna COVID-19 Vaccine | FDA. https://www.fda.gov/emergency-preparedness-and-response/coronavirus-disease-2019-covid-19/spikevax-and-moderna-covid-19-vaccine.

222. Vaxzevria (previously COVID-19 Vaccine AstraZeneca) | European Medicines Agency. https://www.ema.europa.eu/en/medicines/human/EPAR/vaxzevria-previously-covid-19-vaccine-astrazeneca.

223. Sahin, U. *et al.* BNT162b2 vaccine induces neutralizing antibodies and poly-specific T cells in humans. *Nature* 595, 572–577 (2021).

224. Hou, X., Zaks, T., Langer, R. & Dong, Y. Lipid nanoparticles for mRNA delivery. *Nat Rev Mater* 1–17 (2021) doi:10.1038/s41578-021-00358-0.

225. Moghimi, S. M. Allergic reactions and anaphylaxis to lipid nanoparticle-based COVID-19 vaccines. *Mol Ther* 29, 898–900 (2021).

226. McSweeney, M. D., Mohan, M., Commins, S. P. & Lai, S. K. Anaphylaxis to Pfizer/BioNTech mRNA COVID-19 Vaccine in a Patient With Clinically Confirmed PEG Allergy. *Frontiers Allergy* 2, 715844 (2021).

227. Peter, J. *et al.* Allergic reactions to the Ad26.COV2.S vaccine in South Africa. *J Allergy Clin Immunol Global* 1, 2–8 (2022).

228. Hernández-Bello, J. *et al.* Neutralizing Antibodies against SARS-CoV-2, Anti-Ad5 Antibodies, and Reactogenicity in Response to Ad5-nCoV (CanSino Biologics) Vaccine in Individuals with and without Prior SARS-CoV-2. *Nato Adv Sci Inst Se* 9, 1047 (2021).

229. Mendonça, S. A., Lorincz, R., Boucher, P. & Curiel, D. T. Adenoviral vector vaccine platforms in the SARS-CoV-2 pandemic. *Npj Vaccines* 6, 97 (2021).

230. Buchbinder, S. P., McElrath, M. J., Dieffenbach, C. & Corey, L. Use of adenovirus type-5 vectored vaccines: a cautionary tale. *Lancet* 396, e68–e69 (2020).

231. Elzoghby, A. O. Gelatin-based nanoparticles as drug and gene delivery systems: Reviewing three decades of research. *J Control Release* 172, 1075–1091 (2013).

232. Young, S., Wong, M., Tabata, Y. & Mikos, A. G. Gelatin as a delivery vehicle for the controlled release of bioactive molecules. *J Control Release* 109, 256–274 (2005).

233. Foox, M. & Zilberman, M. Drug delivery from gelatin-based systems. *Expert Opin Drug Del* 12, 1547–1563 (2015).

234. Zwiorek, K. *et al.* Delivery by Cationic Gelatin Nanoparticles Strongly Increases the Immunostimulatory Effects of CpG Oligonucleotides. *Pharmaceut Res* 25, 551–562 (2008).

235. Kommareddy, S. & Amiji, M. Poly(ethylene glycol)–modified thiolated gelatin nanoparticles for glutathione-responsive intracellular DNA delivery. *Nanomed Nanotechnol Biology Medicine* 3, 32–42 (2007).

236. Klages-Mundt, N. L. & Li, L. Formation and repair of DNA-protein crosslink damage. *Sci China Life Sci* 60, 1065–1076 (2017).

237. Tretyakova, N. Y., Groehler, A. & Ji, S. DNA–Protein Cross-Links: Formation, Structural Identities, and Biological Outcomes. *Accounts Chem Res* 48, 1631–1644 (2015).

238. Kamla, R. & Bohidar, H. Coacervation in Biopolymers. *J Phys Chem Biophysics* (2014) doi:10.4172/2161-0398.1000165.

239. Rawat, K., Aswal, V. K. & Bohidar, H. B. DNA–Gelatin Complex Coacervation, UCST and First-Order Phase Transition of Coacervate to Anisotropic ion gel in 1-Methyl-3-octylimidazolium Chloride Ionic Liquid Solutions. *J Phys Chem B* 116, 14805–14816 (2012).

240. Reynolds, F., Weissleder, R. & Josephson, L. Protamine as an Efficient Membrane-Translocating Peptide. *Bioconjugate Chem* 16, 1240–1245 (2005).

241. Noguchi, A., Hirashima, N. & Nakanishi, M. Cationic Cholesterol Promotes Gene Transfection Using the Nuclear Localization Signal in Protamine. *Pharmaceut Res* 19, 933–938 (2002).

242. Masuda, T., Akita, H. & Harashima, H. Evaluation of nuclear transfer and transcription of plasmid DNA condensed with protamine by microinjection: The use of a nuclear transfer score. *Febs Lett* 579, 2143–2148 (2005).

243. Kallen, K.-J. *et al.* A novel, disruptive vaccination technology. *Hum Vacc Immunother* 9, 2263–2276 (2013).

244. Sebastian, M. *et al.* A phase I/IIa study of the mRNA-based cancer immunotherapy CV9201 in patients with stage IIIB/IV non-small cell lung cancer. *Cancer Immunol Immunother* 68, 799–812 (2019).

245. Kübler, H. *et al.* Self-adjuvanted mRNA vaccination in advanced prostate cancer patients: a first-in-man phase I/IIa study. *J Immunother Cancer* 3, 26 (2015).

246. Zagato, E. *et al.* Quantifying the Average Number of Nucleic Acid Therapeutics per Nanocarrier by Single Particle Tracking Microscopy. *Mol Pharmaceut* 15, 1142–1149 (2018).

247. Schoenmaker, L. *et al.* mRNA-lipid nanoparticle COVID-19 vaccines: structure and stability. *Int J Pharmaceut* 601, 120586 (2021).

248. Wilfinger, W. W., Mackey, K. & Chomczynski, P. Effect of pH and Ionic Strength on the Spectrophotometric Assessment of Nucleic Acid Purity. *Biotechniques* 22, 474–481 (1997).

249. Arfin, N., Aswal, V. K. & Bohidar, H. B. Overcharging, thermal, viscoelastic and hydration properties of DNA–gelatin complex coacervates: pharmaceutical and food industries. *Rsc Adv* 4, 11705–11713 (2014).

250. Kumar, A. & Dixit, C. K. Advances in Nanomedicine for the Delivery of Therapeutic Nucleic Acids. 43–58 (2017) doi:10.1016/b978-0-08-100557-6.00003-1.

251. Burgess, D. J. & Carless, J. E. Manufacture of gelatin/gelatin coacervate microcapsules. *Int J Pharmaceut* 27, 61–70 (1985).

252. Geggier, S., Kotlyar, A. & Vologodskii, A. Temperature Dependence of DNA Persistence Length. *Biophys J* 100, 76a (2011).

253. Rawat, K., Pathak, J. & Bohidar, H. B. Effect of persistence length on binding of DNA to polyions and overcharging of their intermolecular complexes in aqueous and in 1-methyl-3-octyl imidazolium chloride ionic liquid solutions. *Phys Chem Chem Phys* 15, 12262–12273 (2013).

254. Mao, W. *et al.* Temperature dependence of DNA condensation at high ionic concentration. *Mod Phys Lett B* 30, 1650298 (2016).

255. Gornall, J. L. & Terentjev, E. M. Helix–coil transition of gelatin: helical morphology and stability. *Soft Matter* 4, 544–549 (2008).

256. Gopal, R., Park, J. S., Seo, C. H. & Park, Y. Applications of Circular Dichroism for Structural Analysis of Gelatin and Antimicrobial Peptides. *Int J Mol Sci* 13, 3229–3244 (2012).

257. Mohiti-Asli, M. & Loboa, E. G. Wound Healing Biomaterials. *Part Four Other Funct Biomaterial Dressingsfor Wound Heal* 483–499 (2016) doi:10.1016/b978-1-78242-456-7.00023-4.

258. Hellmund, M. *et al.* Systematic adjustment of charge densities and size of polyglycerol amines reduces cytotoxic effects and enhances cellular uptake. *Biomater Sci-uk* 3, 1459–1465 (2015).

259. Vaz, B., Popovic, M. & Ramadan, K. DNA–Protein Crosslink Proteolysis Repair. *Trends Biochem Sci* 42, 483–495 (2017).

260. Yang, G. *et al.* Assessment of the characteristics and biocompatibility of gelatin sponge scaffolds prepared by various crosslinking methods. *Sci Rep-uk* 8, 1616 (2018).

261. Ulubayram, K., Aksu, E., Gurhan, S. I. D., Serbetci, K. & Hasirci, N. Cytotoxicity evaluation of gelatin sponges prepared with different cross-linking agents. *J Biomaterials Sci Polym Ed* 13, 1203–1219 (2002).

262. Kallen, K.-J. *et al.* A novel, disruptive vaccination technology. *Hum Vacc Immunother* 9, 2263–2276 (2013).

263. Alberer, M. *et al.* Safety and immunogenicity of a mRNA rabies vaccine in healthy adults: an open-label, non-randomised, prospective, first-in-human phase 1 clinical trial. *Lancet* 390, 1511–1520 (2017).

264. Papachristofilou, A. *et al.* Phase Ib evaluation of a self-adjuvanted protamine formulated mRNA-based active cancer immunotherapy, BI1361849 (CV9202), combined with local radiation treatment in patients with stage IV non-small cell lung cancer. *J Immunother Cancer* 7, 38 (2019).

265. TENKUMO, T., ROTAN, O., SOKOLOVA, V. & EPPLE, M. Protamine Increases Transfection Efficiency and Cell Viability after Transfection with Calcium Phosphate Nanoparticles. *Nano Biomed* 5, 64–74 (2014).

266. Sorgi, F., Bhattacharya, S. & Huang, L. Protamine sulfate enhances lipid-mediated gene transfer. *Gene Ther* 4, 961–968 (1997).

267. Cheng, H. *et al.* Efficacy and Safety of COVID-19 Vaccines in Phase III Trials: A Meta-Analysis. *Nato Adv Sci Inst Se* 9, 582 (2021).

268. Wu, Q. *et al.* Evaluation of the safety profile of COVID-19 vaccines: a rapid review. *Bmc Med* 19, 173 (2021).

269. Ciapponi, A. *et al.* Safety of COVID-19 vaccines, their components or their platforms for pregnant women: A rapid review. *Medrxiv* 2021.06.03.21258283 (2021) doi:10.1101/2021.06.03.21258283.

270. Castells, M. C. & Phillips, E. J. Maintaining Safety with SARS-CoV-2 Vaccines. *New Engl J Medicine* 384, NEJMra2035343 (2020).

271. Damase, T. R. *et al.* The Limitless Future of RNA Therapeutics. *Frontiers Bioeng Biotechnology* 9, 628137 (2021).

272. Maruggi, G., Zhang, C., Li, J., Ulmer, J. B. & Yu, D. mRNA as a transformative technology for vaccine development to control infectious diseases. *Mol Ther* 27, 757–772 (2019).

273. Xu, S., Yang, K., Li, R. & Zhang, L. mRNA Vaccine Era—Mechanisms, Drug Platform and Clinical Prospection. *Int J Mol Sci* 21, 6582 (2020).

274. Pardi, N., Hogan, M. J., Porter, F. W. & Weissman, D. mRNA vaccines — a new era in vaccinology. *Nat Rev Drug Discov* 17, 261–279 (2018).

275. Beck, J. D. *et al.* mRNA therapeutics in cancer immunotherapy. *Mol Cancer* 20, 69 (2021).

276. Zhang, H. & Xia, X. RNA cancer vaccines: developing mRNA nanovaccine with self-adjuvant property for cancer immunotherapy. *Hum Vacc Immunother* 17, 2995–2998 (2021).

277. Lint, S. V. *et al.* The ReNAissanCe of mRNA-based cancer therapy. *Expert Rev Vaccines* 14, 235–251 (2014).

278. Heine, A., Juranek, S. & Brossart, P. Clinical and immunological effects of mRNA vaccines in malignant diseases. *Mol Cancer* 20, 52 (2021).

279. Sahin, U., Karikó, K. & Türeci, Ö. mRNA-based therapeutics — developing a new class of drugs. *Nat Rev Drug Discov* 13, 759–780 (2014).

280. Weng, Y. *et al.* The challenge and prospect of mRNA therapeutics landscape. *Biotechnol Adv* 40, 107534 (2020).

281. Tenchov, R., Bird, R., Curtze, A. E. & Zhou, Q. Lipid Nanoparticles□From Liposomes to mRNA Vaccine Delivery, a Landscape of Research Diversity and Advancement. *Acs Nano* 15, 16982–17015 (2021).

282. Shin, M. D. *et al.* COVID-19 vaccine development and a potential nanomaterial path forward. *Nat Nanotechnol* 15, 646–655 (2020).

283. Chatzikleanthous, D., O'Hagan, D. T. & Adamo, R. Lipid-Based Nanoparticles for Delivery of Vaccine Adjuvants and Antigens: Toward Multicomponent Vaccines. *Mol Pharmaceut* 18, 2867–2888 (2021).

284. Zhu, M. Immunological perspectives on spatial and temporal vaccine delivery. *Adv Drug Deliver Rev* 178, 113966 (2021).

285. González-Maeso, J. & Sealfon, S. C. Endocrinology. in *Chapter 5 - Hormone Signaling Via G Protein–Coupled Receptors* 83–105 (2010). doi:10.1016/b978-1-4160-5583-9.00005-8.

286. Gainetdinov, R. R., Premont, R. T., Bohn, L. M., Lefkowitz, R. J. & Caron, M. G. DESENSITIZATION OF G PROTEIN–COUPLED RECEPTORS AND NEURONAL FUNCTIONS. *Neuroscience* 27, 107–144 (2004).

287. Lundstrom, K. Latest development on RNA-based drugs and vaccines. *Futur Sci Oa* 4, FSO300 (2018).

288. Aa, M. A. E. M. van der *et al.* The Nuclear Pore Complex: The Gateway to Successful Nonviral Gene Delivery. *Pharmaceut Res* 23, 447–459 (2006).

289. Ross, R. *et al.* Transcriptional targeting of dendritic cells for gene therapy using the promoter of the cytoskeletal protein fascin. *Gene Ther* 10, 1035–1040 (2003).

290. Moulin, V. *et al.* Targeting dendritic cells with antigen via dendritic cell-associated promoters. *Cancer Gene Ther* 19, 303–311 (2012).

291. Jones, D. L., Brewster, R. C. & Phillips, R. Promoter architecture dictates cell-to-cell variability in gene expression. *Science* 346, 1533–1536 (2014).

292. Andreev, D. E., Terenin, I. M., Dmitriev, S. E. & Shatsky, I. N. Pros and cons of pDNA and mRNA transfection to study mRNA translation in mammalian cells. *Gene* 578, 1–6 (2016).

293. Grun, M. K. *et al.* PEGylation of poly(amine-co-ester) polyplexes for tunable gene delivery. *Biomaterials* 272, 120780 (2021).

294. Gómez-Aguado, I. *et al.* Nucleic Acid Delivery by Solid Lipid Nanoparticles Containing Switchable Lipids: Plasmid DNA vs. Messenger RNA. *Molecules* 25, 5995 (2020).

295. Kaczmarek, J. C. *et al.* Systemic delivery of mRNA and DNA to the lung using polymer-lipid nanoparticles. *Biomaterials* 275, 120966 (2021).

296. Zou, S., Scarfo, K., Nantz, M. H. & Hecker, J. G. Lipid-mediated delivery of RNA is more efficient than delivery of DNA in non-dividing cells. *Int J Pharmaceut* 389, 232–243 (2010).

297. Nasr, S. S. *et al.* Co-Delivery of mRNA and pDNA Using Thermally Stabilized Coacervate-Based Core-Shell Nanosystems. *Pharm* 13, 1924 (2021).

298. Shukla, R. S., Jain, A., Zhao, Z. & Cheng, K. Intracellular trafficking and exocytosis of a multi-component siRNA nanocomplex. *Nanomed Nanotechnol Biology Medicine* 12, 1323–1334 (2016).

299. Lönn, P. *et al.* Enhancing Endosomal Escape for Intracellular Delivery of Macromolecular Biologic Therapeutics. *Sci Rep-uk* 6, 32301 (2016).

300. Erazo-Oliveras, A., Muthukrishnan, N., Baker, R., Wang, T.-Y. & Pellois, J.-P. Improving the Endosomal Escape of Cell-Penetrating Peptides and Their Cargos: Strategies and Challenges. *Pharm* 5, 1177–1209 (2012).

301. Teo, S. L. Y. *et al.* Unravelling cytosolic delivery of cell penetrating peptides with a quantitative endosomal escape assay. *Nat Commun* 12, 3721 (2021).

302. Kulkarni, J. A. *et al.* Design of lipid nanoparticles for in vitro and in vivo delivery of plasmid DNA. *Nanomed Nanotechnol Biology Medicine* 13, 1377–1387 (2017).

303. Wang, Z.-B. & Xu, J. Better Adjuvants for Better Vaccines: Progress in Adjuvant Delivery Systems, Modifications, and Adjuvant–Antigen Codelivery. *Nato Adv Sci Inst Se* 8, 128 (2020).

304. Nordly, P., Madsen, H. B., Nielsen, H. M. & Foged, C. Status and future prospects of lipid-based particulate delivery systems as vaccine adjuvants and their combination with immunostimulators. *Expert Opin Drug Del* 6, 657–672 (2009).

305. Zeng, B. *et al.* Self-adjuvanting nanoemulsion targeting dendritic cell receptor Clec9A enables antigen-specific immunotherapy. *J Clin Invest* 128, 1971–1984 (2018).

306. Kreutz, M. *et al.* Antibody-Antigen-Adjuvant Conjugates Enable Co-Delivery of Antigen and Adjuvant to Dendritic Cells in Cis but Only Have Partial Targeting Specificity. *Plos One* 7, e40208 (2012).

307. Roffê, E. *et al.* A DNA vaccine encoding CCL4/MIP-1β enhances myocarditis in experimental Trypanosoma cruzi infection in rats. *Microbes Infect* 8, 2745–2755 (2006).

308. Bystry, R. S., Aluvihare, V., Welch, K. A., Kallikourdis, M. & Betz, A. G. B cells and professional APCs recruit regulatory T cells via CCL4. *Nat Immunol* 2, 1126–1132 (2001).

309. Chang, T.-T. & Chen, J.-W. Emerging role of chemokine CC motif ligand 4 related mechanisms in diabetes mellitus and cardiovascular disease: friends or foes? *Cardiovasc Diabetol* 15, 117 (2016).

310. Keane, M. P., Strieter, R. M. & Belperio, J. A. Encyclopedia of Respiratory Medicine. *Article Titles M* 1–5 (2006).

311. Förster, R., Davalos-Misslitz, A. C. & Rot, A. CCR7 and its ligands: balancing immunity and tolerance. *Nat Rev Immunol* 8, 362–371 (2008).

312. Förster, R. *et al.* CCR7 Coordinates the Primary Immune Response by Establishing Functional Microenvironments in Secondary Lymphoid Organs. *Cell* 99, 23–33 (1999).

313. Hintzen, G. *et al.* Induction of Tolerance to Innocuous Inhaled Antigen Relies on a CCR7-Dependent Dendritic Cell-Mediated Antigen Transport to the Bronchial Lymph Node. *J Immunol* 177, 7346–7354 (2006).

314. Martín-Fontecha, A. *et al.* Regulation of Dendritic Cell Migration to the Draining Lymph Node. *J Exp Medicine* 198, 615–621 (2003).

315. Bachmann, M. F., Kopf, M. & Marsland, B. J. Chemokines: more than just road signs. *Nat Rev Immunol* 6, 159–164 (2006).

316. Scandella, E. *et al.* Dendritic Cell-Independent B Cell Activation During Acute Virus Infection: A Role for Early CCR7-Driven B-T Helper Cell Collaboration. *J Immunol* 178, 1468–1476 (2007).

Scientific output

1. Nasr, S.S.; Lee, S.; Thiyagarajan, D.; Boese, A.; Loretz, B.; Lehr, C.-M. **Co-Delivery of mRNA and pDNA Using Thermally Stabilized Coacervate-Based Core-Shell Nanosystems.** *Pharm* **2021**, *13*, 1924, doi:10.3390/pharmaceutics13111924.

2. **Proteoid biodynamers for safe mRNA transfection via pH-responsive nanorods enabling endosomal escape (submitted manuscript)**

Sangeun Lee, Sarah S. Nasr, Sari Rasheed, Olga Hartwig, Cansu Kaya, Annette Boese, Marcus Koch, Jennifer Herrmann, Rolf Müller Brigitta Loretz, Eric Buhler Anna K. H. Hirsch and Claus-Michael Lehr

3. **"Dual-loaded Core-Shell mRNA and pDNA Nanocarriers for co-delivery of NA-encoded antigens and adjuvants"**

Sarah S. Nasr, Brigitta Loretz, Claus-Michael Lehr [Short talk, PBP World Meeting-March 2022]

4. **"Protein-based Nanocarriers for Simultaneous Co-transfection of pDNA and mRNA"**

Sarah S. Nasr, Brigitta Loretz, Claus-Michael Lehr [On-demand talk, CRS Virtual Annual Meeting-June 2021]

5. **"Gelatin-Based Nanosystem for Nucleic Acid Delivery"**

Sarah S. Nasr, Brigitta Loretz, Claus-Michael Lehr [Flash talk, CRS-German Chapter Lepziyg 2019]

6. **Thermally Stabilized Core-Shell Nanocarrier for Co-Delivery of plasmid DNA and messenger RNA**

Sarah S. Nasr , Sangeun Lee, Durairaj Thiyagarajan , Annette Boese , Brigitta Loretz and Claus-Michael Lehr [Poster Presentation, BioBarriers 2021]

Acknowledgment

قبل كل شيئ و بعد كل شيئ ، لله الحمد من قبل و من بعد

I would like to preface by collectively thanking everyone who was involved in granting me this transformational opportunity, to experience realizing my life's dream to start a career in 'natural sciences' that have dominated my curiosities since childhood, 'gene therapy' that I first encountered in my early teens and was fascinated by since, drug delivery that I first discovered 8 years ago and that continues to enthrall me a little more every day, and eventually infection research, a crucial cause that can always use new devouts. I thank the circumstances, the timings, and most importantly the endless support of so many people who aided me along this journey.

First, I would like to thank my supervisor Prof. Dr. Claus-Michael Lehr, for being one of the most supportive and open-minded supervisors any student can hope for. Thank you first and foremost for always being enthusiastic about the science, that infectious enthusiasm, positive mindset, and encouragement, even when things were not going as we hoped. Thank you for always teaching me something new in every meeting, we sometimes joked about it, but for me it was the reward for all the journey I had to take all the way from Egypt, to come to your team and learn from you, and you always made it worthwhile. On a personal level thank you for being always a genuinely kind and warm presence throughout my time in Germany.

My second supervisor Dr. Brigitta Loretz, thank you for your both personal and professional support, for always being generous with your time and effort in mentoring me, for always being open to sharing your angle of view, which always encouraged me to try and view things from as many angles as possible. For your honesty and countless good advice. Thank you for allowing me a chance to learn from you and for guiding me through the different phases of this Ph.D.

I would like to thank Prof. Dr. Anna K. Hirsch for taking the time to listen to my progress, and always being very kind in providing useful insight to my project trajectory.

I would also like to thank my collaborator and friend Jr. Prof. Sangeun Lee, for all the fruitful discussions we would have, for showing me so much of her work philosophy, tips, and tricks, and for simply being just a great company in and out of the lab.

I would also like to thank Prof. Carlos A. Guzmán, Dr. Kai Schulz, Dr. Simon Delandre for the constantly stimulating discussion in our Vaccination-club meetings, Dr. Thiago Durairaj, Dr. Marius Hittinger, Dr. Annette Boese for their various contributions either in discussion or technical support that helped me better understand and execute my research.

A big thank you to my friends and labmates, both from DDEL and BION, many faces changed, but everyone has always been extremely helpful and provided a very inclusive work environment: Olga, Mina, Lena, Mohamed, Rebecca, Benedikt, Clementine, Justus, Adriely, Thomas, Max, Eilien, Carla, Alberto, Yun, Sarah F., Samy, Kevin, Lorenz, Neha, Khiet, Xabi, Anna, Eliska, Lise, Brittany, Julia, Alex, just to name a few, thank you all for all the good times.

Our dedicated team of technicians, who never hesitated to support mine or any colleagues' workflows, Annette, Pascal, Petra, Tabea, and Jana, thank you all very much for your time and effort.

A lot of gratitude and many thanks also to the dear office members Karin, Sarah, and Annette for endless help and support with countless logistics over my stay in Germany, you made my life so much easier, and you were always so gracious about it.

I would also like to thank my funding agency the Egyptian Mission's Sector, the Ministry of Higher Education in Egypt, as well as the Egyptian Cultural Office in Berlin for logistic support.

A lot of gratitude goes to the friends who grew to become something a lot more like family over the years. Hanzey, constantly sticking by my side through thick and thin, genuinely, lovingly, you're the sister I never had. Ghamdan, my safehouse, to whom I come with problems and worries, to leave with either solutions, assurance, a good laugh, and always stimulating conversation. Patrick, one of the most genuine friends, kindest hearts, and best cooks tucked away under a whole lot of logic, ready to surprise at any moment with a heart of gold. Samir, always the perfect shopping companion and the dedicated friend. Sarah Menina, the very unlikely combination of extremely adventurous and very wise,you taught me alot, with such kindness on top. Thabet, never a dull moment when you're around even with that ear-bleeds-inducing Egyptian dialect. Robert, great friend, lab companion, biking instructor, hummus aficionado, and favorite German jokester. Carlos, the heart of an Angel, the sense of humor of a devil. Salma and Mina, my two favorite Cairo citizens with all the warmth and fun you brought me. Sarah Laqany for always being such a dedicated friend and sister, building and maintaining such an honest and genuine friendship over the years, despite the distance. I will miss you guys but we kept our friendship alive and thriving for all these years and I am sure we can keep it up.

And to end on the highest note, I would like to thank my family to whom I owe everything that I have or had the pleasure of experiencing or achieving. My parents, who always gave me access to a stimulating life with lots of love and support, and also outlets for creativity and curiosity. Thank you for your endless support to my every endeavor and for nurturing and respecting my differences, for giving me a chance to be independent in a culture like ours, and for always being such great friends, good sports, fun company, and engines of motivation through the darkest times. Thank you, Mama, for being the most supportive and funniest and quirkiest friend and mother anyone can dream of. Thank you,

Papa, for being such a great example in science and men in general, you raise the bar too high. My brother Mohamed for being a partner in crime throughout all our formative years, you taught me tons. To my extended familyAunt Salwa and Uncle Mostafa (may he rest in peace) whom I always considered as my parents as well, thank you for all your amazing love and support throughout the years. To Uncle Hussien and Taunte Christa, thank you so much for being one of the main reasons I could come to Germany, for all your help and genuine encouragement, and for making me feel looked after all these years despite the gaping geographical distance I never felt short of your familial affection. Also Tarek and Yasmin. Love you all guys.

في النهاية،ان لم يكن بك علي غضب فلا أبالي...و لكن عافيتك هي أوسع لي..